REVIEWS OF MODERN PHYSICS, VOLUME 77, OCTOBER 2005

The interaction of relativistic particles with strong crystalline fields

Ulrik I. Uggerhøj

Department of Physics and Astronomy, University of Aarhus, Denmark

(Published 20 October 2005)

Crystals present a uniquely simple environment for the investigation of strong electromagnetic fields. When energetic charged particles are incident on crystals close to major crystallographic directions, their electromagnetic interactions depend crucially on the kinematic conditions. The coherence of the crystalline field can produce very strong electric fields in the rest frame of the particle, exceeding the so-called Schwinger field or quantum critical field. In that domain, the radiation emission takes a substantial part of the electron energy and the "formation zone" changes character. In this review the theory appropriate to the different kinematics domains is described, concentrating on the effects occurring at extreme fields. Properties discussed include strong field synchrotron radiation, channeling radiation, bremsstrahlung, and photon interactions. Applications are given to radiation sources, bending of particle beams, and sources of polarized GeV photons.

CONTENTS

I. INTRODUCTION

It is perhaps surprising that strong crystalline fields allow experimental investigations of phenomena that

 ©2005 The American Physical Society

are otherwise very technically demanding or appear exclusively as astrophysical phenomena. The relevance of such investigations range over quite different phenomena from beamstrahlung, heavy-ion collisions, and $\gamma\gamma$ colliders to the gravitational "analog," Hawking radiation.

In this connection, "strong" means comparable to the quantum-mechanical critical field in the frame of the electron, while "crystalline" refers to the field originating from a periodic arrangement of atoms. Despite the periodicity, the effective field has only a small noncontinuous component in its interaction with a charged particle and the trajectory is therefore locally well described as a segment of a circular path. Therefore although the crystalline fields are purely electric in the laboratory system, the resulting radiation emission becomes of the synchrotron type, as if the field were magnetic.

The aim of this review is to present the "strong-field effects" that are achievable in crystals and to elucidate these effects by the use of experimental results as well as theoretical estimates that at a slight expense of precision offer transparency. Strong-field effects appear as a result of a critical field in the rest frame of the particle and give rise to a quantum suppression of radiation emission in contrast to the classical synchrotron-radiation emission. The reader who wishes to follow a more stringent theoretical route to the strong-field effects is referred to the comprehensive textbook by Baier *et al.* (1998).

Following experiments with electrons impinging on crystals, Stark (1912) published the results of the penetration of charged particles in crystals. He concluded that penetrating particles would be guided in their motion by the very strong interatomic fields of force and that penetration depths along "shafts" in the crystal would be much longer than in amorphous materials. Later, Williams (1935) considered interference in radiative effects for particles passing different nuclei in succession. He concluded that an enhancement or reduction in radiation yield was possible for electrons with energy beyond $137mc^2$, where m is the rest mass of the electron and c the speed of light. However, it was not until the mid 1950s that Dyson and Überall (1955) published a more quantitative evaluation of the enhancement of bremsstrahlung intensity. Their "crude classical argument" was based on the number of atoms within the formation length. Shortly before this, Landau and Pomeranchuk (1953a, 1953b) used the formation length to investigate the suppression of bremsstrahlung due to multiple Coulomb scattering, what is nowadays referred to as the Landau-Pomeranchuk-Migdal (LPM) effect. See Klein (1999) and Uggerhøj (2004a) for recent reviews. In short, the LPM effect appears for photon energies where the multiple scattering over the formation length scatters the radiating particle outside the radiation cone defined approximately by the inverse of the Lorentz factor, $1/\gamma$.

The formation length and the regular atomic positions in a crystal are the necessary features, for example, for an increase in radiation emission compared to incidence on an amorphous foil, the so-called enhancement. Furthermore, the strong electric fields of the lattice nuclei, averaged along the direction of motion, open up the possibility of investigating fields of extreme magnitudes.

When the direction of the penetrating particle nearly coincides with a crystallographic axis or plane, the strong electric fields of the nuclear constituents add coherently such as to obtain a macroscopic, continuous electric field of the order $\mathcal{E}\simeq 10^{11}$ V/cm. This is evidenced by the channeling phenomenon (Lindhard, 1965) or the so-called doughnut scattering (Sørensen and Uggerhøj, 1989) to be discussed below. Therefore in the rest frame of an ultrarelativistic electron with a Lorentz factor of $\gamma\simeq 10^5$, the field encountered becomes comparable to the critical field, $\mathcal{E}_0=m^2c^3/e\hbar=1.32\times 10^{16}$ V/cm. Here, e is the elementary charge and $\hbar$ Planck's constant divided by 2π. The incident particle moves in immensely strong fields over distances up to that of the crystal thickness, i.e., up to several mm. Thereby the behavior of charged particles in strong fields such as $\mathcal{E}_0$—strong-field effects—can be investigated.

The outline of the paper is as follows. After the introduction we present a detailed discussion of the formation length and a few topics from solid-state physics that are the necessary tools for understanding the enhancement of radiation emission. Then, a discussion of channeling and coherent and incoherent bremsstrahlung follows with the main emphasis on showing the phenomena they have in common. A discussion on the possible insufficiency of a classical description for radiation processes then leads to the following main topics: radiation emission and pair production in strong fields. These are first described theoretically and subsequently key experimental results are presented and discussed on the basis of the theory. The last two sections primarily emphasize the relevance of investigations of strong-field effects, first considering related subjects in other branches of physics and finally the many possible applications of the strong-field effects. The main purpose of this review is to show that crystals combined with ultrarelativistic particles offer a uniquely straightforward way of investigating fields of the order $\mathcal{E}_0$.

A. Crystal lattice

The structure underlying any single crystal is the Bravais lattice,

$$\vec{R} = n_1\vec{a}_1 + n_2\vec{a}_2 + n_3\vec{a}_3, \tag{1}$$

which is composed of the primitive vectors $\vec{a}_i$ and n_i is an integer (Ashcroft and Mermin, 1976). From any point in the lattice the crystal looks the same, i.e., its atomic density is periodic, $\rho(\vec{r}+\vec{R})=\rho(\vec{r})$, and therefore so is the potential, $U(\vec{r}+\vec{R})=U(\vec{r})$. The reciprocal lattice represented by $\vec{q}$ is obtained as a Fourier series of the direct lattice and vice versa,

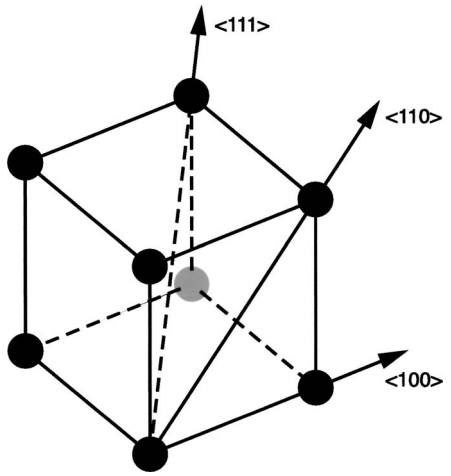

FIG. 1. A primitive cubic lattice with the main crystallographic axes indicated.

$$U(\vec{r}) = \sum_{\vec{q}} G(\vec{q}) e^{-i\vec{q}\cdot\vec{r}}, \tag{2}$$

where $G(\vec{q})$ depends on the particular choice of crystal. Figure 1 shows a primitive cubic lattice and the main crystallographic axes.

B. Strong fields in crystals

To set the scale of an electric field it is natural to combine the four fundamental constants m, e, $\hbar$, and c to obtain an electric field, the so-called critical field,

$$\mathcal{E}_0 = \frac{m^2c^3}{e\hbar}. \tag{3}$$

For electrons, this corresponds to a magnetic field $B_0 = 4.41 \times 10^9$ T. The use of these constants indicates a relativistic (c) quantum ($\hbar$) field for electrons (m, e), i.e., the possibility of electron-positron production for fields of this magnitude. By rewriting the expression slightly to $\mathcal{E}_0 = mc^2/e\lambda\!\!\!^{-}_c$ it is clear that this field corresponds to the production of an electron over a (reduced) Compton wavelength $\lambda\!\!\!^{-}_c$. In a classical analog, the field required to produce a pair is 137 times larger, i.e., a tunneling process reduces the critical field in a quantum theory (Feynman, 1948). The critical field is in many contexts called the "Schwinger field."

Probably the first treatment of a critical field and one of the first indications of the existence of antiparticles was a treatment of electrons impinging on a potential barrier giving rise to a field of the order $\mathcal{E}_0$ (Klein, 1929; Sauter, 1931a, 1931b). This phenomenon—that rapidly became known as the Klein paradox—was one of the first applications of the Dirac equation and has lately received some attention (Nitta *et al.*, 1999; Krekora *et al.*, 2004). In short, the Klein paradox is a reflection probability of an electron incident on a barrier with gradient $\gtrsim \mathcal{E}_0$ exceeding 1 as a result of pair production. An analogous problem may be addressed experimentally within the coming decade by means of strong crystalline fields.

C. Formation length

Ter-Mikaelian first discovered that it takes a relatively long time and therefore a long distance for an energetic electron to create a photon. The interactions of the electron over this "formation zone" affect the radiation spectrum decisively and may lead to enhancement or reduction of total intensity as well as changes in the spectral shape. As observed by Akhiezer and Shul'ga (1982): "It is quite remarkable that the collective phenomena appear at arbitrarily high energies, although at first glance it seems that if the particle wavelength is less than the average distance between the atoms of the material, collective phenomena should not appear and the material should behave as a gas of independent atoms." The "collective phenomena" do not appear due to the particle wavelength, but due to the momentum transfer during the emission process. By the uncertainty relation this transforms into an uncertainty of the exact location where emission takes place and therefore a formation length over which constructive or destructive interference can take place.

1. Classical formation length

Let us consider a couple of approaches to the formation length as they appear in a classical theory. Perhaps the simplest approach is to consider the photon "formed" by the time it takes for a photon to separate from the electron by one reduced wavelength, $\lambda\!\!\!^{-}/2\pi$, and by the corresponding distance of travel of the electron, l_f:

$$\frac{l_f}{v} = \left(l_f + \frac{\lambda\!\!\!^{-}}{2\pi}\right)\frac{1}{c}, \tag{4}$$

which for $v = \sqrt{1-1/\gamma^2}c \simeq c$ yields

$$l_f = \frac{2\gamma^2 c}{\omega}, \tag{5}$$

where v is the speed of the electron and $\gamma = E/mc^2$ the Lorentz factor related to the energy of the electron E. Early approaches to the formation length in QCD were based on this idea (Sørensen, 1992; Gyulassy and Wang, 1994).

A second, more experimentally inclined approach, originates from the emission of synchrotron radiation in a bending magnet with a field B as, for example, in a synchrotron light source. The typical width of emission angles of the photons is $1/\gamma$—resulting from the relativistic transformation of the radiation in the instantaneous rest frame to the frame of the laboratory (Jackson, 1975).

Therefore a detector will not give information on the actual position of radiation emission over the distance a to b; see Fig. 2. It is thus not possible to tell where the

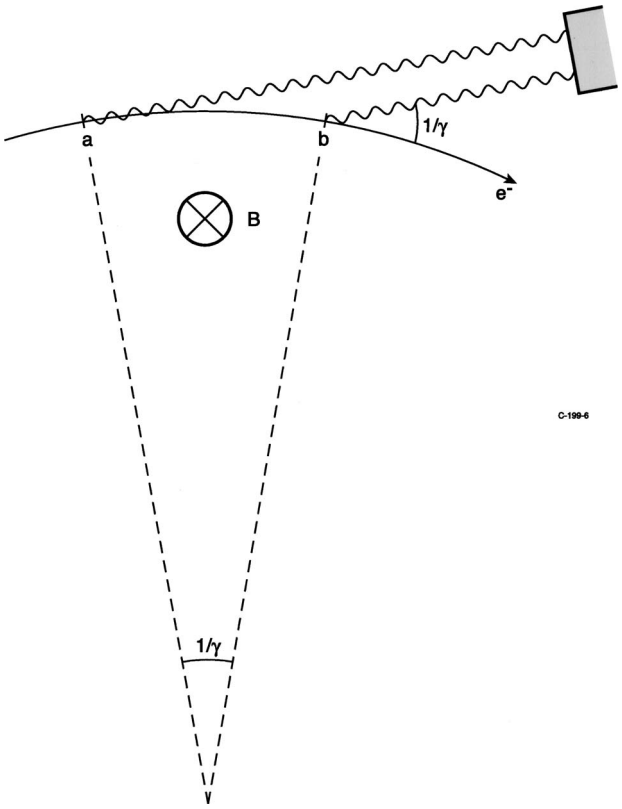

FIG. 2. Synchrotron-radiation emission by an energetic electron traversing a magnetic field B. The typical emission angle $1/\gamma$ makes photon emission from any point within the arc length from a to b indistinguishable by a detector. Therefore the distance ab represents the formation length.

photon was emitted over this length, the formation length. Since the emission angle $1/\gamma$ connects the gyromagnetic curvature radius $r_c=pc/eB$ and the formation length l_f by $l_f=r_c/\gamma$ for small angles, the result is

$$l_f=\frac{pc}{eB\gamma}, \tag{6}$$

where p is the momentum. Since synchrotron radiation has a characteristic frequency $\omega_c=3\gamma^3eB/2p$, Eq. (5) is obtained again, although with a slightly different constant.[1] This constant depends on the choice of characteristic frequency or similarly on the accepted emission angles in Fig. 2, which may as well be chosen as lying in the range $[-1/\gamma;\ 1/\gamma]$.

Following Feinberg (1966), we may also consider the "semibare electron," i.e., the electron and its electric field during the time immediately following a scattering event. Before the scattering event the electron and the electromagnetic field are comoving, whereas the time it takes the field to adjust to the new direction of the electron is finite. In the rest frame of the electron the "regeneration time" t' of the field at position $\vec{x}'$ is proportional to the distance from the electron to $\vec{x}'$, i.e., by a Fourier transform $t'\simeq 1/\omega'$ [see, e.g., Jackson (1975)] where the primed coordinates here denote the rest system. Due to the Lorentz transformations to the frame of the laboratory, $t=t'\gamma$ and $\omega=2\gamma\omega'$, the regeneration time becomes $t\simeq 2\gamma^2/\omega$, which is the same as Eq. (5). This interpretation is very useful for the Ternovskii-Shul'ga-Fomin effect of radiation emission in a thin target (Ternovskii, 1960; Shul'ga and Fomin, 1998), which has an analog in the case of thin crystals (Fomin *et al.*, 1996). In the Ternovskii-Shul'ga-Fomin effect, the radiation yield diminishes for photon energies with formation lengths extending out of the target. In this case, the radiation emission becomes proportional to the logarithm of the target thickness instead of being a linear relationship.

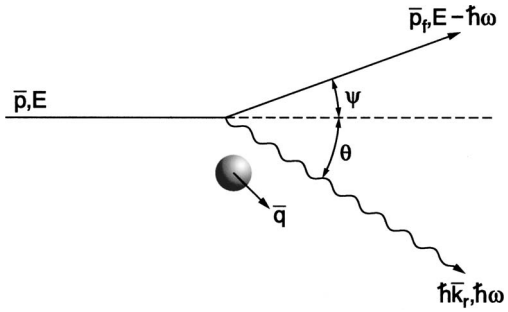

FIG. 3. A schematic diagram showing the photon emission by an energetic lepton in the nuclear field. Angles are exaggerated for clarity.

2. Quantum formation length

In the quantum version, where the recoil imposed on the electron by the emitted photon is taken into account, the formation length can be calculated by use of the longitudinal momentum transfer to the nucleus, $q_\parallel=p-p_f-\hbar\omega/c$, where p and p_f denote the momentum of the electron before and after the radiation event, respectively. The photon propagates in the medium with velocity c/n_r and momentum $\hbar k_r=\hbar n_r k$, where $n_r=\sqrt{\varepsilon(\omega)}=\sqrt{1-\omega_p^2/\omega^2}$ is the index of refraction, $\varepsilon(\omega)$ is the dielectric function, and $\omega_p=\sqrt{4\pi nZ_2e^2/m}$ is the plasma frequency, with n being the number density of atoms and Z_2 the atomic number of the target.

Expanding the longitudinal momentum transfer $\vec{q}_\parallel$ to first order in $1/\gamma$ and applying small-angle approximations, $q_\parallel$ becomes

$$q_\parallel=\frac{\hbar\omega}{2E(E-\hbar\omega)c}\{1+\gamma\gamma_f[\theta^2+\psi^2(E-\hbar\omega)/\hbar\omega+\omega_p^2/\omega^2]\}, \tag{7}$$

where $\gamma_f=(E-\hbar\omega)/mc^2$, ψ is the electron-scattering angle, and θ is the photon emission angle (see Fig. 3). Since $\psi=1/\gamma$ for a penetration depth $l_\gamma=\alpha X_0/2\pi\gg a_0$ the term involving the electron angle can be neglected compared to the ω_p^2/ω^2 term, even when $\omega\lesssim\omega_p$. Here,

[1] A more rigorous derivation of the formation length for synchrotron radiation can be found in the book by Beresteskii *et al.* (1982) where the concept of formation length is attributed to Ter-Mikaelian; see also Feinberg (1994).

$\alpha = e^2/\hbar c$ is the fine-structure constant, a_0 is the Bohr radius, and X_0 is the radiation length. Typical photon angles are $\theta \lesssim 1/\gamma$ such that the allowed range of $q_\parallel$ is given by [see also Timm (1969)]

$$\delta \leqslant q_\parallel \lesssim 2\delta, \tag{8}$$

where δ is equal to the minimum longitudinal momentum transfer. Without a measurement of the photon and electron emission angles θ and ψ, the longitudinal momentum transfer is thus uncertain by an amount $\simeq \delta$. Therefore using the uncertainty relation $l_f = \hbar/\Delta q_\parallel$, the formation length can be obtained by subtracting the minimum longitudinal momentum transfer from Eq. (7) with $\theta \lesssim 1/\gamma$:

$$l_f = \frac{2E(E-\hbar\omega)c}{\omega} \frac{1}{\gamma\gamma_f[\theta^2 + \psi^2(E-\hbar\omega)/\hbar\omega + \omega_p^2/\omega^2]}. \tag{9}$$

For sufficiently high photon energies $\hbar\omega \gtrsim \gamma\hbar\omega_p \simeq \gamma$ (50 eV) the plasma frequency term can be neglected. Thus with this approximation and $\theta \simeq 1/\gamma$, $\psi \simeq 0$, as discussed above, the formation length becomes

$$l_f = \frac{2\gamma^2 c}{\omega^*} \quad \text{with } \omega^* = \omega\frac{E}{E-\hbar\omega} \simeq \omega, \tag{10}$$

where $\hbar\omega$ is the energy of the photon. An alternative approach for the derivation of Eq. (9) is to consider the region of main contributions to the radiation integral as, e.g., in the quasiclassical operator method (Baier and Katkov, 2005a). Similar methods investigating the impact-parameter dependence of various photoprocesses reach the same conclusions in a picture involving momentum transfer as through a more elaborate wave-packet study (Sørensen, 2001).

In the classical or recoilless limit $\hbar\omega \ll E$, Eq. (10) coincides with Eq. (5) as is required. In other cases, e.g., for beamstrahlung in electron-electron collisions, the recoil is substantially different giving rise to strong suppression effects reminiscent of the LPM effect (Baier and Katkov, 2002). As discussed below, beamstrahlung is a result of the interaction of a particle in one bunch with the field of the opposing bunch, and for future linear colliders strong-field effects become decisive for the energy loss due to beamstrahlung.

For pair production, a classical version of the formation length is the length it takes to separate a created pair transversely by two Compton wavelengths $\lambda\!\!\!^{-}_c$ when the pair is emitted with an opening angle $1/\gamma_p$:

$$l_f^{\text{pair}} = 2\gamma_p \lambda\!\!\!^{-}_c \frac{2\gamma_p^2 c}{\omega}. \tag{11}$$

Therefore the formation length increases with the energy of the pair, where $\gamma_p \equiv \hbar\omega/mc^2$.

When calculated properly by means of longitudinal momentum transfer, the formation length for pair production becomes

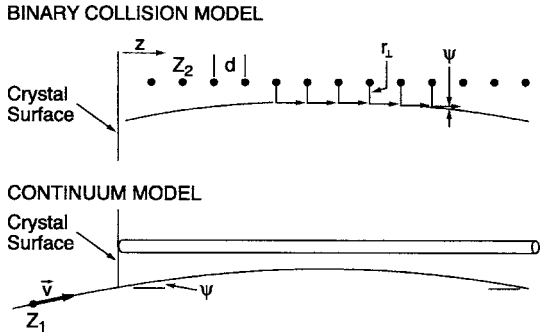

FIG. 4. A schematic drawing of the discrete nature of the scattering centers in a crystal and the resulting continuum approximation. The target atoms with atomic number Z_2 and distance d along the string impose a curved trajectory on the penetrating particle with atomic number Z_1 through binary encounters over the transverse distance $r_\perp$. The resulting trajectory with entrance angle ψ can be accurately described as if being the result of an interaction with a string of continuous charge distribution, i.e., the charges $Z_2 e$ being "smeared" along the direction of motion z.

$$l_f^{\text{pair}} = \frac{2\gamma_p^2 c}{\omega^\#} \quad \text{with } \omega^\# = \frac{\omega}{\eta_+\eta_-}, \tag{12}$$

where $\eta_\pm$ is defined as $E_{e^\pm}/\hbar\omega$, with $E_{e^\pm}$ being the energy of the created electron or positron. It is an important distinction relevant to the strong-field effects that l_f increases with increasing energy of the pair, whereas the formation length for a radiation emission decreases with increasing energy of the emitted photon for a fixed energy of the radiating particle. On the other hand, the similarity between the two formation lengths when expressed as functions of γ, γ_p, ω^*, and $\omega^\#$ reflect the crossing symmetry of the processes.

II. CHANNELING

In the so-called continuum approximation (Lindhard, 1965), charged particles incident on a single crystal with small angles to crystallographic directions experience the collective, screened nuclear fields as if smeared along the string or plane; see Fig. 4. For incidence with angles smaller than the so-called critical angle ψ_c, the particle has a low transverse momentum with respect to the axis or plane of the crystal. Thus it can be restricted to areas away from the nuclei (positively charged particles) or close to the nuclei (negatively charged particles); see Fig. 5.

In this case the particle is channeled and is guided by the lattice such that a separation of the longitudinal and transverse motions is present. The result is a conserved "transverse energy" and therefore a transverse potential $U(r_\perp)$ in which the particle moves:

$$U(r_\perp) = \frac{1}{d}\int_{-\infty}^{\infty} V(r_\perp, z)dz, \tag{13}$$

where $V(r_\perp, z)$ is the atom potential at the location of the projectile. For an introduction to channeling at high

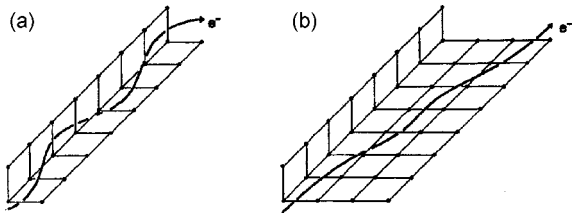

FIG. 5. A channeled negatively charged particle moves near (a) an axis and (b) a plane. From Weinmann, 1998.

energies, see, e.g., Sørensen and Uggerhøj (1989) and Sørensen (1991).

The transverse potential or field obtained by averaging in the longitudinal direction can be obtained from different approximations, e.g., the Lindhard "standard" potential (Lindhard, 1965), the Molière (Molière, 1947), or the Doyle-Turner potential (Doyle and Turner, 1968). An example based on the Doyle-Turner approximation is shown in Fig. 6. The Doyle-Turner potential has been found to be the most precise in predictions of MeV channeling radiation which is very sensitive to the shape of the potential (Andersen *et al.*, 1982). However, Doyle and Turner did not give data for heavy atoms—data of this type have become available only recently (Waasmaier and Kirfel, 1995). The potentials are valid for a static lattice, but thermal effects can be introduced by a Gaussian distribution of the atoms on the lattice. The finite value of the transverse potential shown in Fig. 6 at the location of the atomic strings is due to the inclusion of thermal vibrations.

In the continuum model the transverse motion is given by

$$\frac{d}{dt}\gamma m\dot{r}_\perp = -\frac{d}{dr_\perp}U(r_\perp(t)), \tag{14}$$

where the dot denotes differentiation with respect to time t, and $r_\perp$ is the transverse coordinate; see Fig. 4.

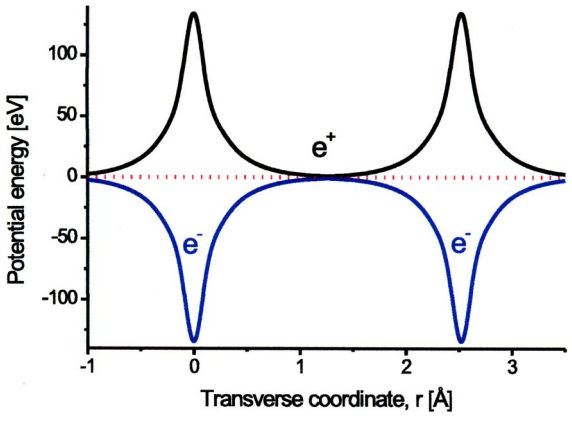

FIG. 6. (Color online) An example of a transverse potential in the continuum approximation for diamond along the ⟨110⟩ axis at room temperature. The main regions for channeled e^- and e^+ are indicated. The Doyle-Turner approximation for the atomic potential has been used.

Neglecting terms of order $1/\gamma^2$, we get for the transverse energy

$$E_\perp = \frac{1}{2}pv\psi^2 + U(r_\perp), \tag{15}$$

where ψ is the particle angle to the axis (Andersen *et al.*, 1983; Bak *et al.*, 1985).

A. Critical angles

Strictly speaking, critical angles are only theoretically well defined for positively charged particles. However, negatively charged particles display similar behavior as a function of angle to crystallographic directions with characteristic angles equal to those for positively charged particles within a factor $\simeq 1-3$.

When the particle approaches the center of the continuum string it has a fair chance—partly due to thermal vibrations—of acquiring a transverse energy exceeding the height of the transverse potential. So for an incident angle ψ_c to the axis where

$$E_\perp = \frac{1}{2}pv\psi_c^2 \simeq U(\rho_t), \tag{16}$$

where ρ_t is a thermal vibration amplitude, the particle may escape the well, i.e., be dechanneled. Using the Lindhard standard potential (Lindhard, 1965), this gives for the axial effect a critical angle for channeling

$$\psi_1 = \sqrt{\frac{4Z_1Z_2e^2}{pvd}}. \tag{17}$$

For the planar motion the critical angle is

$$\psi_p = \sqrt{\frac{4Z_1Z_2e^2nd_pC_La_s}{pv}} \tag{18}$$

and generally $\psi_1 \simeq 3\psi_p$ since the transverse axial and planar potentials differ by about a factor of 10. Here, d_p denotes the planar distance, d is the spacing of atoms along the axial direction, Z_1e is the charge of the penetrating particle, $C_L \simeq \sqrt{3}$ is Lindhard's constant, and a_s is the (Thomas-Fermi) screening distance. The continuum picture does not become invalid beyond the critical angle but may persist out to angles as large as $50\psi_1$. Rigorous mathematical proofs of Lindhard's continuum picture and channeling angles have only recently been published for positively charged particles (Dumas *et al.*, 2000).

B. Positively and negatively charged particles

The interaction potential for negatively charged particles is equal in shape but has the opposite sign as that for positively charged particles; see Fig. 6. So in general channeled negatively charged particles are focused around the nuclei whereas positively charged particles are pushed away. For positive particles the planar potential is nearly harmonic whereas the potential for negative particles is strongly anharmonic. Another difference

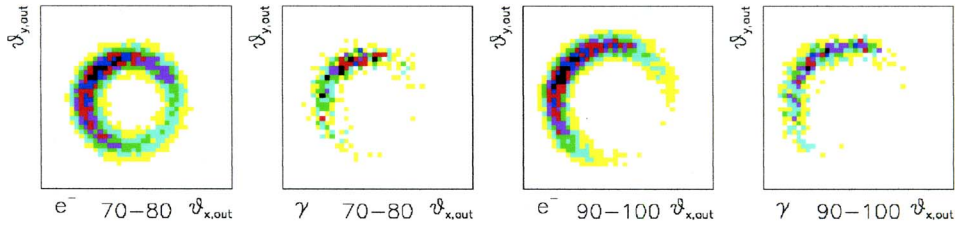

FIG. 7. (Color online) Doughnut formation for 150-GeV electrons after (e^-) and during (γ) their photon emission. The selected incident-polar-angle range is given below each plot of vertical vs horizontal exit angle, $\theta_{x,out} \times \theta_{y,out} \in [-150,\ 150\ \mu\text{rad}] \times [-150,\ 150\ \mu\text{rad}]$. The radiated energy is restricted to the interval 10–70 GeV. Adapted from Kirsebom *et al.*, 2001b.

is that positively charged particles typically move freely from channel to channel while negatively charged particles mostly are bound to one single string.

1. Number of bound states

According to Bohr's correspondence principle, the higher the number of available quantum states, the better a classical description becomes of the phenomenon. For planar-channeled positrons and electrons the approximate numbers of bound states are given as (Andersen *et al.*, 1977)

$$\nu_p^+ \simeq \sqrt{\gamma} Z_2^{1/3} \sqrt{n d_p^3} \tag{19}$$

and

$$\nu_p^- \simeq \sqrt{\gamma} \frac{4a_0}{d_p} \sqrt{n d_p^3}, \tag{20}$$

while for axially channeled positrons and electrons the numbers are

$$\nu_s^+ \simeq \gamma \frac{1}{\pi} \frac{d}{a_0} Z_2 \frac{1}{n d^3} \tag{21}$$

and

$$\nu_s^- \simeq \gamma \frac{4a_0}{d_p} Z_2^{1/3}, \tag{22}$$

where the number for positrons is the number of states per unit cell for below-barrier particles. As an example, for silicon the numbers are $\nu_p^+ \simeq 2.5$, $\nu_p^- \simeq 1.1$, $\nu_s^+ \simeq 34$, and $\nu_s^- \simeq 4$, for 1 MeV in the (110) plane and ⟨110⟩ axis, respectively (Andersen *et al.*, 1977). As the number of states are proportional to $\sqrt{\gamma}$ and γ for planar and axial channeling, it is seen that the *motion* of GeV channeled particles is well described by classical theory.

2. Reversibility and blocking

The focusing of negatively charged particles around atomic strings or planes leads to an increase in the yield of close-encounter processes. As a consequence of the "rule of reversibility" (Lindhard, 1965), the time-reversed process of directing a beam into the crystal to observe, for example, Rutherford backscattering, corresponds to the emission of particles from the string or plane and observation at the location of the external beam source. Therefore if the close-encounter processes are suppressed as for positively charged particles, the emission of positively charged particles in that crystallographic direction must be suppressed as well. This is referred to as "blocking."

3. Doughnut scattering

In the continuum model the angular momentum L_ϕ with respect to the axis is conserved—giving an effective potential U_{eff} equal to

$$U_{\text{eff}} = U(r_\perp) + \frac{L_\phi^2}{2mr_\perp^2} \tag{23}$$

for interaction with a *single* string.

For incidence along an axial direction with large angles $\psi_1 < \psi \lesssim 50\psi$, but still in the continuum approximation, the penetrating particle scatters off *many* strings of atoms, preserving the polar angle in each collision (due to conservation of $E_\perp$) while changing the azimuthal angle in a stochastic fashion (Akhiezer *et al.*, 1991). This leads to the so-called doughnut scattering: The beam will reach an equilibrium state in azimuthal angles giving a uniform doughnut in angle space; see Fig. 7. This happens once the ensemble of particles has traversed a length given for $\psi \leqslant \psi_1$ by (Linhard, 1965)

$$\lambda_\perp^< \simeq \frac{4\psi}{\pi^2 n d a_s \psi_1^2} \tag{24}$$

and for $\psi \geqslant \psi_1$ roughly as (Andersen *et al.*, 1980)

$$\lambda_\perp^> \approx 4\lambda_\perp^< \frac{\psi^2 u_1}{\psi_1^2 a_s}, \tag{25}$$

where u_1 is the one-dimensional thermal vibration amplitude of the lattice atoms.

C. High-energy channeling radiation

By channeling radiation we mean the coherent emission of photons due to the lattice structure of the crystal structure, subject to the condition that the particle is channeled. Traditionally, channeling radiation is separated into three groups depending on the energy of the penetrating particle: At low energies, $\simeq$10–100 MeV, the transverse potential contains a limited number of states when quantized such that a classical description is insufficient; see Eqs. (19)–(22). At intermediate energies,

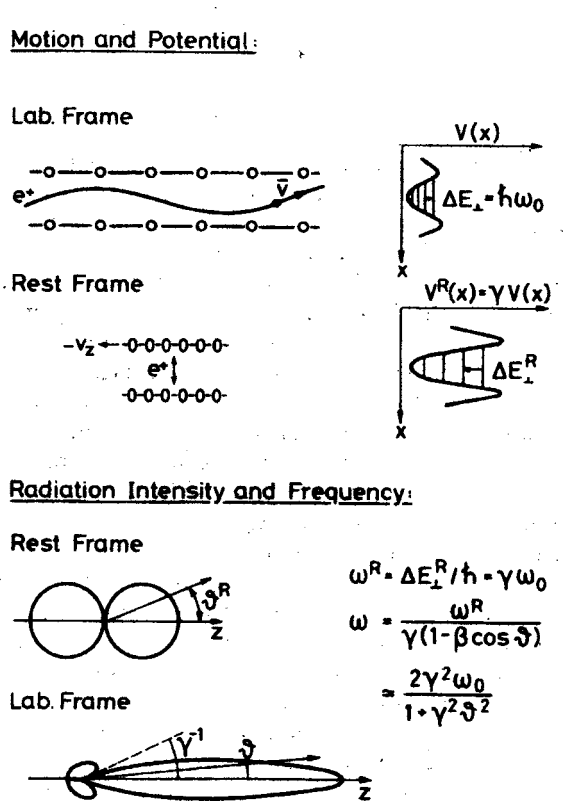

FIG. 8. Illustration of Lorentz transformations between the laboratory and the rest frame for a radiating planar-channeled positron with $\gamma=3$. From Andersen *et al.*, 1983.

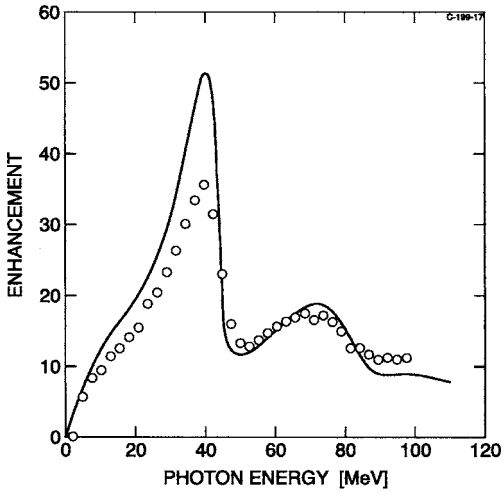

FIG. 9. High-energy channeling radiation for 6.7 GeV/c positrons incident parallel to the (110) plane in a silicon crystal. The experimental result shown by open dots is compared to a calculated spectrum shown by a solid line. The calculation is on an absolute scale and enabled an identification of the erroneous assignment of the beam energy of 7 GeV such that the points are slightly modified compared to the original data (Bak *et al.* 1985). From Sørensen and Uggerhøj, 1989.

$\simeq$100 MeV–1 GeV, the number of states is so high that, according to the correspondence principle, a classical calculation of the motion is a good approximation. At high energies, above about 1 GeV, the dipole approximation is no longer justified because the longitudinal velocity varies as a result of a relativistic transverse momentum. This means that as the energy is increased, the appropriate description varies from a quantized transverse potential, through the dipole approximation in classical electrodynamics, to a stage where transverse relativistic effects must be taken into account. It is one aim of the following to show that yet another stage is achieved when the multi-GeV region is considered. Figure 8 shows an example of a $\gamma=3$ planar-channeled positron. In the particle rest frame, the transverse potential in the frame of the laboratory is boosted by the Lorentz factor. Transforming back to the frame of the laboratory, the emission angles become peaked in the forward direction with a characteristic angle $1/\gamma$ and the emission frequency is boosted by another factor of 2γ in the forward direction.

The time dependence of γ initially neglected in Eq. (14) makes the longitudinal motion differ from a uniform translation. In the few-GeV region this deviation is significant—here photon emission can change γ drastically. Moreover, when the transverse momentum $p_\perp$ becomes relativistic the longitudinal velocity $\beta_z c$ is affected since (neglecting terms of order $p_\perp/p_\parallel$)

$$\beta_z^2 = \beta^2 - \beta_x^2 \simeq 1 - \frac{1}{\gamma^2}\left[1 + \left(\frac{p_\perp}{mc}\right)^2\right] \tag{26}$$

such that the longitudinal motion becomes nonconstant, even in the absence of direct forces in this direction. An explanation for this can be found in the interaction of the particle possessing a relativistic transverse velocity with the magnetic field in the average rest frame of the longitudinal motion. This field imposes a force in the longitudinal direction which depends on the transverse velocity, i.e., the transverse position and direction in the channel, such that a "figure-eight" motion results (Baier *et al.*, 1981; Bak *et al.*, 1985).

Figure 9 shows an example of channeling radiation obtained at an energy of 6.7 GeV. The sharp peak observed at $\hbar\omega\simeq 40$ MeV is due to below-barrier transitions. The upper $\hbar\omega\simeq 80$ MeV peak originates from above-barrier particles that interact with the crystalline planes with an oscillation period that is approximately twice as large (Akhiezer and Shul'ga, 1982) as well as emission of higher harmonics (Bak *et al.*, 1985).

III. BREMSSTRAHLUNG

Another way to approach the channeling radiation is from theory of bremsstrahlung, which only needs to be generalized to coherent sources. This is described below, starting from the theory for incoherent sources, progressing through coherent bremsstrahlung, and ending up with the connection to channeling radiation.

A. Incoherent bremsstrahlung

The cross section for radiation emission in an amorphous foil—incoherent bremsstrahlung—can be found from the Bethe-Heitler formula (Bethe and Heitler, 1934; Heitler, 1954), which is given to good accuracy by

$$\frac{d\sigma}{d\hbar\omega} = \frac{16}{3} Z_2^2 \alpha r_e^2 \frac{1}{\hbar\omega}\left[1 - \frac{\hbar\omega}{E} + \frac{3}{4}\left(\frac{\hbar\omega}{E}\right)^2\right] \ln(183 Z_2^{-1/3}), \tag{27}$$

where $r_e = e^2/mc^2 = \alpha \lambda\!\!\!^{-}_c = \alpha^2 a_0$ is the classical electron radius and the logarithmic factor indicates complete screening, $\gamma \gg 1$. From this, the radiation length can be found,

$$\frac{1}{X_0} = \frac{n}{E}\int_0^E \hbar\omega \frac{d\sigma}{d\hbar\omega} d\hbar\omega = 4 Z_2^2 \alpha n r_e^2 \ln(183 Z_2^{-1/3}). \tag{28}$$

An incident particle statistically loses all but $1/e$ of its energy by emission of bremsstrahlung in passing a foil of thickness X_0. Equations (27) and (28) include only the scattering off the nucleus. The contribution from the target electrons can be taken approximately into account by the replacement $Z_2^2 \to Z_2(Z_2+1)$, which brings Eq. (28) into good agreement with tabulated values for the radiation length (Tsai, 1974).

B. Coherent bremsstrahlung

The Bethe-Heitler cross-section differential in angles and photon energy can be represented in terms of momenta $\hbar q_\parallel$, $\hbar q_\perp$ transferred longitudinally and perpendicularly to the direction of motion (Ter-Mikaelian, 1972; Sørensen, 1983). The allowed values of $q_\parallel$ and $q_\perp$ are given by [Timm, 1969; see also Eq. (8)]

$$0 \leqslant q_\perp \lesssim 1/\lambda\!\!\!^{-}_c, \tag{29}$$

$$\delta \leqslant \tilde{q}_\parallel \lesssim 2\delta \tag{30}$$

since collimation to angles less than the radiation cone $1/\gamma$ is usually beyond experimental capability at sufficiently high energy. In $\tilde{q}_\parallel = q_\parallel - \lambda\!\!\!^{-}_c q_\perp^2/2\gamma$ the subtracted term gives a curvature to the "Überall pancake," i.e., to the three-dimensional formation zone which has the shape of a pancake in the reciprocal lattice; see Fig. 10.

To first order in $(\lambda\!\!\!^{-}_c q_\perp)^2$ the Bethe-Heitler cross section, Eq. (27), then becomes (Ter-Mikaelian, 1972)

$$\frac{d\sigma}{d\omega} = \frac{2 Z_2^2 r_e^2 \alpha}{\pi \gamma^2 c}\int d^3q \frac{q_\perp^2 [1 - F(q)]^2}{q^4 \tilde{q}_\parallel^2} \times \left(1 + \frac{\lambda\!\!\!^{-2}_c \omega \delta}{c} - \frac{2\delta}{\tilde{q}_\parallel} + \frac{2\delta^2}{\tilde{q}_\parallel^2}\right). \tag{31}$$

Here δ denotes the inverse of the formation length, Eq. (10), and $F(q) = Z_2^{-1}\int \exp(i\vec{q}\cdot\vec{r})\rho(\vec{r}) d^3\vec{r}$ is the atomic form factor which takes the screening into account through the term $[1 - F(q)]^2$.

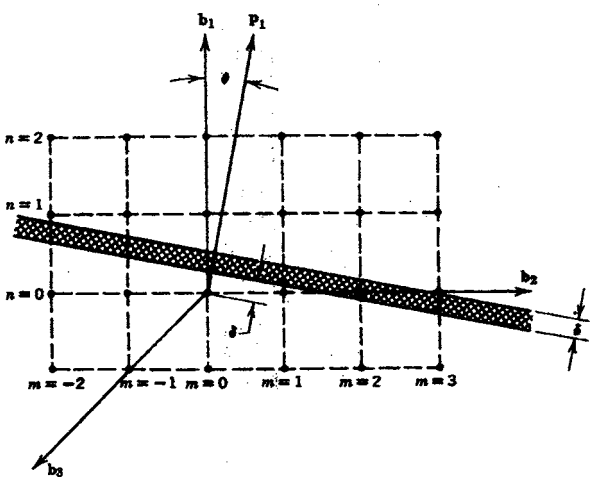

FIG. 10. An illustration of a section of the "Überall pancake" (hatched area, curvature neglected). The main part of the emitted radiation comes from reciprocal-lattice points for which the projection on the momentum vector $\vec{p}_1$ lie in the range given by Eq. (30). The reciprocal lattice is spanned by the primitive reciprocal-lattice vectors $\vec{b}_i$. From Ter-Mikaelian, 1972.

For N atoms, the single interaction potential V must be replaced by a sum over all interactions $\Sigma_{n_i} V(\vec{r} - \vec{r}_{n_i})$, where $\vec{r}_{n_i}$ denotes the position of atom n_i. Thus the differential cross section for N atoms becomes (Sørensen and Uggerhøj, 1989)

$$\left.\frac{d\sigma}{d\hbar\omega d^3q}\right|_N = \left.\frac{d\sigma}{d\hbar\omega d^3q}\right|_s \left|\sum_{n_i} e^{-i\vec{q}\cdot\vec{r}}\right|^2, \tag{32}$$

where the subscript s denotes the single-atom cross section. The last term yields N in the case of an amorphous substance since the mixed terms are of random phases and sum to zero. Therefore the incoherent cross section, Eq. (27), becomes proportional to the number of atoms within the formation length, which explains the $\propto 1/\hbar\omega$ behavior that is also found in Eq. (10).

For a static single crystal in the limit $N \to \infty$ we get (Sørensen, 1983; Sørensen and Uggerhøj, 1989)

$$\left|\sum_{n_i} e^{-i\vec{q}\cdot\vec{r}}\right|^2 = \frac{N(2\pi)^3}{N_0 \Delta}|S(\vec{g})|^2 \sum_{\vec{g}} \delta(\vec{q} - \vec{g}) \tag{33}$$

similar to diffraction from a grating; see also Palazzi (1968). Here N_0 is the number of atoms in the unit cell of volume Δ, $\delta(\vec{q} - \vec{g})$ is the Dirac delta function, and $S(\vec{g})$ is the structure factor for the lattice in question (Ashcroft and Mermin, 1976).

Again to first order in $(\lambda\!\!\!^{-}_c q_\perp)^2$ the expression then becomes

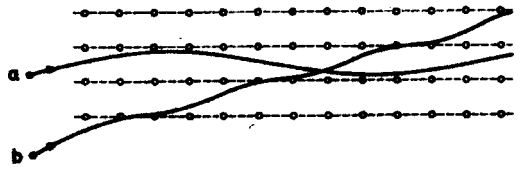

FIG. 11. Two particle trajectories in a crystal lattice. Track (a) gives rise to the emission of channeling radiation while (b) leads to coherent bremsstrahlung. From Andersen *et al.*, 1980.

$$\frac{d\sigma}{d\omega}=\frac{N(2\pi)^3}{N_0\Delta}\frac{2Z_2^2r_e^2\alpha}{\pi\gamma^2c}\sum_{\vec{g}}|S(\vec{g})|^2\frac{g_\perp^2[1-F(g)]^2}{g^4\tilde{g}_\parallel^2}\times\left(1+\frac{\lambda\!\!\!^{-2}_c\omega\delta}{c}-\frac{2\delta}{\tilde{g}_\parallel}+\frac{2\delta^2}{\tilde{g}_\parallel^2}\right),\tag{34}$$

where $\tilde{g}_\parallel=g_\parallel-\lambda\!\!\!^{-}_c g_\perp^2/2\gamma$. We note the similarity between Eqs. (31) and (34).

The interpretation of Eq. (34) is that the coherent cross section only becomes appreciable when the recoil momentum is equal to a vector of the reciprocal lattice [perhaps even clearer from the delta function in Eq. (33)], i.e., when the wavelength of emitted radiation is an integer times the direct lattice spacing of atoms in the chosen direction. This gives rise to "coherent peaks," i.e., enhancements that can be highly polarized; see, e.g., Palazzi (1968), Timm (1969), and Ter-Mikaelian (2001).

At this point it is worthwhile to comment on the use of formation lengths. A collimation of the photon emission angles will result in less radiation (a "sharpening" of the leading edge of the coherent peak) even though the formation length according to Eq. (9) gets longer. This is due to the corresponding shortening of the relevant zone in the reciprocal lattice, i.e., fewer reciprocal-lattice points contribute to the radiation. There is thus not a one-to-one correspondence between the number of atoms within the formation length and the radiation yield.

In the transverse-potential picture, coherent bremsstrahlung can be regarded as free-free transitions, i.e., transitions among states above the potential barrier, while channeling radiation originates from bound-bound transitions within the potential well (Andersen *et al.*, 1980, 1981); see Fig. 11.

A relatively recent example of coherent bremsstrahlung spectra at high energy is shown in Fig. 12. As the angle to the plane increases the theoretical values based on the first Born approximation, shown by solid lines, become a better approximation to the data, shown by crosses. Applying the second Born approximation (Shul'ga and Syshchenko, 2002) could possibly improve the agreement between theory and experiment shown in Fig. 12.

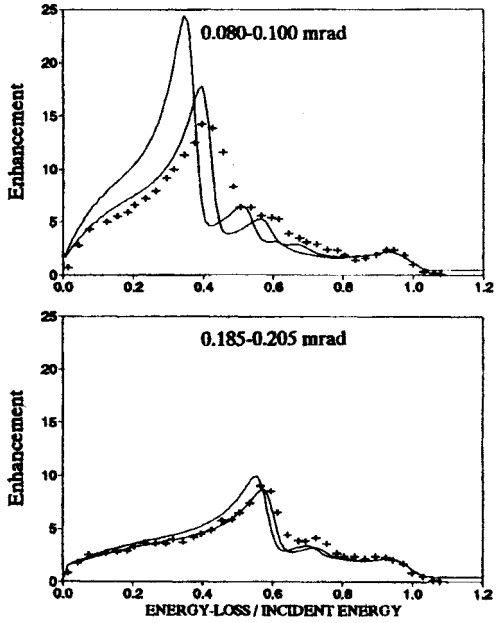

FIG. 12. Radiation from 150-GeV electrons incident on 0.6-mm Si with different angular intervals to the (110) plane as indicated. The enhacement is with respect to an amorphous target of the same material and thickness. The polar angle to the ⟨110⟩ axis is 8.2 mrad. From Medenwaldt *et al.*, 1991.

IV. QUANTUM OR CLASSICAL DESCRIPTION?

At sufficiently high energies, the motion of particles in a crystal—even when channeled—becomes quasiclassical. On the other hand, as the radiation may carry away a substantial fraction of the energy and momentum of the emitting particle, the radiation emission itself must be described as a quantum process.

A. Particle motion

In considering the quantization of the electron motion in a crystal, one may estimate the number of levels in a harmonic oscillator [as for a planar-channeled positron; see also Eq. (19)] of potential height U_0 from $\nu\hbar\omega=U_0=\gamma m\omega^2(d_p/2)^2/2$ to be

$$\nu=\frac{1}{\hbar}\sqrt{\frac{\gamma mU_0}{2}}\frac{d_p}{2}\propto\sqrt{\gamma},\tag{35}$$

which is of the order of a thousand at 100 GeV. In the case of an electron in a magnetic field, one may evaluate the level distance with respect to the energy $\hbar\omega/E$ by use of $L=\nu\hbar$ and the Lorentz force which leads to

$$\frac{1}{\nu}=\frac{\hbar\omega}{E}=\frac{B}{B_0}\frac{m^2c^2}{p^2}=\kappa_f\frac{m^2c^2}{p^2},\tag{36}$$

where κ_f is the actual field in units of the critical field. Clearly, even for channeled particles and for large κ_f the motion is quasiclassical according to the correspondence principle as long as the electron fulfills the weak criterion $\gamma\gg\sqrt{\kappa_f}$.

B. Emission of radiation

With respect to the recoil in the emission process, we utilize a classical calculation of the synchrotron-

radiation emission in a magnetic field which leads to a spectrum that extends to $\omega_c \simeq 3\gamma^3 eB/2p = 3\gamma^3\omega_0/2$ (Jackson, 1975), i.e.,

$$\frac{\hbar\omega_c}{E} \simeq \frac{3\gamma B}{2B_0} = \frac{3\gamma\kappa_f}{2} = \frac{3\chi}{2}, \tag{37}$$

which for sufficiently large γ exceeds 1. Here ω_0 is the Larmor angular frequency and χ is the strong-field parameter to be defined shortly. Thus for γ values beyond a certain point, the classically calculated radiation spectrum extends beyond the available energy (Schwinger, 1954; Tsai, 1973; Tsai and Yildiz, 1973; Sørensen, 1991). In this case a quantum treatment is obviously necessary: "… the condition for quantum effects to be unimportant is that the momenta of the radiated quanta be small compared with the electron momentum" (Schwinger, 1954).

Following Nikishov and Ritus (1964) and Berestetskii *et al.* (1971), we can construct three dimensionless invariants from the electromagnetic field strength tensor $F_{\mu\nu}$ and the momentum four-vector p^ν (or, in the case of a photon, $\hbar k^\nu$):

$$\chi^2 = \frac{(F_{\mu\nu}p^\nu)^2}{m^2c^2\mathcal{E}_0^2}, \tag{38}$$

$$\Xi = \frac{F_{\mu\nu}^2}{\mathcal{E}_0^2} = \frac{2(\vec{B}^2 - \vec{\mathcal{E}}^2)}{\mathcal{E}_0^2}, \tag{39}$$

$$\Gamma = \frac{e_{\lambda\mu\nu\rho}F^{\lambda\mu}F^{\nu\rho}}{\mathcal{E}_0^2} = \frac{8\vec{\mathcal{E}}\cdot\vec{B}}{\mathcal{E}_0^2}, \tag{40}$$

where $e_{\lambda\mu\nu\rho}$ is the antisymmetric unit tensor and contraction is indicated by repeated indices. For an ultrarelativistic particle moving across fields $\mathcal{E} \ll \mathcal{E}_0$, $B \ll B_0$ with an angle $\theta \gg 1/\gamma$, the invariants fulfill $\chi \gg \Xi, \Gamma$ and $\Xi, \Gamma \ll 1$. The relation of χ to the fields $\vec{\mathcal{E}}$ and $\vec{B}$ is given by (Berestetskii *et al.*, 1971)

$$\chi^2 = \frac{1}{\mathcal{E}_0^2 m^2 c^4}[(\vec{p}c \times \vec{B} + E\cdot\vec{\mathcal{E}})^2 - (\vec{p}c\cdot\vec{\mathcal{E}})^2]. \tag{41}$$

For an ultrarelativistic particle moving perpendicularly to a pure electric or pure magnetic field this reduces to

$$\chi = \frac{\gamma\mathcal{E}}{\mathcal{E}_0} \quad \text{or } \chi = \frac{\gamma B}{B_0}, \tag{42}$$

which is implicit in Eq. (37). Due to $\mathcal{E}_0$ and γ being proportional to m^2 and $1/m$, respectively, we note that χ scales with $1/m^3$ such that, for example, the coherent production of muon pairs becomes appreciable only at energies $207^3 \approx 10^7$ times larger than electron-positron pairs.

As discussed in the Introduction, for the emission of radiation it is the trajectory that is decisive. Therefore it is insignificant if the field responsible for the path is electric or magnetic and they may be used indiscriminately. Since χ is invariant, γB (or $\gamma\mathcal{E}$) is the same in any reference system and thus it is reasonable to transform to the electron frame. In this reference system, by definition the Lorentz factor of the electron is 1 and the field present in the frame of the laboratory is boosted by $\gamma = E/mc^2$, where E is the energy of the electron in the laboratory. This means that the field in the rest frame of the electron can become critical for achievable γ values.

C. Classical recoil

What happens to Eq. (37) if the recoil imposed on the electron by the photon emission is taken into account? In this section let the barred values denote the values where recoil (momentum $\hbar\omega/c$ lost to the photon) is taken into account and unbarred values denote variables in which this is not the case. The discussion follows Jackson's (1975, Sec. 14.4) closely. The time interval in which a finite pulse is detected by an observer is related through a Fourier decomposition to its frequency components. A comparison between the time duration of the pulse with and without account of energy loss of the particle in the emission process therefore gives an estimate of the effect of recoil. After emission of the photon, the particle Lorentz factor becomes

$$\bar{\gamma} = \gamma\left(1 - \frac{\hbar\omega}{E}\right) \tag{43}$$

since $E = \bar{E} = \gamma mc^2$ is the initial energy of the projectile and $\bar{\gamma}mc^2 = E - \hbar\omega$. The emission frequency will not diminish

$$\bar{\omega} = \omega. \tag{44}$$

Thus the critical frequency will be

$$\bar{\omega}_c \simeq 3\bar{\gamma}\gamma^2\bar{\omega}/2 = \omega_c\left(1 - \frac{\hbar\omega}{E}\right) \tag{45}$$

since the radiation cone is limited by γ, whereas the particle moves with velocity $\bar{\beta}c = c\sqrt{1 - 1/\bar{\gamma}^2}$ after the emission (i.e., on the average $\sqrt{\bar{\beta}\beta}$). In combination, the radiation cone and the velocity determine the duration of the pulse in a manner similar to that in the discussion connected to Fig. 2. Suppose now the radiation emitted has the critical frequency $\hbar\omega = \hbar\bar{\omega}_c$, then

$$\frac{\hbar\bar{\omega}_c}{\bar{E}} = \frac{\hbar\omega_c}{E}\left(1 - \frac{\hbar\omega_c}{E}\right), \tag{46}$$

which is the modification of photon frequencies sought. In the limit $\hbar\omega_c/E \ll 1$ the usual behavior is obtained, $\hbar\omega_c/E \simeq \hbar\bar{\omega}_c/\bar{E}$.

Thus the modifications of photon frequencies ω^* and $\bar{\omega}$ in Eqs. (10) and (44) take into account the recoil, i.e., it "represents a QED correction to classical electrodynamics" (Kimball *et al.*, 1986), but the corrections can in a qualitative manner be found from classical electrodynamics.

V. RADIATION EMISSION IN STRONG FIELDS

Equations (10) and (12) show the formation length in the laboratory frame. What is the formation length in the particle rest frame?

Let us consider pair production first. In the frame with a Lorentz factor of $\gamma_p \equiv \hbar\omega/mc^2$, the formation length would become Lorentz contracted by γ_p: $l_f^{\text{pair}}/\gamma_p = 2\gamma' \lambda\!\!\!^{-}_c/\gamma_p \simeq \lambda\!\!\!^{-}_c/2$, where $\gamma' \equiv \hbar\omega\eta_+\eta_-/mc^2$. This is roughly what one would expect for pair production in a strong field[2] since for $\chi=1$ a pair can be created over $2\lambda\!\!\!^{-}_c$.

Turning to radiation emission, the formation length in the rest frame of the radiating electron with the emission of $\xi=\hbar\omega/E$ leads to

$$\frac{l_f^{\text{rad}}}{\gamma} = \frac{2\gamma^* \lambda\!\!\!^{-}_c}{\gamma} = \frac{2\lambda\!\!\!^{-}_c(1-\xi)}{\xi}, \tag{47}$$

which is $2\lambda\!\!\!^{-}_c$ for $\xi=\frac{1}{2}$ and decreases with increasing ξ. Here, $\gamma^* = \gamma(1-\xi)/\xi$. Bearing in mind the definition of the critical field where mc^2 is produced over $\lambda\!\!\!^{-}_c$, it is natural to expect that the formation length is given by the so-called field deflection length $\lambda\!\!\!^{-}_\gamma$, i.e., the length over which the particle is deflected by an angle $1/\gamma$ by the transverse force $F_\perp$:

$$\lambda\!\!\!^{-}_\gamma = \frac{\mathcal{E}_0}{\mathcal{E}}\lambda\!\!\!^{-}_c = \frac{\lambda\!\!\!^{-}_c}{\kappa_f} = \frac{mc^2}{F_\perp} \tag{48}$$

leading to $\lambda\!\!\!^{-}_\gamma/\gamma = \lambda\!\!\!^{-}_c/\chi$ such that the effective length for radiation decreases with increasing χ. Thus by setting $\lambda\!\!\!^{-}_\gamma = l_f^{\text{rad}}$, according to Eq. (47) the diminishing field deflection length leads to a "preference" for radiation closer to the edge of the spectrum:

$$\xi = \frac{2\chi}{2\chi+1} \tag{49}$$

as is indicated in the discussion of critical frequencies, Eq. (37). The basis of this is the inverse dependence of the formation length on the photon energy. This behavior, with a minor modification, is also obtained in the more accurate constant field approximation (CFA) to be discussed below.

In amorphous materials the length over which a particle statistically scatters a rms angle $1/\gamma$ due to multiple Coulomb scattering is given approximately by

$$l_\gamma = \frac{\alpha}{2\pi} X_0, \tag{50}$$

where α is the fine-structure constant and X_0 the radiation length. This is one possible starting point to describe the shortening of the formation zone in the LPM effect (Hansen *et al.*, 2004; Uggerhøj, 2004a). It leads—as for the case of λ_γ—to a higher radiation yield at high energies compared to lower energies and an increase of the effective radiation length at sufficiently high energies (Hansen *et al.*, 2003).

[2]Alternatively, the length it takes to deflect a created positron of $p=\frac{1}{2}\gamma mc$ by an angle $\theta=1/\gamma$ with respect to the photon direction in a critical ($\chi=1$) B field is $2\lambda\!\!\!^{-}_c/2$.

TABLE I. Comparison of threshold values for the strong-field effect from Eq. (51) and Baier *et al.* (1998).

	Estimate, Eq. (51)	Baier *et al.* (1998)
Si ⟨110⟩, 293 K	102 GeV	120 GeV
Ge ⟨110⟩, 280 K	74 GeV	70 GeV
Ge ⟨110⟩, 100 K	45 GeV	50 GeV
W ⟨110⟩, 293 K	14 GeV	22 GeV
W ⟨110⟩, 77 K	8 GeV	13 GeV

A. Threshold for strong-field effects

As an estimate of the peak electric field originating from an axis in a crystal, one may set $\mathcal{E} \simeq U_0/\sqrt{2}eu_1$, where U_0 is the transverse-potential height. This can, for instance, be seen in Fig. 6 where $u_1 \simeq 0.1$ Å and $U_0 \simeq 140$ eV leads to $\mathcal{E} \simeq 1$ kV/Å, i.e., a field of the order 10^{11} V/cm. For a good summary of relevant crystal parameters, see, e.g., Gemmell (1974). From the definition of the critical field and χ in Eq. (37) it follows that the "threshold," $\chi=1$, for the quantum effects is obtained for

$$\hbar\omega_t = \gamma_t mc^2 = mc^2 \frac{\sqrt{2}u_1 mc^2}{U_0 \lambda\!\!\!^{-}_c}, \tag{51}$$

where the field becomes critical in the Lorentz frame boosted with γ_t or $\hbar\omega_t/mc^2$. Table I compares the values obtained from Eq. (51) with the more accurate ones obtained in the constant field approximation (Baier *et al.*, 1998), where $\hbar\omega_t$ is defined as the energy at which the probability for the coherent strong-field mechanism equals the Bethe-Heitler value.

As Eq. (51) is a rather crude estimate, it is not surprising that there is some disagreement. Nevertheless, Eq. (51) is a good estimate of the energy of onset of strong-field effects. Furthermore, it directly explains the origin—namely, that the field in the rest frame becomes critical.

B. The classical limit of synchrotron radiation

Since it is the trajectory that is decisive for the emission of radiation and the interaction with the continuous electric field imposes a curved trajectory, see Fig. 4, it can be expected that the radiation emission is synchrotronlike. Therefore classical synchrotron-radiation emission is described in short below, followed by the important phenomenon of synchrotron-radiation emission under recoil of the emitting particle. The latter takes place when χ gets sufficiently large.

According to classical electrodynamics, the intensity per unit frequency and unit solid angle emitted by a charged particle in synchrotronic motion can be expressed as (Jackson, 1975)

$$\frac{d^2I}{d\omega d\Omega} = \frac{e^2}{4\pi^2 c}\left| \int_{-\infty}^{\infty} \frac{\vec{n}\times[(\vec{n}-\vec{\beta})\times\dot{\vec{\beta}}]}{(1-\vec{\beta}\cdot\vec{n})^2} \times \exp\{i\omega[t-\vec{n}\cdot\vec{r}(t)/c]\}dt \right|^2, \tag{52}$$

where $\vec{\beta}(t)=\vec{v}(t)/c$ and $\vec{n}$ denotes the direction of photon propagation. Equation (52) leads to a counting spectrum (Sørensen, 1991) by use of $dN_\gamma/d\xi=(1/E)\hbar\omega\cdot dP/d\hbar\omega$, where the emitted power is $P=\omega_0 I/2\pi$, $\omega_0=eB/p$:

$$\frac{dN_\gamma}{d\xi} = \frac{\alpha c}{\sqrt{3}\pi\lambda\!\!\!^{-}_c}\frac{1}{\gamma}\left(2K_{2/3}(\delta_c) - \int_{\delta_c}^{\infty} K_{1/3}(t)dt\right), \tag{53}$$

where $\delta_c=2\xi/3\chi$, $\xi=\hbar\omega/E$, K_ν is the modified Bessel function of order ν, and χ is the invariant strong-field parameter defined in Eq. (42), $\chi=\gamma Be\lambda\!\!\!^{-}_c/mc^2$.

C. The constant field approximation (CFA)

1. Radiation emission

The classical spectrum of synchrotron radiation becomes modified when quantum corrections are taken into account, as for emission in a sufficiently strong field. According to Schwinger (1954), Schwinger and Tsai (1978), and Lindhard (1991) following the correspondence principle, the approximate quantum spectrum can be found by a replacement of variable in Eq. (53). The substitution $\omega\to\omega^*=E\omega/(E-\hbar\omega)$ in the right-hand side of Eq. (53) will take into account the quantum (recoil) effects [see also Berestetskii *et al.* (1971), Eqs. (59.9) and (59.20), where the same result is derived from the semiclassical approach]:

$$\xi^* \equiv \frac{\hbar\omega^*}{E} = \frac{\hbar\omega}{E-\hbar\omega} = \frac{\xi}{1-\xi}, \tag{54}$$

where, as above, $\xi=\hbar\omega/E$. This substitution reappears in the definition of the formation length, Eq. (10), in going from the classical limit to the accurate expression. The result is a modification of Eq. (53) where $\delta_c=2\xi/3\chi \to \delta_q=2\xi/3(1-\xi)\chi$ leading to

$$\frac{dN_\gamma}{d\xi} = \frac{\alpha c}{\sqrt{3}\pi\lambda\!\!\!^{-}_c}\frac{1}{\gamma}\left(2K_{2/3}(\delta_q) - \int_{\delta_q}^{\infty} K_{1/3}(t)dt\right). \tag{55}$$

In the constant field approximation [Baier *et al.* (1983) and Kimball *et al.* (1983); reviewed in Kimball and Cue (1985) and Baier *et al.* (1989a)] the corresponding result for emission of radiation is

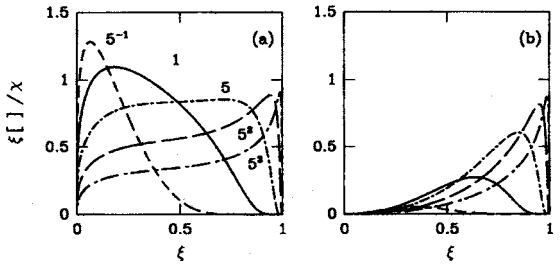

FIG. 13. Synchrotron radiation in a strong field, where (a) the power spectrum is rescaled by χ according to Eq. (56) and (b) the contribution from the spin; see text for details. The labels on the curves denote the value of χ which are in both cases $\chi=5^{-1}$ (dashed), $\chi=1$ (solid), $\chi=5$ (dash-dotted), $\chi=5^2$ (long-dashed), and $\chi=5^3$ (long-dash-dotted). Adapted from Sørensen, 1991.

$$\frac{dN_\gamma}{d\xi} = \frac{\alpha c}{\sqrt{3}\pi\lambda\!\!\!^{-}_c}\frac{1}{\gamma}\left[\left(1-\xi+\frac{1}{1-\xi}\right)K_{2/3}(\delta_q) - \int_{\delta_q}^{\infty} K_{1/3}(t)dt\right], \tag{56}$$

where as found above $\delta_q=2\xi/3(1-\xi)\chi$. Figure 13(a) shows the term in square brackets from Eq. (56) multiplied by ξ/χ to obtain a power spectrum and to normalize by χ such that the spectra become comparable.

In Fig. 13(b) is shown the contribution from the spin (see Berestetskii *et al.*, 1971 [Eq. (59.20)], Lindhard (1991), and Sørensen (1991)), where the first factor depends on the spin, i.e., the difference between (a) and the bracket term from Eq. (55) multiplied by ξ/χ; see Sørensen (1991). Clearly, the end of the spectrum is seriously affected by the spin for high energies. This contribution originates in Lindhard's approach from the replacement of the Thomson cross section for the virtual photon scattering by the Klein-Nishina cross section which takes recoil and spin into account.

As a result of the quantum correction, the total radiated intensity for the classical emission is, according to Schwinger, reduced by a factor $1-55\sqrt{3}\lambda\!\!\!^{-}_c\omega_0\gamma^2/16c$ due to first-order quantum corrections when $\chi\ll 1$ (Schwinger, 1954). Including the second-order term, we find the reductions for small and large values of χ are (Berestetskii *et al.*, 1971)

$$I/I_{\rm cl} = 1 - 55\sqrt{3}\chi/16 + 48\chi^2, \quad \chi\ll 1, \tag{57}$$

$$I/I_{\rm cl} \simeq 1.2\chi^{-4/3}, \quad \chi\gg 1. \tag{58}$$

Figure 14 shows the approximate expression

$$I/I_{\rm cl} \simeq [1+4.8(1+\chi)\ln(1+1.7\chi)+2.44\chi^2]^{-2/3} \tag{59}$$

valid for a wide range of χ values (Baier *et al.*, 1998).

From this it is clear that the emission of synchrotron radiation is already affected at fairly small values of χ. A graphical representation compared to measured values is given in the articles of Baier *et al.* (1986c) and Belkacem *et al.* (1988).

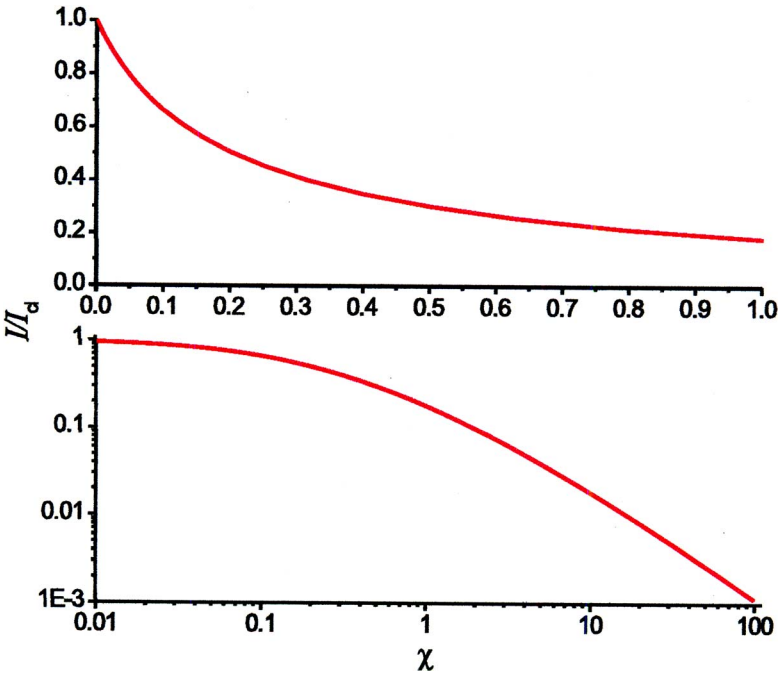

FIG. 14. (Color online) The intensity I of synchrotron radiation as a function of χ, normalized to the classical value I_{cl} obtained for $\chi \to 0$. The upper part shows the region $0 \leqslant \chi \leqslant 1$ on a linear scale while the lower part shows the region $0.01 \leqslant \chi \leqslant 100$ on a logarithmic scale.

At this point it is worth noting that even though the quantum corrections imply a *reduction* compared to the classical synchrotron law, the emission probabilities in the quantum regime are still *enhanced* in a crystal with respect to the Bethe-Heitler value, due to the coherence. The enhancement is here defined as the emission probability for an aligned crystal in units of the random value.

The "end point" of the radiation spectrum, $\hbar\omega_c$—beyond which the frequencies are exponentially suppressed—is found in the CFA (Artru, 1988; Baier *et al.*, 1989b) as being the approximate fraction of the incident energy:

$$\frac{\hbar\omega_c}{E} \simeq \frac{\chi}{1+\chi} \tag{60}$$

in good agreement with the estimate of the critical frequency, Eqs. (46) and (49) combined with Eq. (37).

There is therefore nothing extraordinary in the "emission under recoil" in terms of the emission process in itself, except that one has to take conservation of energy and momentum as well as spin into account. It therefore seems natural that a full quantum-mechanical calculation of these phenomena using the Dirac equation concludes that ultrarelativistic channeling does not involve quantum effects which are not included in the semiclassical treatment (Augustin *et al.*, 1995). On the other hand, what is remarkable is the large enhancement with respect to random incidence which is a result of the large field in the rest frame of the emitting particle and the coherence. So, even though the emission process can be calculated reliably in a semiclassical theory, it shows a drastic change from the usual classical behavior.

Thus crystals give us the opportunity to investigate the behavior of synchrotron radiation in the region where quantum effects become decisive in the spectrum. Moreover, crystals open up the possibility of investigating modifications to the radiation spectrum of a "nonsynchrotron" character, i.e., when the trajectory is better approximated by segments of nonconstant acceleration (Khokonov and Nitta, 2002).

For a single crystal, the strong-field parameter χ is approximately given by (Baier *et al.*, 1998)

$$\chi \simeq \frac{U_0 \gamma \hbar}{m^2 c^3 a_s}, \tag{61}$$

where a_s is the screening distance and U_0 is a measure of the height of the transverse potential. This leads, for example, for tungsten to $\chi_W \simeq 3$, at an energy of 100 GeV. For the energies 30 and 300 GeV the energy losses are reduced by factors of 6 and 45, respectively, compared to the classical synchrotron radiation (Kononets, 1988).

Table II summarizes the behavior of the intensity I, the radiation probability W, and the critical energy $\hbar\omega_c$, with γ for the two limits $\chi \gg 1$ and $\chi \ll 1$ (Kononets, 1988). Note that the radiation probability and pair-production probability have the same behavior with γ (or γ_p) in both the quantum and classical limits, in agree-

TABLE II. Behavior with γ for the intensity, radiation and pair-production probability, and the characteristic energy of emission for the quantum and classical limits.

	$\chi \gg 1$	$\chi \ll 1$
$I \propto$	$\gamma^{2/3}$	γ^2
$W \propto$	$\gamma^{-1/3}$	γ^0
$\hbar\omega_c \propto$	γ	γ^2

ment with expectations from crossing symmetry.[3] These drastic changes in behavior with γ from the classical to the quantum limit have so far only been investigated by means of the strong fields in crystals, which thus provide unique tools for tests of QED as shown from experimental results below.

2. Variations with energy, material, and temperature

The conclusion from Eqs. (51) and (61) is that the strong-field effects appear at lower energies the higher the Z of the crystal and the lower the temperature. The maximum enhancement, on the other hand, decreases with increasing Z since the maximum achievable formation length before the onset of the self-suppressing field deflection is inversely proportional to Z. Furthermore, the maximum enhancement is only slightly dependent on temperature. Nevertheless, it can be useful to cool a crystal intended to serve as a target for conversion of photons simply to reduce the threshold below the region of typical energies of the impinging photons and by these means obtain a significant increase in enhancement. This is due to the deeper transverse potential in a cooled crystal of high Z, which implies a high field and thus $\chi=1$ at a lower value of γ.

Clearly, the crystal material, orientation, and temperature are crucial parameters for an application as a target for conversion of photons.

3. Characteristic angle for CFA

Following Sørensen (1987), conservation of transverse energy leads to

$$\frac{p^2}{2\gamma m}\psi_0^2 = \frac{p^2}{2\gamma m}(\psi_0 + \Delta\psi)^2 - U_0, \tag{62}$$

where ψ_0 and $\Delta\psi$ denote the incident and deflection angle, respectively. For $\Delta\psi \ll \psi_0$ this gives

$$\Delta\psi = \frac{1}{\gamma}\frac{U_0}{mc^2}\frac{1}{\psi_0} \tag{63}$$

such that the angle

$$\Theta_0 = \frac{U_0}{mc^2} \tag{64}$$

separates two regions where the deflection angle is larger than or smaller than the opening angle of the emission cone, $1/\gamma$. Thus it separates the regions where the radiation has dipole nature, $\psi \gg \Theta_0$, and where it has a synchrotron nature, $\psi \ll \Theta_0$. Θ_0 is the so-called Baier angle. This characteristic angle does not depend on energy [see Cue and Kimball (1984) for a different approach] such that at relatively high energies, roughly when $\gamma \simeq 2mc^2/U_0$, i.e., a few GeV for axes in Si and Ge, we have $\psi_c < \Theta_0$ since $\psi_c \propto 1/\sqrt{\gamma}$. Thus the strong-field regime extends beyond the channeling regime for particles with energy above a few GeV. Furthermore, in accordance with the continuum approximation, the field registered by a particle incident at this angle can be considered constant along the string.

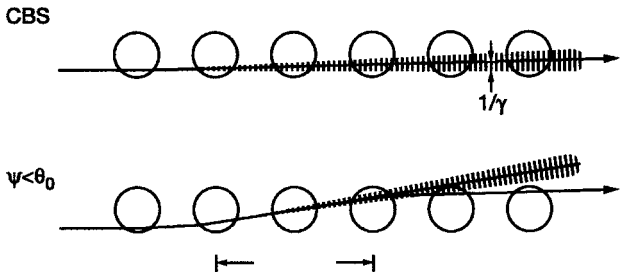

FIG. 15. Emission of bremsstrahlung by a charged particle crossing a string of atoms. In the upper part, the deflection due to the field from the string is sufficiently small such that coherent superposition can take place over many atoms—this is the limit with an angle $\psi > \Theta_0$ to the axis. The lower part reflects the increased deflection when incident with an angle $\psi < \Theta_0$ to the axis, which results in a shorter distance for the coherent superposition. From Sørensen, 1987.

From Eq. (63) and Fig. 15 it is again possible to conclude a "self-suppression" effect of the strong field. Coherence takes place within the "$1/\gamma$ zone" which becomes shorter and shorter as ψ_0 decreases since $\Delta\psi$ increases (Pedersen *et al.*, 1986, 1987), so the strong-field enhancement is smaller than the enhancement calculated from coherent theory (first Born approximation).

An alternative derivation shows the constant field more explicitly:

$$\Delta\mathcal{E} = \frac{U}{u_1 e} - \frac{U}{(u_1 + \Delta x)e} \lesssim \mathcal{E} = \frac{U}{u_1 e} \Rightarrow \Delta x \lesssim u_1. \tag{65}$$

Then

$$\Delta x = \frac{\psi_0 \lambda\!\!\!^{-}_c \mathcal{E}_0}{\mathcal{E}} = \frac{\psi mc^2 u_1}{U} \tag{66}$$

is the transverse displacement over the formation length, Eq. (48). By use of Eq. (65), this leads to $\psi \lesssim \Theta_0$ again with Θ_0 given by Eq. (64), i.e., under the assumption that the field deflection length is the formation length, the field can be considered constant during the creation process for incidence inside Θ_0.

Due to the thermal motion of the lattice nuclei, there is always an incoherent component of radiation. For a comparison of theory and experiment, it is necessary to add this contribution—a slightly modified Bethe-Heitler cross section, see, e.g., Ter-Mikaelian (1972, p. 60)—to the CFA contribution.

[3]Of course, pair production is always a quantum process so the separation between classical and quantum limits are understood as those belonging to the synchrotron-radiation case, i.e., $\chi \ll 1$ and $\chi \gg 1$. Likewise, the pair-production probability for $\chi \ll 1$ is understood as the dominant process, i.e., the Bethe-Heitler contribution, since the coherent part is exponentially small in this region of χ.

D. Virtual photon density

An alternative approach shows the interaction strength more explicitly in a picture where the penetrating particle interacts with the field seen as virtual photons. Following Baier *et al.* (1989b) the flux of equivalent photons can be calculated as

$$J_q = \frac{\gamma}{4\pi e^2}\frac{|G(q)|^2}{\hbar c|q_\parallel|}q_\perp^2, \tag{67}$$

where the strength of the potential is expressed through $|G(q)|$; see Eq. (2). In the interaction region of approximate size in the rest frame, $V_r \simeq 2\pi\hbar\lambda\!\!\!^{-2}_c/\gamma q_\parallel$ [given by the volume restricted by the inverse of Eqs. (29) and (30)], the resulting number of photons $N_q \simeq J_q V_r$. The strength of the interaction is then given by

$$\alpha N_\gamma = \alpha\sum_q N_q \simeq \sum_q \frac{|G(q)|^2 q_\perp^2}{m^2c^4q_\parallel^2}. \tag{68}$$

From $|G(q)| \simeq U_0$ and $q_\parallel \simeq q_\perp\theta_0$ then follows

$$\alpha N_\gamma \approx \left(\frac{U_0}{mc^2\theta}\right)^2 \tag{69}$$

from which it is seen that there are two regions of angles separated by $\Theta_0 = U_0/mc^2$. For $\alpha N_\gamma \gg 1$ the interaction is similar to a constant field, while for $\alpha N_\gamma \ll 1$ perturbation theory is valid.

E. Spin processes

The first calculation of the photon spectrum emitted by "particles of arbitrary spin moving in an arbitrary electromagnetic field" was done by Baier and Katkov (1967). Earlier, Sokolov and Ternov (1964) considered polarization and spin effects for electrons moving in a homogeneous, constant magnetic field. However, their realization that the spin influences the spectrum decisively for large values of χ was not discussed as an observable phenomenon. Nevertheless, radiation intensities were calculated for spin 0, $\frac{1}{2}$, and 1. In fact, the influence of spin was left out of many discussions of quantum effects: "quantum effects in synchrotron radiation originate in two ways: from the quantisation of the motion of the electron, and from the quantum recoil when a photon is emitted" (Berestetskii *et al.*, 1971; Baier *et al.*, 1998).

The first discussion of the possibility of observing spin flips in axial channeling was by Bagrov *et al.* (1984), but these results were later questioned by Greiner's group (Augustin *et al.*, 1995) based on a calculation starting from the Dirac equation. Spin flip in planar channeling, which requires energies about a factor of 10 higher, is discussed by Baryshevskii and Grubich (1983).

Later, Lindhard (1991) showed that the contribution from the spin can be derived from a Weizsäcker-Williams-type calculation. He and Sørensen (Sørensen, 1991) convincingly demonstrated that the contribution from the spin dominates the hard end of the photon spectrum as soon as $\chi \gg 1$; see Fig. 13. This means that—apart from the reverse action of the photon on the electron, the recoil—an additional quantum effect of the spin of the electron influences the spectrum, as also discussed in the book by Sokolov and Ternov (1986).

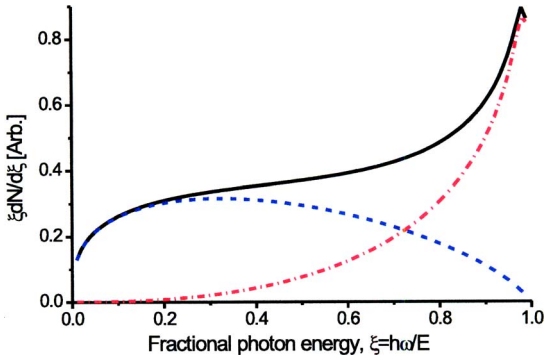

FIG. 16. (Color online) Synchrotron radiation in a strong field, where the solid line is the total spectrum according to Eq. (56), the dash-dotted line shows the contribution from the spin, and the dashed line is the contribution neglecting the spin; see text for details. The value of χ is set to 100.

Why the spin exerts its influence can be seen by a rough but simple argument (Kirsebom *et al.*, 2001a): The energy of a magnetic moment $\vec{\mu}$ at rest in a magnetic field $\vec{B}$ is given by

$$E_\mu = -\vec{\mu}\cdot\vec{B}. \tag{70}$$

Therefore spin-flip transitions of electrons with $\mu = e\hbar/2mc$ have an energy $\Delta E_\mu = e\hbar B/mc$ in the rest system. In this system, the purely electric field in the crystal is, by the Lorentz transformation, converted into a magnetic field $B = \gamma\beta\mathcal{E}_{\rm lab}$ plus an electric field which does not influence $\vec{\mu}$. Transformation back to the laboratory frame yields a factor γ (as in the case of channeling radiation arising from transitions in the transverse potential) such that the result is

$$\Delta E_\mu = \gamma^2\beta\frac{\mathcal{E}}{\mathcal{E}_0}mc^2 = \chi\beta\gamma mc^2, \tag{71}$$

which is equal to the initial energy of the electron E when $\chi\beta = 1$. This simple estimate shows why the radiation from spin flip concentrates near the end point of the spectrum. An analogous behavior appears for synchrotron radiation where the typical fractional photon energy, Eq. (37), becomes equal to 1 for $\chi = 2/3$ and the recoil of the photon must be taken into account as discussed above.

Asymptotically, the spin contribution becomes $\xi dN/d\xi \propto [\xi^7/(1-\xi)]^{1/3}\chi^{2/3}$ for $\chi \to \infty$ such that it is strongly peaked at the upper end of the spectrum. An example is given in Fig. 16 where the value of χ is set to 100.

In the process of radiative polarization of the electron, the typical time of spin-flip transitions τ is given by (Baier *et al.*, 1970; Schwinger and Tsai, 1974; Sokolov and Ternov, 1986)

$$\tau = \frac{8\hbar}{5\sqrt{3}\alpha m}\left(\frac{B_0}{B}\right)^3 \frac{1}{\gamma^2} = \frac{8\hbar}{5\sqrt{3}\alpha m}\frac{\gamma}{\chi^3} \tag{72}$$

such that $c\tau$ becomes 15 μm for a 150-GeV electron in a $\chi=1$ field. Therefore a substantial fraction of the radiation events originate from spin-flip transitions as one gets to and beyond $\chi \simeq 1$, even in a target as thin as 0.1 mm. Theoretical studies (Baryshevskii and Tikhomirov, 1989) point to the possibility of obtaining polarized positrons in a similar manner, by planar channeling through bent crystals of lengths about 1 mm.

F. Doughnut-scattering suppression

Suppression due to doughnut scattering can be stronger than the LPM effect due to multiple Coulomb scattering. Let the particle be incident with a fixed angle ψ to the axis and deflected through an azimuthal angle ϕ. Then the change in angle becomes $\theta \simeq 2\psi \sin(\phi/2) \simeq \phi\psi$. Setting this equal to $2/\gamma$, an estimate for the length over which the particle scatters outside the radiation cone is obtained (Bak *et al.*, 1988b):

$$l_{\gamma d} = \left(\frac{\phi}{2\pi}\right)^2 \lambda_\perp = \frac{\lambda_\perp}{\gamma^2\psi^2\pi^2}, \tag{73}$$

with $\lambda_\perp$ given by Eqs. (24) and (25). The length $l_{\gamma d}$ can become smaller than l_γ, even along an axis where multiple Coulomb scattering is enhanced for negatively charged particles. Therefore if the incident particles doughnut scatter sufficiently over one formation length, suppression of radiation may result; see also Uggerhøj (2004a).

The energy below which the radiation emission is suppressed by doughnut scattering can be estimated by use of Eqs. (10), (24), (25), and (73) as

$$\hbar\omega \leqslant (\hbar c\gamma^4\pi^4\psi_1^2 a_s dn/2)\psi \tag{74}$$

for electrons inside the critical angle and

$$\hbar\omega \leqslant (\hbar c\gamma^4\pi^4\psi_1^4 a_s^2 dn/8u_1)\psi^{-1} \tag{75}$$

for electrons outside the critical angle. Since $\psi_1^2 \propto 1/\gamma$, the doughnut-scattering suppression energies show a γ^3 and γ^2 dependence, respectively.

VI. PHOTONS IN STRONG FIELDS

By crossing symmetry, the radiation-emission and pair-production processes are intimately related. Thus it is natural to use the constant field approximation also for pair creation where the field is considered constant over the pair formation length. Furthermore, a couple of higher-order processes, photon splitting and Delbrück scattering, become enhanced in a strong field.

A. Pair production

It is useful to show by a qualitative argument why the condition $\chi \geqslant 1$ is sufficient to create a pair (Bassompierre *et al.*, 1995). If the formation length is $\lambda_\gamma = \lambda\!\!\!^{-}_c \mathcal{E}_0/\mathcal{E}$ then the formation time is $\Delta t = mc/e\mathcal{E}$. During this time a pair can be created if the energy conservation is violated by $\Delta E = 2\sqrt{p^2c^2+m^2c^4} - 2pc \simeq mc^2/\gamma$. Then the Heisenberg uncertainty principle $\Delta E \Delta t \simeq \hbar$ implies $mc^2/\gamma\mathcal{E}e\lambda\!\!\!^{-}_c \simeq 1$, i.e., $\chi \simeq 1$.

1. Total and differential rates

The pair-production probability differential in the normalized energy of one of the final-state particles, $\eta_\pm$, is given in the CFA as (Baier *et al.*, 1984, 1998)

$$\frac{dN_p}{d\eta_+} = \frac{\alpha}{\sqrt{3}\pi\lambda\lambda\!\!\!^{-}_c}\frac{mc^2}{\hbar\omega}\left[\left(\frac{1-\eta_+}{\eta_+} + \frac{\eta_+}{1-\eta_+}\right)K_{2/3}(\delta) - \int_{\delta_p}^{\infty} K_{1/3}(t)dt\right], \tag{76}$$

where $\delta_p = 2/3\,\eta_+\eta_-\chi$. Note here the similarity with the "substitution rule" in the coherence length, Eq. (12), going from ω to $\omega^{\#} = \omega/\eta_+\eta_-$ such that one can derive $\delta_p = 2/3\,\eta_+\eta_-\chi$ from δ_c merely on the basis of crossing symmetry. It should be noted, however, that due to the redistribution of channeled particles the calculation of radiation becomes more complicated than pair production for angles smaller than Lindhard's critical angle.

The differential probability develops a pronounced minimum around $\eta = E_{e^\pm}/\hbar\omega = 1/2$ and peaks at $\eta \simeq 1.6/\chi$ for large χ. This—combined with the fact that the strong-field radiation emission tends toward the end point of the spectrum—means that as the energy increases beyond the region where χ is of the order 100, an electromagnetic shower develops as essentially one energetic particle or photon, followed by many low-energy particles (Baier, Katkov, and Strakhovenko, 1987, 1995; Medenwaldt *et al.*, 1989b; Baurichter *et al.*, 1995). Again, this behavior is reminiscent of the behavior of the LPM effect for pair production [see, for example, Klein (1999)] which yields a preference for highly asymmetric pairs. This arises due to the similarity between the influence of the lengths λ_γ and l_γ, Eqs. (48) and (50).

The strong-field pair-production probability per unit time is given as (Baier *et al.*, 1998)

$$W_p = \frac{\alpha m^2 c^4}{6\sqrt{3}\pi\hbar^2\omega}\int_1^\infty \frac{8u+1}{u^{3/2}\sqrt{u-1}}K_{2/3}(\eta)du, \tag{77}$$

where $\eta = 8u/3\chi$. In the limit $\chi \ll 1$ the probability is exponentially small,

$$W_p \simeq \frac{3\sqrt{3}\alpha m^2 c^4 \chi}{16\sqrt{2}\hbar^2\omega\exp(8/3\chi)}, \tag{78}$$

while in the limit $\chi \gg 1$ the result is

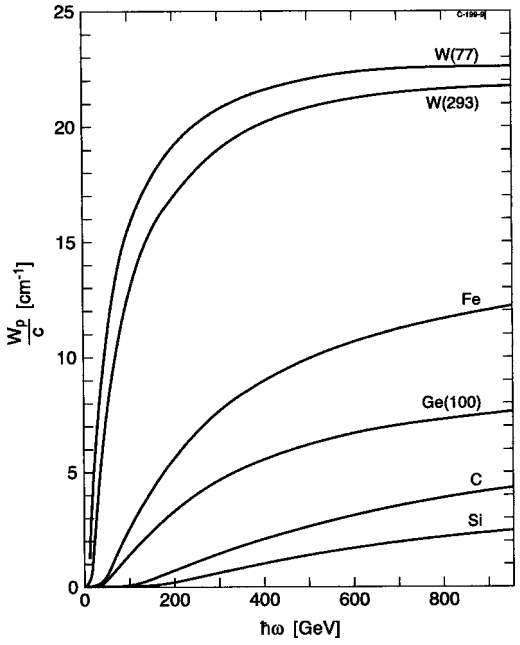

FIG. 17. Pair-production probability as a function of energy by a photon incident along the ⟨111⟩ axis for C, Si, Fe, and W and along ⟨110⟩ for Ge. The temperature, if different from 293 K, is given in the brackets. The values are according to the constant field approximation (CFA). Adapted from Baier *et al.*, 1985, 1998.

$$W_p \simeq \frac{0.38\alpha mc^2 B}{B_0 \hbar \chi^{1/3}}, \tag{79}$$

i.e., the probability actually diminishes once the energy surpasses the domain where $\chi \simeq 10$ (Baier *et al.*, 1998).

A good approximation to the cross section for all values of χ is given as (Erber, 1966)

$$\frac{dN_p}{dt} = \frac{4}{25}\frac{\alpha mc}{\lambda\!\!\!^{-}_c \hbar \omega} K_{1/3}^2\left(\frac{4}{3\chi}\right), \tag{80}$$

while a more precise (accuracy quoted as better than 3%) expression is given in the book by Baier *et al.* (1998) in which the probability has been averaged over photon polarization.

The exponential suppression at low values of χ in Eq. (78) can be interpreted as a tunneling process where "energy borrowed from the background field" (Kurilin, 1999) makes possible a process which is forbidden in vacuum.

2. Enhancements in crystals

Pair production attains a maximum enhancement of (Baier *et al.*, 1989a)

$$\eta_\gamma^{\max} \simeq \eta_{\mathrm{PP}}^{\max} = \frac{W_{\mathrm{CFA}}^{\max}}{W_{\mathrm{BH}}} \simeq \frac{U_0 m a_s d}{3Z_2^2 \alpha^2 \hbar^2 \ln(183 Z_2^{-1/3})}. \tag{81}$$

Note that according to Eq. (79) the effect is self-suppressing at high energies as indicated in the discussion of the formation length. The maximum enhancement, which can reach values of $\simeq 150$ for both pair production and radiation emission, is roughly inversely proportional to Z_2 and appears at an energy of approximately 100 times the threshold energy $\hbar\omega_t$, i.e., in the (multi-)TeV region.

Figure 17 shows calculated values for the total pair-production probability per unit distance in the constant field approximation for a number of crystals. The rapid onset of the coherent mechanism and the saturation at large energies is clear with the chosen energy scale, in particular for *W*.

For moderate χ, i.e., in the region just above threshold, the strong-field yield behaves as roughly proportional to the formation length. This means that the distribution of pairs peaks at $\eta_+ = 1/2$ (as $l_f \propto \eta_+ \eta_-$ does), whereas for very high energies it tends to a spectrum similar to the Bethe-Heitler for random incidence.

3. Suppression of incoherent contribution

Another effect of the self-suppression type is the reduction of the incoherent contribution due to coherent effects (Tikhomirov, 1987a; Kononets, 1999). It is analogous to the self-suppression effect as a result of the diminishing formation length in a strong crystalline field, only in this case the suppression is from the incoherent contribution.

The LPM suppression in pair production for presently available accelerator energies is negligible (Uggerhøj, 2004a). Even for a possibly near-future few-TeV electron beam generating bremsstrahlung photons, an experimental assessment of the magnitude of the effect would be extremely demanding. However, crystals may in fact present a possibility for measuring LPM suppression in pair production with beams in the few-hundred GeV region available today. The main reason is that the photon conversion into pairs in an aligned crystal takes place predominantly where the field is strongest, i.e., at small transverse distances from the string of nuclei, $r_\perp \simeq u_1$; see also Artru *et al.* (1993). At this transverse location, the multiple Coulomb scattering is drastically increased—by up to three orders of magnitude! For this reason, one may expect the threshold for LPM suppression to decrease by approximately the same three orders of magnitude corresponding to a replacement of TeV by GeV (Baryshevskii and Tikhomirov, 1986). However, it is only the incoherent contribution that becomes suppressed and, since the coherent contribution quickly dominates the pair-production cross section, the strong incoherent suppression becomes a small correction to the total yield except near the threshold for strong-field effects where the incoherent contribution plays a significant role (Tikhomirov, 1987b; Baier and Katkov, 2005b).

4. Corrections to the CFA

First-order corrections to Eqs. (56) and (76) in the field of a crystal axis are proportional to θ^2 where θ is the angle to the axis. The correction term in $W = F_1 + (mc^2\theta/U_0)^2 F_2$ has a positive coefficient F_2 at small energies, a negative coefficient at high energies (Baier *et al.*, 1989a), and changes sign at an energy of roughly

$7\hbar\omega_t$. Thus for energies larger than about $7\hbar\omega_t$ the maximum conversion probability takes place for perfect alignment with the axis, $\theta=0$.

B. Trident production

Oscar Klein was one of the first doing calculations using the Dirac equation. In 1929 he looked at the reflection probability of an electron from a potential barrier supplied by an electric field. Klein (1929) and later Sauter (1931a, 1931b) found that the probability for reflection exceeded 1 for electric fields beyond $m^2c^3/e\hbar$, i.e., when the field is so high that an electron transported over a Compton wavelength yields mc^2. Nowadays, this process is understood as pair production, which—not knowing of the positron—was an impossible conclusion for Klein and it is therefore known as the Klein paradox. Processes similar (but not identical) to Klein pair production are, for example, addressed in heavy-ion collisions in which the local field during the collision may become "supercritical" resulting in pair production (Greiner *et al.*, 1985).

Lately, the interest in the Klein paradox has been revived through theoretical studies with wave packets (Nitta *et al.*, 1999) and space-time resolved simulations (Krekora *et al.*, 2004) that reach very different conclusions concerning the probability of positron production by electrons, $e^-\rightarrow e^-e^+e^-$ so-called trident production, in a strong field. In the paper by Krekora *et al.* (2004) it is claimed that "the incoming electron suppresses the pair production."

Due to the invariance of the parameter $\chi=\gamma\mathcal{E}/\mathcal{E}_0$, it is possible to probe field strengths of the order of those relevant for the Klein paradox in single crystals. The only difference in the three dimensionless invariants describing the problems of trident production in crystals and the Klein paradox, Eqs. (38)–(40), is that in the latter case Ξ is of the order 1. The relation $\chi\gg\Xi,\Gamma$, still holds for both cases.

In fact, calculations of the drastic increase of trident production in crystals compared to an amorphous material have existed for almost two decades (Kimball and Cue, 1985). One result is shown in Fig. 18. A measurement of the trident-production process requires the use of several thicknesses of foils since the competing process where the electron radiates a *real* photon that subsequently produces a pair depends on the square of the thickness, whereas trident production has a linear dependence. Furthermore, the ratio of probabilities for trident production to that of the cascade process involving a real photon in the intermediate step can be estimated as $l_f/\Delta t_f$ (Baier *et al.*, 1998) such that the required foil thickness must be of the order one formation length. This is a rather modest thickness—even for a 250-GeV electron producing a 1-GeV pair it is 0.1 mm, but it seems possible to discern the signal from background effects, especially in view of the huge enhancement and the fact that it increases with increasing energy of the primary electron.

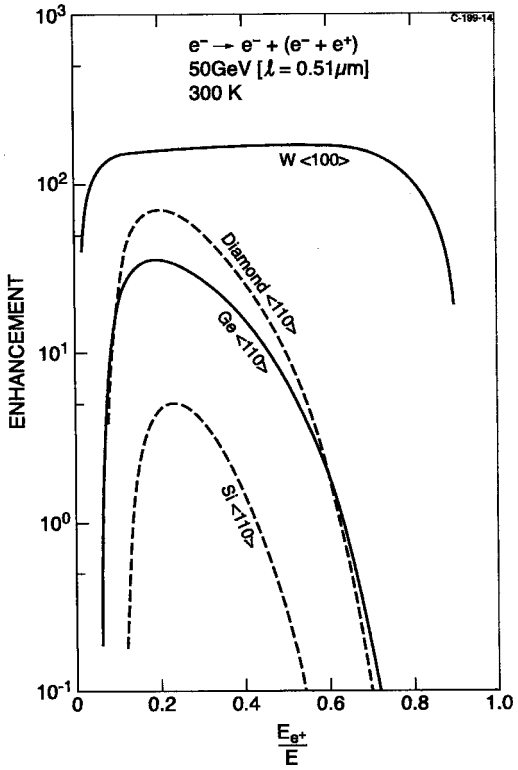

FIG. 18. Enhancement over random incidence for trident production of four different crystals. The electron energy is 50 GeV and the horizontal scale is the fractional energy taken by the positron. Adapted from Kimball and Cue, 1985.

C. Photon splitting

With prospects of being able to address the question of the Higgs mechanism by clean production of Higgs particles in $\gamma\gamma$ collisions (Schäfer *et al.*, 1990), the behavior of photons in crystals has been examined. The key idea is to have two counterpropagating electron beams interacting in a crystal. Since the photons for both electron beams are produced near the atomic strings, an enormous effective increase in luminosity can be expected (Schäfer *et al.*, 1990). This boost in luminosity could be further increased if the photons were "channeled" by Delbrück scattering, but calculations indicate that this is not the case (Klenner *et al.*, 1994).

In his paper on what is now called the Weizsäcker-Williams method (Williams, 1935) in which he also discussed interference effects in crystals, Williams was the first to discuss the possibility of photon splitting. Similar to elastic Delbrück scattering, photon splitting is an inherently nonlinear process. It has recently been observed in amorphous matter (Akhmadaliev *et al.*, 1997, 2002) but hitherto not in crystals. In an earlier experiment, Jarlskog *et al.* (1973) reached the wrong conclusions due to the difficulty of discerning the true events from background effects (Baier *et al.*, 1974).

The coherent photon splitting probability $W_{\gamma\rightarrow\gamma\gamma}$ in a crystal has been calculated to exceed the amorphous value for achievable energies $\hbar\omega\simeq 300$ GeV (Baier, Milstein, *et al.*, 1987). Already at 150 GeV an increase of

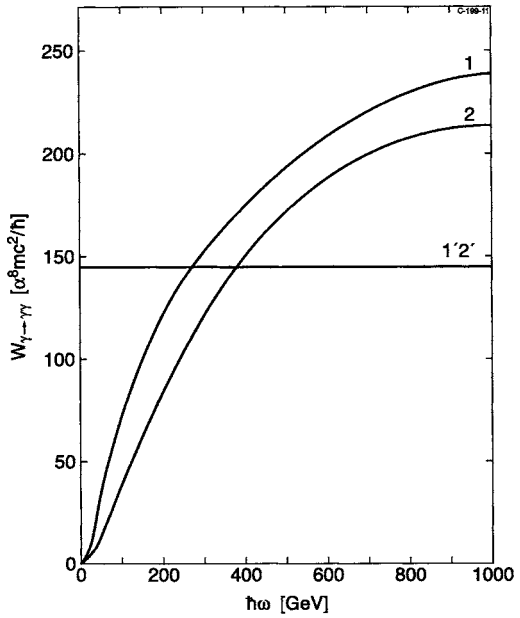

FIG. 19. The photon splitting probability $W_{\gamma\to\gamma\gamma}$ in W along the ⟨111⟩ axis as a function of photon energy. Curve 1 is $W_{\gamma\to\gamma\gamma}$ in the strong field at 77 K, curve 2 is $W_{\gamma\to\gamma\gamma}$ in the strong field at 293 K, and curves 1′ and 2′ denote the random (amorphous) value. Adapted from Baier *et al.*, 1987.

about 50% is to be expected along the ⟨111⟩ axial direction in a cooled W crystal; see Fig. 19. This opens up the possibility of a measurement where many systematic effects may be drastically reduced by a comparison of the aligned and random spectra—for example, the multiphoton content of the incident beam. The main background process is $e^-\to e^+\gamma e^-\gamma$, where each of the produced leptons lose almost their entire energy to a photon. In a crystal the probability of this is strongly energy dependent, at least for energies in the neighborhood of threshold (see, however, Fig. 33 for higher energies). Furthermore, to avoid conversion of one or both of the two produced photons, the target must be of the order one *effective* radiation length—a thickness that also depends strongly on energy. To give an estimate for the scale of the cross section, the photon-splitting process for $\chi\gg 1$ is approximately $0.3(\alpha/\pi)^2\simeq 1.6\times 10^{-6}$ times smaller than that of pair production. The measurement of photon splitting is a complicated problem in experimental physics, in particular, for crystals; see also Baier, Milstein, *et al.* (1986).

D. Delbrück scattering

In the picture of the Dirac sea where all negative-energy states are filled with electrons, Delbrück scattering is an elastic scattering of the photon off the negative-energy electrons. The process is necessarily elastic since there are no vacant negative-energy states the struck electron can end up in (Schumacher, 1999). Delbrück scattering is one of the few nonlinear QED processes that have been studied experimentally during many years.

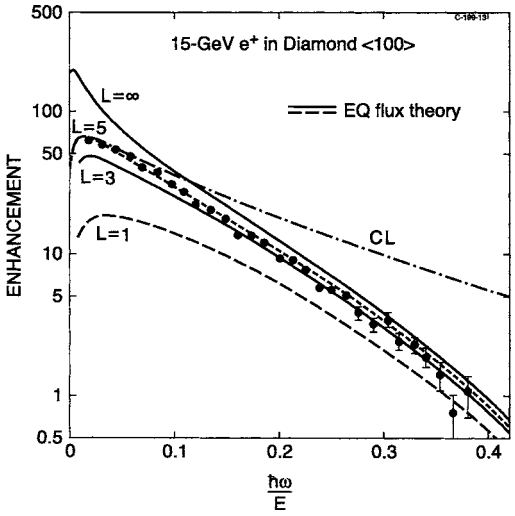

FIG. 20. Relative enhancement of photons for 15-GeV positrons directed along the ⟨100⟩ axis in diamond. The curves show calculated values based on the theory of Kimball and Cue (1984a) with L as an effective path length in μm. A classical spectrum is shown by the dot-dashed line (CL). Adapted from Cue *et al.*, 1984.

In the article of Klenner *et al.* (1994) the process of Delbrück scattering in a strong crystalline field is considered, with photons of energies up to 25 GeV and incidence along the ⟨110⟩ axis in Ge at room temperature. Unfortunately, the crucial parameter χ for this case is only up to 0.12, i.e., barely in the strong-field regime, whereas 200-GeV photons would give $\chi\simeq 1$ and up to $\chi\simeq 6$ in tungsten. Nevertheless, for 10-GeV photons incident very close to the axial direction $\theta=1$ μrad Augustin *et al.* (1995) calculate an azimuthal scattering angle ϕ of about 200 μrad, even in this comparatively weak field. However, the observed scattering angle would be of the order $\phi\theta$ and since the scaling is approximately $\phi\propto 1/\theta$, the result is far below the current state-of-the-art experimental resolution $\Delta\psi\simeq 5$ μrad *unless* the strong-field behavior enhances the scattering angle by a large factor.

VII. EXPERIMENTS

In the early 1980s under the heading "new crystal-assisted pair-creation process," experiments in the strong crystalline fields began (Kimball *et al.*, 1983; see also Baier *et al.*, 1983). It was shown that photons incident on crystals along an axis will pair produce with a probability that is higher than that of an amorphous target and that the differential spectrum (in $\eta_\pm$) is completely different. Shortly after, the first experimental results followed.

A. Radiation emission

The first observation of quantum recoil effects in synchrotron radiation is shown in Fig. 20 (Cue *et al.*, 1984), an experiment performed at the Stanford Linear Accel-

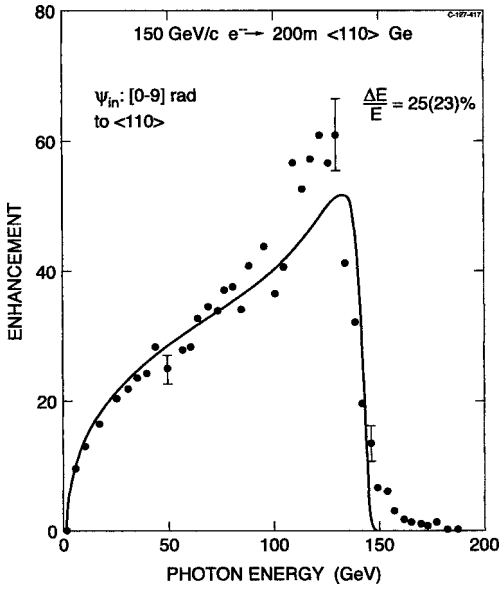

FIG. 21. Enhancement of radiation yield for 150-GeV electrons incident within 9 μrad to the $\langle 110\rangle$ axis of a 0.2-mm Ge crystal. The dots are experimental points and the line represents the calculated value based on the CFA. Adapted from Medenwaldt *et al.*, 1989a.

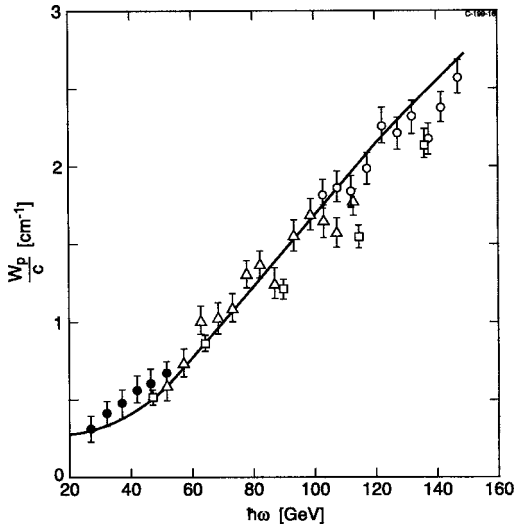

FIG. 22. Pair-production yield for photons incident along the $\langle 110\rangle$ axis of a 1.4-mm Ge crystal cooled to 100 K (Balkacem *et al.*, 1986a, 1987). The constant field approximation is shown by the solid. Adapted from Baier *et al.*, 1998.

erator Center (SLAC). A collimated beam of 4-, 15-, and 17.5-GeV positrons was directed along the $\langle 100\rangle$ axis in a diamond crystal. The results confirmed the newly developed theory (Kimball and Cue, 1984a, 1984b) treating the radiation emission as synchrotronlike, dividing the particle trajectory into nearly circular segments, and summing the appropriately weighted contributions. As seen from the figure, already at these values of χ a significant suppression of the radiation yield results as compared to the classically calculated value.

A few years later, the so-called "Belkacem peak" was discovered (Belkacem *et al.*, 1986b)—an enhancement of radiation yield with a sharp peak at $\xi \simeq 0.85$ from 150-GeV electrons passing a thin Ge crystal at axial alignment. The first results showed an enhancement of about 8, but this was due to an averaging over the beam width of $\simeq 30$ μrad. Figure 21 shows a later measurement where the angle of incidence is restricted to less than 9 μrad to the axis and in this case the enhancement becomes as high as 60 (Medenwaldt *et al.*, 1989a). Furthermore, the expected value for the enhancement based on the CFA, shown in Fig. 21 as a solid line, fits the data very well (Baier *et al.*, 1991). The Belkacem peak, initially hoped to be a sign of new physics, was shown to be a result of pileup of multiple photon emission (Medenwaldt *et al.*, 1990).

B. Pair production

Since the mid 1980s a number of increasingly detailed experiments have been performed employing strong crystalline fields. The first experiments confirmed the strong-field behavior with relatively poor statistics, being able to assess an enhancement of pair creation and radiation emission (Belkacem *et al.*, 1984, 1985; Cue *et al.*, 1984), but averaged over large slices in energy and incident angle.

Figure 22 shows a measurement of the enhanced pair-production yield for photons incident along the $\langle 110\rangle$ axis of a 1.4-mm Ge crystal cooled to 100 K (Belkacem *et al.*, 1986a, 1987). A CFA calculation added to the Bethe-Heitler value is shown as the solid line (Kimball and Cue, 1985; Baier *et al.*, 1998). The tremendously good agreement gives compelling evidence for the physical interpretation as a strong-field effect.

Moreover, the behavior of the enhancement with angle for different energy intervals, Fig. 23, is in very good agreement with calculated values and shows the expected behavior of the correction term discussed in Sec. VI.A.4, i.e., the maximum enhancement tends towards perfect alignment for higher photon energies. Alternatively, by assuming a "trial trajectory" that takes the field nonuniformity into account, a single compact expression allows us to calculate the enhancement as a function of angle to good accuracy (Nitta *et al.*, 2004).

The initial, comparatively crude, experiments were later refined substantially. One example was the NA43 experiment at CERN which during the last few runs had upgraded the detector assembly giving plenty of new opportunities for investigations. The NA43 experiment was performed in the North Area of the CERN SPS. The beam (H2) was a tertiary one containing either electrons, positrons, or pions with energies ranging from about 10 to 300 GeV. As the beam is produced by conversion of photons originating typically from π^0 decay, it is very pure. The later version of the experimental setup of NA43 is shown in Fig. 24. Its main components were six drift chambers (DCs) in conjunction with magnets. DC1, DC2, and DC3 defined the entry and exit angles and positions on a first crystal. Downstream of a magnet, B8, DC4 was used in a tagging system where the primary

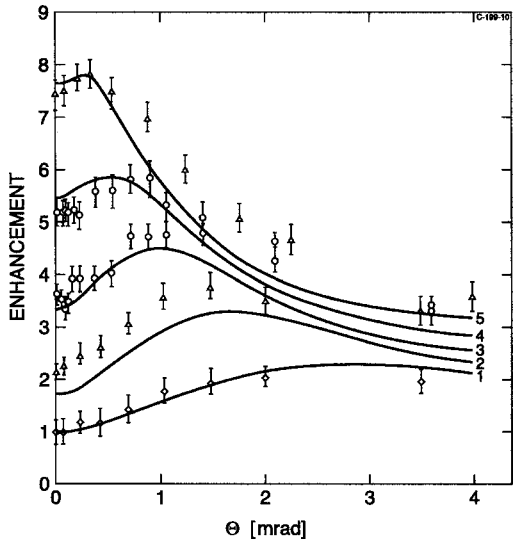

FIG. 23. Enhancement as a function of angle of pair-production yield for photons incident along the ⟨110⟩ axis of a 1.4-mm Ge crystal cooled to 100 K (Belkacem *et al.*, 1986a, 1987). The energy intervals are as follows: line 5, 120–150 GeV; line 4, 90–120 GeV; line 3, 60–90 GeV; line 2, 40–60 GeV; and line 1, 22–40 GeV. The lines are calculated values from Baier *et al.* (1988a). Adapted from Baier *et al.*, 1998.

e^+/e^- were deflected. The deflection was registered in DC4, from which the radiated energy was found. The energy was also determined from a downstream lead-glass array, intercepting either photons or undeviated electrons (or, in the case of generated pairs, positrons). Finally, DC5 and DC6 were placed downstream of a magnet, Tr6, in front of which a second conversion crystal or amorphous foil was positioned. The last two drift chambers and the magnet Tr6 were used as a magnetic pair spectrometer to determine the momentum of the pair produced in the converter—and thus the momentum of the photon.

In one setup, the first goniometer held a 0.7-mm-thick diamond crystal, whereas at the position of the second goniometer an amorphous foil was placed. This type of setup was suited for measurements of the photon multiplicity. In front of the second target, a scintillator Sc9 was positioned to reject those events where a photon converted upstream. Immediately downstream of the second target, two counters, a solid-state detector, and a scintillator Sc11 detected the pairs produced in the crystal. Photon multiplicities were measured by a 1-mm amorphous Cu converter followed by the 0.5-mm-thick solid-state detector. For normalization and background subtraction random (nonaligned) directions and "no-target" measurements were performed. The angular resolutions on incident and exit sides of the first goniometer were $\simeq 5$ μrad. By means of the drift chambers it was possible to select specific areas of the target crystals and thereby check the stability and possible bending of the crystal in both the on- and off-line analysis.

In this detector system the photon multiplicities were measured with the solid-state detector, but the pair spectrometer could also be used. For the solid-state-detector system, the lowest photon energy was ≈ 0.5 GeV determined by the solid angle subtended by the detector and the opening angle of the pairs, $\simeq mc^2/\hbar\omega$. In the pair spectrometer used for photon multiplicities the minimum photon energy was around 5 GeV, determined by the deflection power of Tr6 and the geometry of DC5 and DC6. Thus the detected multiplicity with the two systems generally differ by a factor $\simeq 2$, but show the same trend (Kirsebom *et al.*, 2001b). For the pair spectrometer the specific energy of each converting photon is measured, whereas when using the solid-state detector only the total energy of all photons is measured in the calorimeter.

The spectrometer was also used to find the direction of the emitted photons. Since the photons are emitted within $1/\gamma$, which is comparable to the angular resolution of the combined DCs, the approximate particle direction at the moment of photon emission could be measured. In this way, not only the angular distribution of the electron beam can be measured in front of and behind the first crystal, but also the direction of the elec-

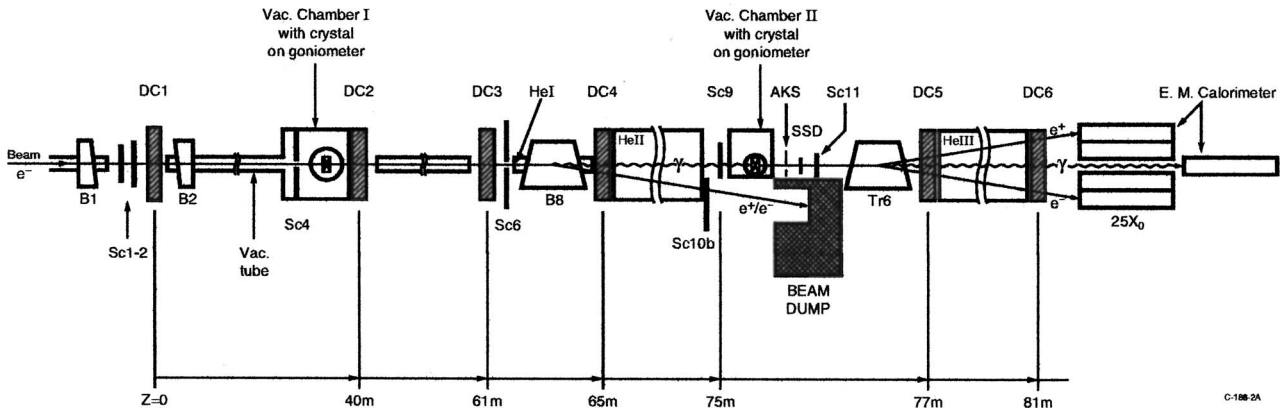

FIG. 24. A schematical drawing of the setup used in NA43. The abbreviations are B1, B2, B8, and Tr6, magnetic dipoles; DC1-6, drift chambers; Sc1-2, Sc4, Sc6, Sc9, Sc10b, Sc11, scintillator counters; AKS, "anti-K-short" scintillator counter; HeI-III, helium vessels; and SSD, solid-state detector.

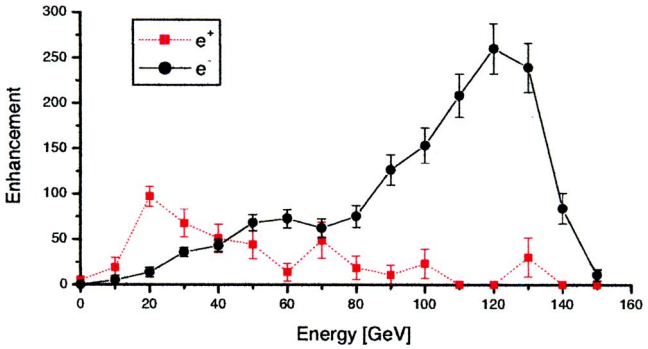

FIG. 25. (Color online) Enhancement as a function of energy for an incident angle of 0–5 μrad. A spectrum produced by 149-GeV electrons and positrons incident around the ⟨110⟩ axis in 0.7-mm diamond. Adapted from Kirsebom *et al.*, 2001b.

tron while emitting the photon *inside* the crystal can be detected, see below.

Figure 25 shows results obtained for 149-GeV electrons and positrons incident close to the ⟨110⟩ axis in 0.7-mm diamond (Kirsebom *et al.*, 2001b). It can be seen that there is a big difference between electrons and positrons due to the redistribution of particles inside the channeling region (Baier *et al.*, 1986b). Furthermore, as expected from the CFA, the enhancement is much larger for diamond than for germanium; cf. Fig. 21.

A similar experiment to NA43 was performed by the CERN NA46 Collaboration which aimed to search for neutral particles produced in the strong crystalline field (discussed below). The NA46 experiment is shown schematically in Fig. 26. As for the NA43 experiment, the main elements were tagged photons produced by incoherent bremsstrahlung in a foil (LR), a crystalline target (XTAL), a long baseline (≃80 m), a position-sensitive microstrip detector (μS), a pair spectrometer consisting of a magnet and three double multiwire proportional chambers (MWPC), and finally a lead-glass calorimeter (CAL). The use of a microstrip detector and a long baseline gave excellent position and angular resolution of $\sigma_{\theta_x}=\sigma_{\theta_y}=0.2$ μrad. This was, however, to some extent

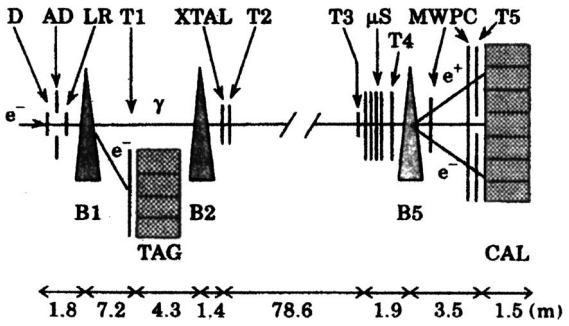

FIG. 26. A schematical drawing of the setup used by NA46. The abbreviations are B1, B2, and B5, magnetic dipoles; TAG and CAL, lead glass calorimeters; LR, target foil; XTAL, crystal target; μS, microstrip detector; MWPC, multiwire proportional chambers; and D, AD, T1-5, scintillator counters. From Bassompierre *et al.*, 1993.

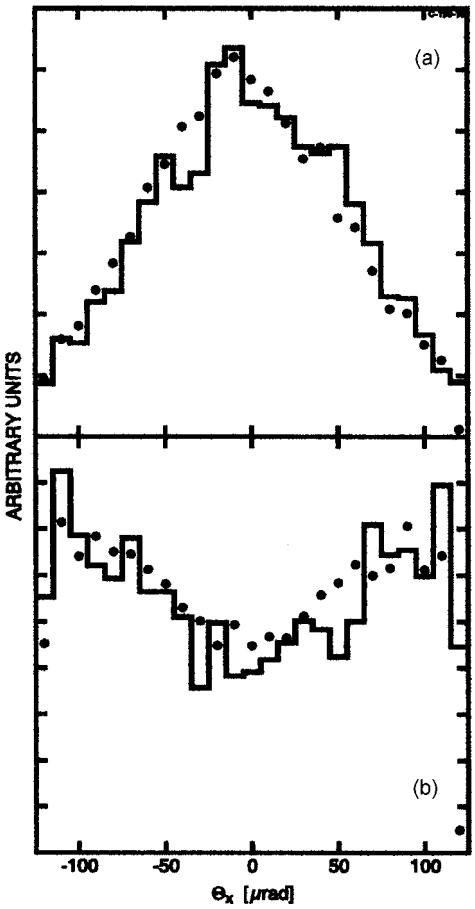

FIG. 27. Angular distribution of particles produced in a 0.42-mm-thick Ge crystal by photons within an energy range of 83–133 GeV: (a) the emerging electrons and (b) positrons. The dots are experimental points and the histograms are results from a Monte Carlo code based on pair production in strong crystalline fields. Adapted from Artru *et al.*, 1993.

spoiled by the beamwidth of 8 mm, which resulted in a final resolution of $\sigma'_{\theta_x}=\sigma'_{\theta_y}\simeq 25$ μrad.

Figure 27 shows experimental results obtained as a "by-product" by NA46 and compared to the results of a Monte Carlo code. Since the pair production predominantly takes place where the field is strongest, i.e., close to the atomic string, the produced electrons are almost all channeled giving rise to an enhancement of yield [Fig. 27(a)], while the positrons show a "blocking" effect of yield suppression along the axial direction [Fig. 27(b)]. An interesting effect, the so-called "side slip" (Artru, 1988; Artru and Bignon, 2001) corresponding to the pair being produced noncollinearly with the photon, was too small to be considered significant in the experiment and was not included in the simulation.

C. Coherent resonances in strong fields

Distinct coherent resonance peaks develop in the radiation and pair-production spectra as the entry direction of the electron or photon is tilted out along a plane, maintaining a relatively small angle to the axis. In this

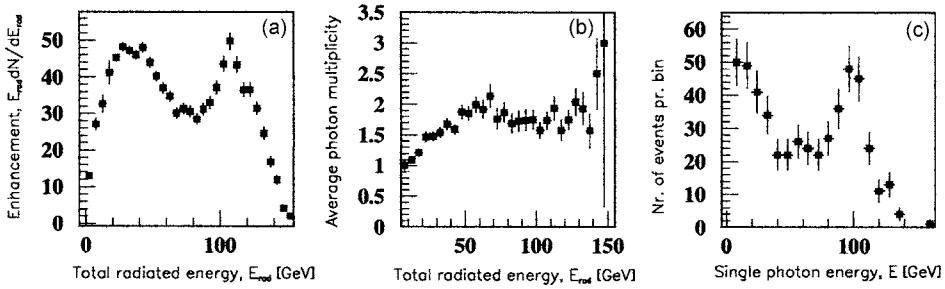

FIG. 28. 149-GeV electrons on the (111) plane of 0.7-mm diamond, 0.6 mrad to the ⟨110⟩ axis. (a) The radiation enhancement as a function of total radiated energy, (b) the photon multiplicity, and (c) the number of photons emitted as a function of the energy of the photon given that the sum of photon energies exceeds 100 GeV. From Kirsebom *et al.*, 2001b.

case, the coherent resonances are obtained in passing the periodically spaced axes in the plane, in a way analogous to the passage of the planes for coherent bremsstrahlung and coherent pair production.

1. Radiation emission

In the early 1990s it was found both experimentally by NA43 (Medenwaldt *et al.*, 1992) and theoretically by Baier *et al.* (1992) that electrons of energies in the hundred-GeV range incident on a single crystal with a small, nonzero angle to the axis along a plane would lead to a peak of high-energy photons; see Fig. 28 where a later example is given (Kirsebom *et al.*, 2001b). Furthermore, the increase of yield of such photons with respect to the emission from the equivalent amorphous material was found experimentally to be around 50 for diamond.

The appearance of this peak is ascribed to a coherent resonance obtained when the electron passes the strings forming the plane in the so-called strings-of-strings region. It is thus reminiscent of the usual coherent phenomenon obtained when the electron passes planes, see Fig. 11, only in this case it is the crystallographic axes and not the planes that lead to coherent structures in the spectrum. Therefore the position of the peak in the spectrum is found as (Kononets and Tupitsyn, 1994)

$$\hbar\omega_{\mathrm{CR}} = E\left(1 + \frac{A_{\mathrm{ax}} d_a}{n_i 2\pi 2\gamma\lambda\!\!\!^{-}_c \sin\theta}\right)^{-1}, \tag{82}$$

where $A_{\mathrm{ax}}=1.282$, d_a is the transverse distance between the traversed atomic strings, θ is the angle to the axis, and n_i is an integer—the peaks in coherent bremsstrahlung are obtained by replacing A_{ax} by $A_{\mathrm{pl}}=1$ and d by d_p and setting θ as the angle to the plane. The fact that $A_{\mathrm{ax}}\neq 1$ is due to the deflection in the strong field as shown in a comprehensive paper on the calculation of the coherent peaks (Kononets and Tupitsyn, 1994). They based their theory on the semiclassical approximation, CFA. Since the radiation peak consists of hard photons ($\simeq$100 GeV) typically followed by a single soft photon ($\lesssim$20 GeV), see Fig. 28(c), it is a potential source for hard γ rays.

2. Pair production

A similar phenomenon is obtained for pair production where the coherent pair-production mechanism of the strings gives rise to peaks, notably in the spectrum differential in the fractional energy carried by one of the leptons (Bak *et al.*, 1988a; Kononets and Tupitsyn, 1993). An example of a measurement is shown in Fig. 29 (Kirsebom *et al.*, 1998) where, unfortunately, the scatter of points prevents a clear proof of the effect. Even under

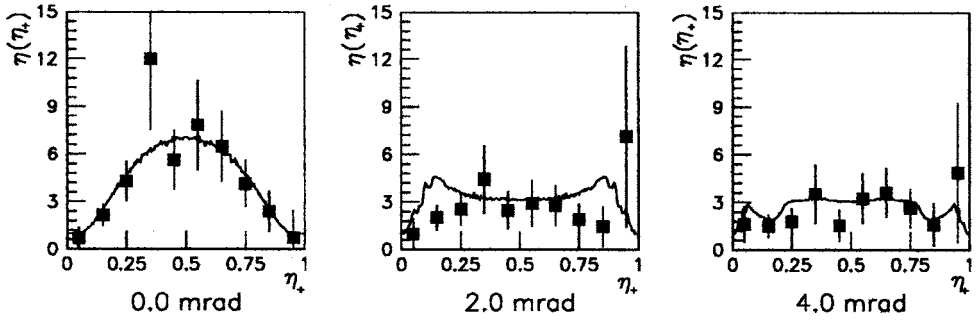

FIG. 29. Differential enhancement of pair production for photons in the energy interval 80–100 GeV incident around the ⟨110⟩ axis in a germanium crystal cooled to 100 K. Filled squares are results of the pair spectrometer and the line represents the theoretical values according to Kononets (1996). The results are shown for the three angles 0, 2, and 4 mrad to the ⟨110⟩ axis on the (110) plane. Adapted from Kirsebom *et al.*, 1998.

axial alignment a coherent mechanism may lead to a resonance structure as discussed by Cue and Kimball (1987).

D. Radiation cooling

The influence of radiation cooling on the motion of GeV particles through crystals was widely discussed since the Belkacem peak was found in the photon spectrum from 150-GeV electrons traversing germanium crystals (Belkacem *et al.*, 1986b). Initial estimates of the cooling effect were given already by Baryshevskii and Dubovskaya (1977). In this context, radiation cooling is understood as radiative transitions downwards in the transverse potential that may or may not lead to angular cooling, the decrease of transverse emittance through reduction of the exit angle compared to the entry angle.

Following the Belkacem peak, several groups studied radiation cooling (Tikhomirov, 1987a, 1989; Artru, 1988; Kononets and Ryabov, 1988). Later on, radiation from very thin crystals was investigated experimentally and the results showed that photon spectra from high-energy electrons or positrons were strongly influenced by multiphoton effects (Medenwaldt *et al.*, 1989a, 1990). These experiments resulted in new calculations of radiation emission (Artru, 1990; Kononets and Ryabov, 1990a, 1990b; Baier *et al.*, 1991; Beloshitski *et al.*, 1991; Khokonov, 1992; Kononets, 1992) where radiative cooling—feeding into channeling states for above-barrier particles—was a necessary ingredient.

NA43 provided a demonstration of radiative and angular cooling for 149-GeV electrons or positrons traversing Si crystals (Kirsebom *et al.*, 1996; Baurichter *et al.*, 1997). It was found that the cooling effect is absent for positrons as well as for electrons with incident angles inside the channeling region. On the other hand, for electrons with incident angles larger than ψ_1 a strong cooling was found, i.e., $\psi_{\rm out} < \psi_{\rm in}$.

The situation can be understood from the continuum approximation: the transverse energy $E_\perp = \gamma m v^2 \psi^2/2 + U(r_\perp)$ is conserved between photon emission events and the direction of v remains unchanged during the emission process while γ decreases. From this, a relation between $\psi_{\rm out}$ and $\psi_{\rm in}$ was obtained by Kononets [for details, see Baurichter *et al.* (1997)]:

$$\langle \theta_{\rm out}^2 \rangle = \langle \theta_{\rm in}^2 \rangle + \frac{2}{E - \hbar\omega}[U(r_\perp^0) - \langle U \rangle_f] - \frac{2}{E}[U(r_\perp^0) - \langle U \rangle_i], \tag{83}$$

where symbols $\langle \cdots \rangle_i$ and $\langle \cdots \rangle_f$ denote the averaging over initial and final states of the radiating particle, respectively. The transverse coordinate where the γ emission event takes place is denoted as $r_\perp^0$. For positrons the main contribution to the radiation comes from transverse locations $r_\perp^0$ where the transverse potential is high, i.e.,

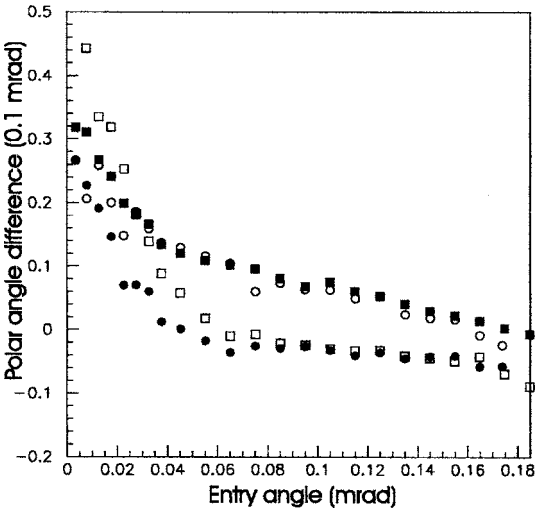

FIG. 30. Polar-angle differences for 149-GeV electrons, positrons, and their respective photons. The filled squares show the electron angle difference calculated from the angle at the moment of photon emission and the entry angle, i.e., $\theta_\gamma - \theta_{\rm in}$, and the filled dots show the same for the positron. The open squares show the electron angle difference calculated from the exit angle and the entry angle, i.e., $\theta_{\rm out} - \theta_{\rm in}$, and the open dots show the same for the positron. Adapted from Kirsebom *et al.*, 2001b.

$$U(r_\perp^0) > 0 \quad \text{and } |\langle U \rangle_f|, |\langle U \rangle_i| \ll |U(r_\perp^0)|, \tag{84}$$

which gives

$$\langle \theta_{\rm out}^2 \rangle - \langle \theta_{\rm in}^2 \rangle \simeq 2\left(\frac{1}{E - \hbar\omega} - \frac{1}{E}\right) U(r_\perp^0). \tag{85}$$

Now, θ is unchanged when the particle crosses the target surface. Thus since $U(r_\perp^0) > 0$ for positrons, it follows that $\langle \theta_{\rm out}^2 \rangle > \langle \theta_{\rm in}^2 \rangle$, i.e., positrons experience angular heating, even though the transverse energy is reduced.

For electrons $U(r_\perp^0) < 0$ for the main region of emission close to the nuclei and there are two important regions of angle of incidence:

$$\text{(a) } \theta_{\rm in} \ll \psi_1, \qquad \text{(b) } \theta_{\rm in} > \psi_1. \tag{86}$$

In case (a) the radiation emission and multiple scattering result in capture to high-lying states in the potential well as shown by experimental results (see Fig. 31). This is because the low surface transmission of electrons brings them to states only slightly above the well where the probability of radiating photons of relatively low energy is high. Thus the low transverse kinetic energy before radiation is converted into a high transverse kinetic energy originating from the depth of the potential well, i.e., angular heating: $\langle \theta_{\rm out}^2 \rangle > \langle \theta_{\rm in}^2 \rangle$. Even though a photon is emitted the transverse emittance increases! In case (b) angular cooling results, $\langle \theta_{\rm out}^2 \rangle < \langle \theta_{\rm in}^2 \rangle$. For details, see Kononets (1999).

Figure 30 shows data for 149-GeV electrons incident along the $\langle 110 \rangle$ axis in a 0.7-mm diamond crystal. As a

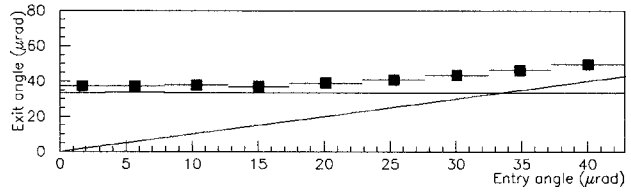

FIG. 31. An example of radiative capture for 149-GeV electrons in 0.7-mm diamond. Shown are exit angles θ_{out} as a function of entry angles with respect to the $\langle 110\rangle$ axis, θ_{in}, for an interval of radiated energy, $0-E/3$. The full squares with error bars denote the data points, and the lines indicate $\theta_{\text{out}}=\theta_{\text{in}}$, and the critical angle of the exiting electron, $\psi_1(\overline{E^{\text{exit}}})$, where the average energy loss, $\overline{\Delta E}$, for each θ_{in} bin has been used with $\overline{E^{\text{exit}}}=E-\overline{\Delta E}$. The critical angle for 149-GeV electrons in this configuration is 30 μrad. Adapted from Kirsebom *et al.*, 2001b.

measure of the angular cooling after penetration, the parameter $\Delta_\theta=\theta_{\text{out}}^2-\theta_{\text{in}}^2$ can be introduced. The physical meaning of Δ_θ is a measure of the angular cooling effect. For large positive values the beam is radiatively heated upon traversal while for values below zero it "shrinks" in the transverse directions.

For randomly oriented multiple scattering by a 149-GeV e^- in a 0.7-mm-thick $\langle 110\rangle$ diamond crystal, $\Delta_\theta=110$ μrad^2. For $\theta_{\text{in}}\geqslant\psi_1$ the competing processes of radiative cooling and multiple scattering result in $\Delta_\theta<0$, i.e., the cooling effect can more than compensate for the multiple scattering. For $\theta_{\text{in}}\ll\psi_1$ it is found that $\theta_{\text{out}}\simeq\psi_1(E_{\text{exit}})$, where $\psi_1(E_{\text{exit}})$ is the critical angle corresponding to the exit electron energy; see Fig. 31. This means—as is the basis of the discussion connected to Eq. (86)—that the electrons are captured in high-lying states in the potential. They are thus transferred from the random to the channeled beam. For positrons Δ_θ is always positive and large, corresponding to strong angular heating (Kirsebom *et al.*, 2001b).

The radiative cooling scales as $(\delta\langle\theta^2\rangle/\delta L)_{\text{rad}}\propto Z^3$ for small χ and $(\delta\langle\theta^2\rangle/\delta L)_{\text{rad}}\propto Z^2/E$ for $\chi\gg 1$ (Kononets, 1999). Compared to the multiple scattering $(\delta\langle\theta^2\rangle/\delta L)_{\text{ms}}\propto Z^2/E^2$ this means that the net radiative cooling is expected to be much stronger at higher energies.

These results clearly show that electrons incident on crystals outside the channeling region are cooled and thereby can be captured into the channeling region. For practical use, unfortunately, these cooled electrons have lost and dispersed a considerable amount of energy—i.e., the total emittance (transverse and longitudinal) is not getting smaller.

It is also possible to estimate the main region of transverse positions $r_\perp$ where photon emission takes place. This can be done by a comparison of incident and exit angles for electrons and positrons together with emission angles for the photons that they respectively emit. The angle of photon emission is found by tracking the produced pair in the pair spectrometer to find the production vertex; see Fig. 7. By a comparison with the incident electron track, the angle of the electron during emission θ_γ is found.

Figure 30 shows the difference between exit and incidence polar angles as a function of entry angle. Here a clear correspondence is seen between positrons and "electron photons" and also between electrons and "positron photons" in the incident angle region (60–160 μrad). Because of the surface transmission, the continuum potential is low for nearly all particles, $U(r_{\perp\text{in}})\simeq 0$ at the point of particle entrance. We get the polar angle θ_γ at the point of photon emission, $r_{\perp\gamma}$, by setting the small emission angle to zero and as a first approximation neglecting the multiple Coulomb scattering,

$$\frac{1}{2}pv\theta_{\text{in}}^2=\frac{1}{2}pv\theta_\gamma^2+U(r_{\perp\gamma}) \tag{87}$$

giving

$$\Delta_\gamma=\theta_\gamma^2-\theta_{\text{in}}^2=\frac{-2U(r_{\perp\gamma})}{pv}, \tag{88}$$

i.e., for the photons originating from electrons $[U(r_{\perp\gamma})<0]$ Δ_γ should be positive and vice versa for positrons.

From Fig. 30 it is found that $\theta_\gamma^2-\theta_{\text{in}}^2$ for electron photons is positive, which is only possible for $U(r_\perp)$ large (Kirsebom *et al.*, 2001b)—corresponding to a strong field. The conclusion from these experiments is that the hard photons are emitted close to the nuclei, i.e., at small $r_\perp$. This experimental finding is in sharp contrast to some calculations (Augustin *et al.*, 1995).

In Fig. 30 it can also be clearly seen that positrons are heated over the whole incident angle region similar to electrons incident in the channeling region, whereas electrons outside the channeling region are cooled.

A more thorough investigation of the polar-angle difference as a function of single photon energy shows another interesting result: the harder the photon, the closer to the axis it is produced (Kirsebom *et al.*, 2001b).

E. Spin flip

Figure 32 shows experimental results from Kirsebom *et al.* (2001a) for the emission power of photons from a 243-GeV electron in 0.2-mm W $\langle 111\rangle$, aligned close to the axis but outside the channeling region. The experimental values are in fair agreement with the curve where spin-flip transitions are included and are clearly different from the calculation excluding spin effects. The calculations shown are simply the quantum synchrotron-radiation-emission values for the value of χ found from Eq. (61), but more elaborate calculations reach essentially the same conclusion (Korol *et al.*, 2002).

F. Quantum suppression

The energy loss in classical synchrotronic motion in a constant field is proportional to E^2, whereas the energy loss due to incoherent bremsstrahlung from a foil is proportional to E. Thus for the classical region of radiation

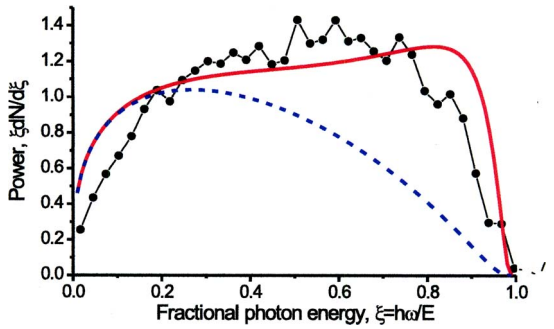

FIG. 32. (Color online) Power spectrum of radiated photons $\xi dN/d\xi$ for 243-GeV electrons aligned 0.3 mrad from the axis in 0.2-mm W ⟨111⟩. Filled circles denote the experimental points and the lines (solid, including spin; dashed, excluding spin) the calculated values. Adapted from Kirsebom *et al.*, 2001a.

emission from synchrotronic motion in a crystal, an enhancement proportional to E is expected. Analogously, in the extreme quantum case an enhancement proportional to $E^{-1/3}$ is expected; see Table II. As seen from Fig. 33, the situation at a few hundred GeV in W is between these two extremes, showing clearly the onset of quantum suppression. Experimentally, the enhancement is defined as the ratio of effective radiation lengths, $\eta = X_0^{\mathrm{BH}}/X_0^{\mathrm{SF}}$, where X_0^{BH} is the Bethe-Heitler value for the radiation length and X_0^{SF} is the effective radiation length for the strong-field case. A high-Z crystal in a hundred-GeV beam thus gives the opportunity of investigating a "quantum synchrotron," i.e., synchrotron-radiation emission in the quantum regime.

Baier's group (Baier *et al.*, 1986a, 1998) has given a "rough estimate" of the enhancement η:

$$\eta \simeq \frac{mca_s}{3Z_2\alpha\hbar \ln(183Z_2^{-1/3})}, \quad 1 < \chi < 15. \tag{89}$$

In the case of tungsten, this estimate of the enhancement becomes $\eta \simeq 9$, whereas Kononets estimates from a calculation based on the CFA that $\eta \simeq 7$ from about 30 GeV to a few thousand GeV (Kononets, 1988). Clearly, the rough estimates are in very good agreement with experiment, and they show that in this region the dependence on energy can be neglected to a first approximation.

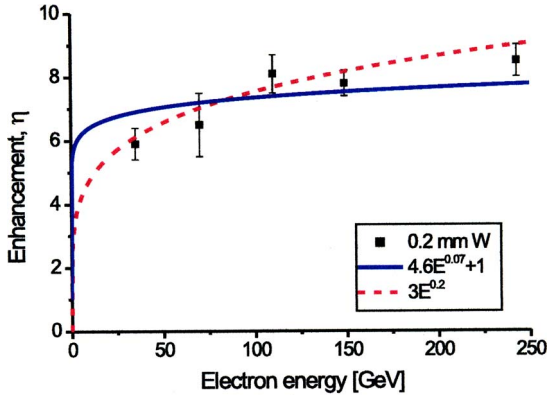

FIG. 33. (Color online) The enhancement η for radiation emission from 0.2-mm W ⟨111⟩. The points with error bars are the experimental values, the dashed line is a least-squares fit by $\eta = aE^b$, and the solid line is a fit with $\eta = aE^{0.07}+1$, where a and b are free parameters. Adapted from Kirsebom *et al.*, 2001a.

The dotted line shown in Fig. 33 is a least-squares fit by $\eta = aE^b$ to extract the exponent in the power law for this particular energy region, which from Eq. (59) should be 0.07 and comes out as 0.19 ± 0.04. These exponents are in fair agreement considering the simplicity of the fitting function which does not include, for example, the incoherent contribution or the variation with χ. To include the incoherent contribution and the expected power from Eq. (59) (averaged over $[1 \leqslant \chi \leqslant 10]$), the solid line in Fig. 33 is a fit with $\eta = aE^{0.07}+1$, where a is a free parameter. The agreement between data and these simple estimates is satisfactory, although the enhancement becomes slightly low.

VIII. NONCRYSTALLINE STRONG FIELDS

A. Astrophysical strong fields

Following a semiclassical argument (Duncan, 2000) we can calculate the excitation energy of an electron in a strong magnetic field B_0. From the gyration radius $r_c = p_\perp c/eB$ and the uncertainty relation $r_c p \simeq \hbar$ we get a semiclassical gyration radius $r_c = \lambda\!\!\!^{-}_c \sqrt{B_0/B}$ and from $\omega \simeq c/r_c$ we finally get the relative excitation energy in a strong field,

$$\frac{\hbar\omega}{mc^2} \simeq \sqrt{\frac{B}{B_0}}, \tag{90}$$

which shows that the gyration becomes relativistic in fields $B \gtrsim B_0$; see also Eq. (36). There is substantial evidence that pulsars with fields at and above this strength—so-called magnetars—exist. A recent example is the $\simeq 10^{11}$ T magnetar detected in the soft gamma repeater SGR 1806-20 (Ibrahim *et al.*, 2003) which yielded a giant flare at the end of 2004 (Yamazaki *et al.*, 2005).

B. Strong fields in nuclear collisions

As a measure of the electric field a $1s$ electron is exposed to, let us consider the ratio of this field to the critical field, $\mathcal{E}_{1s}/\mathcal{E}_0 = \alpha^3 Z^3$, where effects such as relativistic corrections, reduced mass, and extension of the nucleus are neglected. Clearly, for a nuclear charge number of $Z = 137$ a $1s$ electron is in a strong field. Equivalently, the binding energy "dives" into the negative-energy continuum for $Z = 137$ (and for extended nuclei $Z \simeq 172$) and a pair is created. During the collision of two nuclei with a combined charge exceeding $172|e|$, a quasimolecular state with a very short existence may be generated from which positron emission has been observed. So by means of collisions of heavy nuclei, strong-field QED may be investigated. However, since the nuclear collision is of extremely short duration,

$\approx 10^{-22}$ s, the strong field in this case is far from constant. For a review see, e.g., Greiner *et al.* (1985).

C. Strong laser fields

Another technically demanding example of investigations of strong fields is in multi-GeV electron collisions with terawatt laser pulses in which nonlinear Compton scattering and so-called Breit-Wheeler pair production are observed (Burke *et al.*, 1997; Bamber *et al.*, 1999). Breit-Wheeler pair production is the production of an electron-positron pair in a photon-photon collision. In order to get sufficient energy in the center-of-mass system to pair produce, at least one of the photons must be very energetic. This has been achieved by nonlinear Compton backscattering of laser photons off an intense, high-energy electron beam. In nonlinear Compton backscattering, several photons are absorbed but only one is emitted. In this case χ is again a crucial parameter. For a future $\gamma\gamma$ collider, these strong-field effects must be avoided in order not to deplete the photon beams produced by Compton backscattering off intense laser pulses (Chen and Telnov, 1989). Moreover, the effect of the electron spin becomes even stronger in the case of interactions with strong laser fields as compared to crystalline strong-field effects (Khokonov *et al.*, 1998, 2002).

Other theoretical schemes proposed to produce fields approaching the Schwinger limit is by laser reflection off a relativistic "mirror" made by a propagating wakefield in a plasma (Bulanov *et al.*, 2003) or an x-ray free-electron laser interacting with a relativistic ion (Müller *et al.*, 2003).

D. Strong fields in beam-beam interactions

In the construction of linear colliders an important phenomenon is the emission of beamstrahlung due to the interaction of one electron bunch with the electromagnetic field from the opposing electron bunch. In the rest frame of one bunch the field of the other bunch is boosted by a factor $2\gamma^2$ and may approach or even exceed critical-field values. The emission of beamstrahlung can be expressed as a function of χ (often called Υ in the accelerator physics community), which for the Stanford Linear Collider is small $\simeq 10^{-3}$ but of the order unity for the next-generation linear colliders (Chen and Yokoya, 1988). Thus for these future colliders $\gamma\gamma$ collisions may be generated from the beams themselves or special bunch structures must be applied to avoid rapid beam deterioration from strong-field effects (Blankenbecler and Drell, 1988).

For a future linear collider operating in the "quantum regime," the beamstrahlung spectrum becomes similar to the spectrum shown in Fig. 16; see solid line in Fig. 34.

E. Unruh effect and Hawking radiation

The equivalence between the temperature of the Hawking radiation from a black hole and the temperature of the vacuum in a constantly accelerated frame (Davies, 1975; Unruh, 1976) has been widely discussed—the so-called Unruh effect. As channeled particles are subject to enormous fields and accelerations, outlines for possible detection schemes using strong crystalline fields have been proposed (Darbinian *et al.*, 1989; MacDonald, 1998). Darbinian *et al.* (1989) estimated that a planar-channeled positron with $\gamma \gtrsim 10^8$ will emit Unruh radiation as intense as the incoherent bremsstrahlung. These estimates, however, do not take into account the subtleties connected to the inherently nonconstant acceleration for a channeled particle.

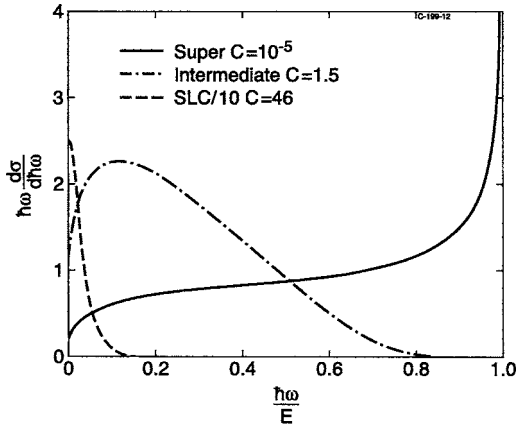

FIG. 34. Three examples of beamstrahlung power spectra where the horizontal scale is the fractional photon energy and the constant C here is approximately equal to $1/\chi$. Adapted from Blankenbecler and Drell, 1987.

The Unruh effect gives rise to a Planckian photon spectral distribution at a temperature

$$T = \frac{\hbar a}{2\pi k_B c}, \tag{91}$$

where a is the acceleration and k_B the Boltzmann constant. Several other methods have been proposed to explore the problem of measuring the Unruh temperature experimentally. For an overview of these methods and a review of the literature on the subject see, e.g., Rosu (2004).

Along this line of thought, a fascinating analogy exists between the critical field and the Hawking radiation from a black hole. The gravitational acceleration at the Schwarzschild radius $R_S = 2GM/c^2$ equals $g(R_S) = c^4/4GM$, where G is Newton's constant and M the mass of the black hole. Setting this equal to the acceleration at the critical field $g_0 = e\mathcal{E}_0/m = c^2/\lambda\!\!\!^{-}_c$ the condition $\lambda\!\!\!^{-}_c = 2R_S$ is obtained, i.e., the black hole can emit particles with a wavelength that is as large as or larger than the hole itself. This is approximately what is obtained in a full analysis of the Hawking radiation (Davies, 1978) and the analogy becomes even more compelling by interpreting the field as a temperature as is done for the Unruh effect, Eq. (91): $T_0 = e\mathcal{E}_0\hbar/2\pi m k_B c$ (Müller *et al.*, 1977) and inserting $g(R_S) = c^4/4GM$ in-

stead of $g_0 = e\mathcal{E}_0/m$ in T_0 to get the correct Hawking temperature (Greiner *et al.*, 1985):

$$T_0 = \frac{\hbar c^3}{8\pi GMk_B}. \tag{92}$$

The Hawking radiation can thus be viewed as a critical-field phenomenon and it is easy to see why light black holes are "hotter" than heavy ones—the gradient $g(R_S)$ is simply larger allowing shorter wavelenghts to be emitted.

F. The geomagnetic field as a strong field

With facilities such as the Pierre Auger Observatory (Watson, 1998) for the detection of ultra-high-energy cosmic rays of energies in the EeV (10^{18} eV) region and orders of magnitude above, pair production and photon emission in the magnetic field of the Earth become increasingly relevant. This phenomenon was first studied by Pomeranchuk (1940), later revived by McBreen and Lambert (1981), and recently by, e.g., Stanev and Vankov (1998), as well as in extended air-shower simulations (Plyasheshnikov and Aharonian, 2002). One important issue in this context is the possibility of distinguishing photon-initiated extended air showers from those initiated by protons or heavy nuclei. Such a distinction may shed light on the question of "top-down" (topological defects, massive X particles) or "bottom-up" (acceleration of known particles) mechanisms (Stanev, 1998; Olinto, 2000; Shinozaki *et al.*, 2002).

The behavior of an EeV electromagnetic shower initiated in the Earth's magnetic field and that of a GeV shower in a crystal (Baurichter *et al.*, 1999) are intimately related. This is because the decisive χ is about equal in the two cases and their developments are both affected by, for example, multiple scattering and LPM effect (Uggerhøj, 2003).

Figure 35 shows a calculation based on Eq. (77) similar to that shown in the articles of McBreen and Lambert (1981) or Stanev and Vankov (1998) [who use the simpler Eq. (80)] to determine the conversion probability of a photon in the geomagnetic field. A dipole field with values of 0.25 and 0.528 G at the surface of the Earth has been assumed. This corresponds to the planned and constructed sites of the Pierre Auger Observatory. The close analogy between the two processes makes crystals a suitable testing ground for the development of computer codes to simulate the behavior of extended air showers.

Finally, for sufficiently energetic photons even the intergalactic fields will appear as a strong field and generally speaking the Universe thus will become "opaque" to these photons. As intergalactic fields are quite weak, $\approx 10^{-12}$ T, this happens at very high energies only.

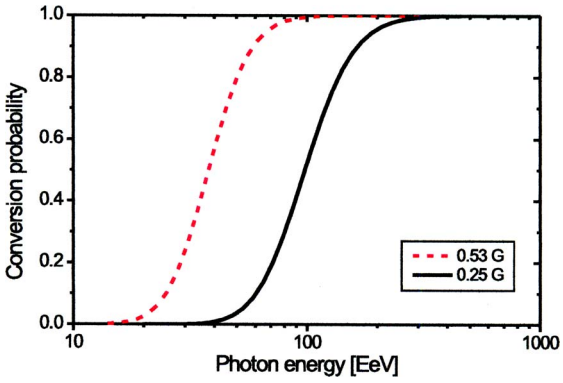

FIG. 35. (Color online) The conversion probability of a photon in the geomagnetic field as a function of photon energy for energies in the region 10^{19}–10^{21} eV (10–1000 EeV). The dashed line represents the conversion probability for a magnetic field corresponding to the site of the southern part of the Pierre Auger Observatory and the solid line represents that corresponding to the northern part. Adapted from Uggerhøj, 2003.

IX. APPLICATIONS OF STRONG CRYSTALLINE FIELDS

A. Radiation sources

The ideal radiation source is simple, monochromatic, tunable, and intense (possibly even coherent). In the following we show that crystals as radiation sources fulfill many of these criteria.

1. Strings-of-strings radiation

The appearance of a high-energy-photon peak from electrons traversing a crystal in a planar orientation, but with a small angle ($\lesssim$1 mrad), to a low-index axis is ascribed to a coherent resonance. This resonance is obtained when the electron passes the strings forming the plane in the strings-of-strings region. As discussed above it is similar to the usual coherent phenomenon obtained when the electron passes planes and is therefore a tunable γ source. One experiment (Kirsebom *et al.*, 1999) was performed to verify the expectation that these so-called strings-of-strings photons were linearly polarized; see below.

The position of the peak in the spectrum is found as for "standard" coherent bremsstrahlung from Eq. (82). The enhancement observed, ranging up to around 50 for diamond [see Fig. 28(a)] is in good agreement with the value expected from the CFA (Baier *et al.*, 1992).

The radiative cooling may be helpful in producing a strong γ source. For normal channeling radiation the useful incident-angle region is very narrow, especially in the GeV region since the critical angle narrows as $1/\sqrt{p}$. The cooling effect increases this incident-angle region as above-barrier particles may be captured into channeling states.

2. Crystalline undulator

With a superperiodicity imposed by either ultrasound (Korol *et al.*, 1998), strain in Si-Ge interfaces (Mikkelsen and Uggerhøj, 2000), or surface defects (Bellucci *et al.*, 2003, 2004) it is theoretically possible to generate high-intensity, nearly monochromatic radiation in a crystalline undulator (Korol *et al.*, 1998, 1999, 2001, 2002; Avakian *et al.*, 2001). Although it is advantageous to use positrons to generate radiation because of decreased multiple scattering (Krause *et al.*, 2000; Mikkelsen and Uggerhøj, 2000) it is desirable to investigate the behavior of electrons, in particular, in view of its potentialities as an efficient positron source with low output emittance. In this case, the strong-field effect must be avoided in order not to deplete the penetrating positron beam (Mikkelsen and Uggerhøj, 2000). A long-term goal is to investigate the potential of a crystalline undulator as a γ-ray laser, i.e., in the stimulated emission mode (Krause *et al.*, 2001). This would require positron densities of the order 10^{21} cm^{-3} (Korol *et al.*, 1999; Krause *et al.*, 2001), only about two orders of magnitude less than the electron density in a typical metal. Although at first sight this might seem far-fetched, (electron) densities of the order 10^{21} cm^{-3} are actually available at the final focus test beam at SLAC and theoretical schemes to increase this by a factor of 30 have been devised (Emma *et al.*, 2001). Furthermore, it is known from experimental tests that a diamond crystal bears no visible influence from being irradiated by the final focus test beam, whereas amorphous aluminum simply evaporates (Krejcik, 2001).

The use of the Bormann effect of x-ray transmission has also been proposed to accelerate channeled muons in superlattice crystals (Tajima and Cavenago, 1987).

B. Bent crystals

The following section on ions (from protons to lead) in bent crystals can be seen as a short digression from the main theme, strong crystalline fields, where strong is understood as comparable to the critical field in the particle rest frame. Such fields may barely be achievable for protons from the coming Large Hadron Collider with 7-TeV protons channeled along an axis in a heavy crystal such as tungsten, but are not experimentally relevant yet. However, with this interpretation of a strong as compared to a normal—or even superconducting—magnet field, it turns out that crystalline fields for ions are indeed strong.

The guidance of channeled particles in a crystal persists even if the crystal is slightly bent, such that the particle may be deviated from its original direction of motion as in a magnetic dipole. Since the fields that are responsible for this deviation are the extremely strong fields present near the lattice nuclei, the corresponding bending strength can reach a magnitude of several thousand tesla. It is therefore possible to design a crystalline "kicker" with an equivalent deflection power of 10 T m by use of a device that is of the order 0.1 m long.

A comprehensive review of channeling in bent crystals, with emphasis on the contributions from the Russian groups, can be found in the book by Biryukov *et al.* (1997). Baurichter *et al.* (2000) have given a concise introduction to the field along with a summary of the results obtained at the CERN SPS. In these texts extensive reference lists are included. For a short introduction to the field, see Møller (1995).

1. Bending of particle beams

When one considers the strong fields in a crystal it is apparent that a crystal has a superb bending power. One can calculate the equivalent magnetic field $B=\kappa p/Z_1 e$ corresponding to the so-called critical curvature κ_c discussed below as

$$B_c[\mathrm{T}] = 1.5 \times 10^3 Z_2 n d_p \ (\text{Å}^{-2}). \tag{93}$$

This critical field is $B_c \simeq 2500$ T for a silicon crystal. Clearly Eq. (93) shows that a high-Z material is preferable for deflection.

2. Critical curvature

There is a certain curvature at which the particles will dechannel in a bent crystal due to the centrifugal force that tends to increase the interactions with the lattice nuclei. Estimating this curvature, it was found that as long as the curvature fulfills the condition

$$\kappa \leqslant \kappa_c = \frac{\pi Z_1 Z_2 e^2 N d_p}{p v} \tag{94}$$

the charged particle can channel in a bent crystal. The minimum radius of curvature $R_c = 1/\kappa_c$ at 7 TeV is 11.5 and 5.48 m for the (110) planes in Si and Ge, respectively. As κ_c is approached a rising fraction F, the so-called dechanneling fraction, is lost from the channeled states and is therefore unable to follow the curvature through the whole crystal.

3. Dechanneling

The length L_D over which a planar-channeled beam of protons in a straight crystal has been reduced to the fraction $1/e$ of the initial intensity by transfer to nonchanneled states by multiple scattering is given for $\gamma \gg 1$ by (Biryukov *et al.*, 1994)

$$L_D = \frac{256}{9\pi^2} \frac{p\lambda\!\!\!^{-}}{\ln(2\gamma mc^2/I_Z) - 1} \frac{a_s d_p}{Z_1 e^2}, \tag{95}$$

where I_Z is the ionization potential. Equation (95) has been shown to be in good agreement with measured values of L_D at room temperature over a fairly wide range of energies. At 7 TeV, the values of L_D for Si and Ge are 2.9 and 2.5 m which, as will be shown shortly, by far exceed the dimensions of the crystals proposed for use.

4. Model for deflection efficiency

Since the straight crystal dechanneling favors small crystal lengths and the curvature favors long crystal

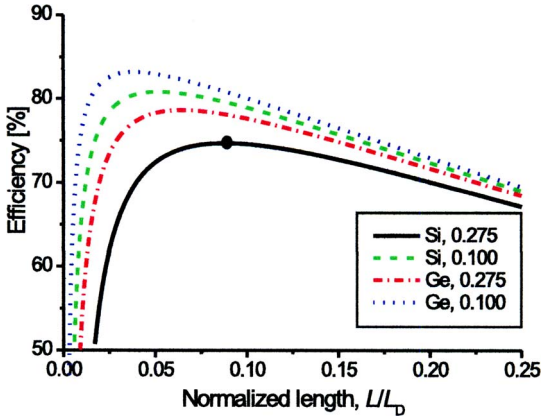

FIG. 36. (Color online) Efficiency as a function of normalized length L/L_D at 7 TeV according to Eq. (96) for Ge (110) and Si (110). The solid line is for Si bent to $\theta=0.275$ mrad, the dash-dotted line for Ge bent to $\theta=0.275$ mrad, the dashed line for Si bent to $\theta=0.100$ mrad, and the dotted line for Ge bent to $\theta=0.100$ mrad. The values $\eta_F=3$ and $\varepsilon_S=0.9$ were used (see text). Shown by a filled dot is the efficiency, Eq. (99), at optimum length, Eq. (98), for Si bent to an angle $\theta=0.275$ mrad (Uggerhøj and Uggerhøj, 2005).

lengths (for fixed angle), there is an optimum crystal length which depends on the angle and which is only weakly dependent on energy when the length is expressed in units of the dechanneling length (Baurichter *et al.*, 1996). Given $\eta_F=F_D\kappa_c/\kappa\simeq 3$, where F_D is the dechanneling fraction, the approximate deflection efficiency is (Baurichter *et al.*, 2000)

$$\varepsilon_{\text{appr.}}=\varepsilon_S\exp\left(-\frac{L}{L_D}\right)\left[1-\eta_F\frac{\theta}{(L/L_D)L_D\kappa_c}\times\left(1+2\frac{L}{L_D}\right)\right], \tag{96}$$

where

$$L_D\kappa_c=\frac{256}{9\pi}\frac{Z_2Nd_p^2a_s}{\ln(2\gamma mc^2/I)} \tag{97}$$

is only logarithmically dependent on energy and is 0.251 and 0.451 for Si and Ge along (110) at 7 TeV. Here L denotes the crystal length and the crystal is assumed to have a uniform curvature.

Equation (96) has a maximum at the optimum length

$$\frac{L}{L_D}=-\frac{1+\sqrt{1-4(2-L_D\kappa_c/\eta_F\theta)}}{2(2-L_D\kappa_c/\eta_F\theta)} \tag{98}$$

with an efficiency value at this maximum of

$$\varepsilon_{\text{max}}^{\text{appr.}}\simeq\varepsilon_S\left[\left(1-\sqrt{\frac{\eta_F\theta}{L_D\kappa_c}}\right)^2-2\frac{\eta_F\theta}{L_D\kappa_c}\left(1-\sqrt{\frac{\eta_F\theta}{L_D\kappa_c}}\right)\right]. \tag{99}$$

An example of values is given in Fig. 36 for the Large Hadron Collider relevant case $\theta=0.275$ mrad. The surface transmission has been set to $\varepsilon_S=0.9$, a realistic but somewhat arbitrary value. The angle $\theta=0.100$ mrad is also shown to display the weak dependence of the optimum efficiency on angle.

5. Extraction of particles

Multipass extraction schemes yield extraction efficiencies that are higher than the single-pass extraction for beam divergencies larger than the planar critical angle. The reason is that particles that encounter the crystal and are not channeled will not necessarily be lost and may be extracted on a later turn in the machine. Furthermore, parameters of the accelerator lattice, such as the betatron amplitude function that determines the beam size and divergence, become important for the extraction efficiency.

An actual implementation of a crystalline extraction device at the coming Large Hadron Collider at CERN has recently been proposed (Uggerhøj and Uggerhøj, 2005). This would enable a nearly continuous beam of 7-TeV protons extracted towards the Large Hadron Collider beam dump with an intensity of $\simeq 5\times 10^8$ per second and a horizontal emittance as low as 20 μm μrad.

6. Detection of spin of short-lived particles

Analagous to a top possessing an angular momentum in the gravitational field of the earth, a moving particle possessing a magnetic moment will precess in an inclined magnetic field. Therefore since the field in a bent crystal is equivalent to a strong magnetic field, a charged particle with spin s and magnetic moment $\mu=g_\mu\mu_B s$ will precess during the passage of a bent crystal if the spin and magnetic field are inclined. Here, g_μ is the gyromagnetic ratio, $\mu_B=e\hbar/2mc$, $\mu_N=e\hbar/2m_pc$, the Bohr magneton and the nuclear magneton, respectively, and m_p is the mass of the proton. For an ultrarelativistic particle with $g_\mu\neq 2$ the connection between the spin precession θ_s and the change of momentum direction θ_p is (see also Baryshevskii, 1979, for an early discussion of the effect)

$$\theta_s=\frac{g_\mu-2}{2}\gamma\theta_p. \tag{100}$$

Therefore if $\gamma\gg 1$, a polarized beam will appear with a markedly different polarization after the bending, even if the bending angle is small. Since the distance over which it will precess through a given angle in a crystal is drastically shortened compared to that in a magnet, one may use this effect to measure magnetic moments of short-lived particles. This effect has been used in a proof-of-principle experiment to measure the magnetic moment of the Σ^+ (Chen *et al.*, 1992), a hyperon with $\mu=2.46\mu_N$, and a short proper lifetime $c\tau=2.4$ cm.

To take this further, it has been proposed that the magnetic moments of charmed baryons be measured by use of the spin precession in bent crystals. For these, the typical lifetime is shorter than for hyperons by a factor

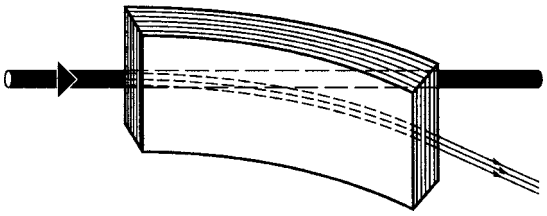

FIG. 37. A schematical drawing of extraction of particles from the halo of a circulating beam by means of a bent crystal. From Møller, 1995.

≈500, so very short crystals have to be used (Baublis *et al.*, 1994; Samsonov, 1996). In this case a high-Z crystal would be preferable (see Fig. 37).

C. Ultralow emittance beams

Inspired by the phenomenon of radiative cooling discussed in Sec. VII.D in which the transverse emittance diminishes, the quantum excitation-free radiation emission in a single crystal has been explored (Huang *et al.*, 1995, 1996). The idea is that analogous to the behavior in a synchrotron, radiation emission leads to beam cooling. Moreover, as a channeled beam is in a "continuous focusing environment," the recoil imposed by the radiation emission may be taken by the crystal as a whole, possibly leading to an exceptionally low emittance. In their papers, Huang and co-workers show that the transverse action—and thereby the emittance—decreases exponentially towards the minimum value $\hbar/2$, corresponding to the ultralow emittance of half of the Compton wavelength. This applies as long as the radiation is in the undulator regime where the angle of emission is larger than the pitch angle. However, their approach explicitly does not take into account multiple scattering. Including this effect, the damping effect originating from the photon emission becomes antidamping, except possibly with the imposition of very specific conditions on the beam incidence and crystal type (Baier and Katkov, 1997; Uggerhøj, 2004b). The calculations with inclusion of multiple scattering match at least qualitatively that of experimental results on the cooling mechanism (Baurichter *et al.*, 1997; Uggerhøj, 2004b).

D. Generation of polarized GeV photons

The so-called spin crisis in high-energy physics, which deals with the question of the origin of the spin of the nucleon, has attracted a great amount of interest during the last decades and several experiments have been performed or are being designed to solve this important puzzle; see, e.g., Adams *et al.* (1997). One way to approach the problem is through photoproduction of charmed mesons, using circularly polarized high-energy photons. The advantage is that in the case of circular polarization—as opposed to linear—the helicity of the photon is a well-defined quantity such that from the distribution of the decay products of the meson one may derive the influence of the spin of the struck parton or gluon.

Circularly polarized photons can be produced by Compton backscattering of laser light, but this requires an extremely powerful laser and a very dense electron beam (Ginzburg *et al.*, 1983). On the other hand, circularly polarized photons can be produced by passing an unpolarized electron beam of any density through a crystalline target where the electrons emit linearly polarized gamma rays. These photons can—according to an old idea (Cabibbo *et al.*, 1962)—be converted into circularly polarized photons in the equivalent of a "quarter-wave" plate; see also Baryshevskii and Tikhomirov (1982, 1989). In such a device the difference between the real parts of the indices of refraction times the photon frequency must equal $\pi/2$ over the thickness of the crystal, i.e., $\mathrm{Re}(n_{r\perp}-n_{r\parallel})\omega\Delta t_f/c=\pi/2$ such that one component of the polarization vector gains a phase factor $e^{i\pi/2}$ with respect to the other to generate circular polarization.

Photons can be converted efficiently into electron-positron pairs by means of another aligned crystal as was, for example, done in the NA48 experiment at CERN (Moore *et al.*, 1996). If the photons are indeed polarized, one may expect a birefringence effect (a dependence on the photon polarization of the pair-production yields) of the conversion crystal from symmetry of the processes $e^-+\bar{\gamma}\rightarrow e^-+\gamma$ (bremsstrahlung) and $\gamma+\bar{\gamma}\rightarrow e^-+e^+$ (pair production), where $\bar{\gamma}$ denotes a virtual photon of the crystalline field.

Substantial interest in the application of polarized high-energy photons from crystals for photoproduction experiments has been expressed at CERN (Bilokon *et al.*, 1983; Bussey *et al.*, 1983; Apyan *et al.*, 1998a, 2001), at Fermilab (Kasper, 1996), and at SLAC (Apyan *et al.*, 1998b). Another proposal is to generate polarized $e^{\pm}$ beams by means of bent crystals as the $\gamma\rightarrow e^+e^-$ conversion target (Baryshevskii and Tikhomirov, 1988).

1. Linear polarization

One of the experiments performed by the NA43 Collaboration was concerned with the proof of linear polarization of the strings-of-strings radiation and a detection of a birefringent effect in the conversion of these photons into electron-positron pairs (Kirsebom *et al.*, 1999).

As shown above, ultrarelativistic electrons incident on a crystal near the axis along a plane generate very energetic radiation (the so-called strings-of-strings radiation) which may be utilized as a source of high-energy photons. The experimental result (Kirsebom *et al.*, 1999) indicated a substantial degree of linear polarization, in contrast to calculations that (later) showed a rather modest polarization degree of the high-energy peak (Darbinyan and Ter-Isaakyan, 1999, 2002; Strakhovenko, 2002). As already stated by Kirsebom *et al.* (1999), the admixture of channeling radiation that could not be deconvoluted in the experiment was a possible cause of misinterpretation of the ≈10% asymmetry

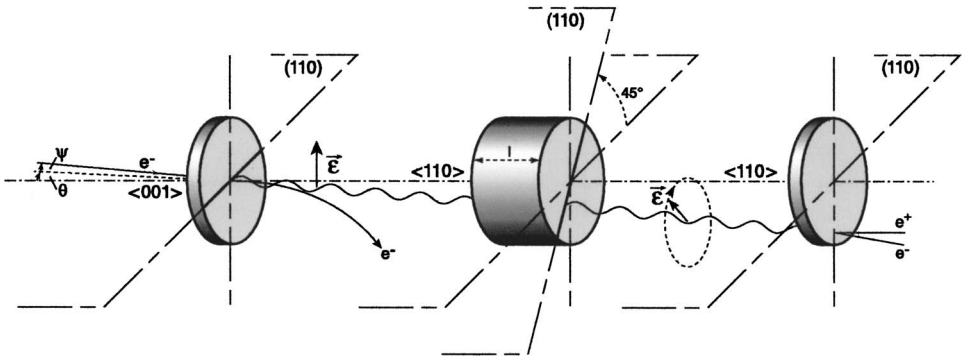

FIG. 38. An outline of the setup used in NA59. The leftmost crystal produces energetic, linearly polarized photons by electrons incident with an angle $\theta=5$ mrad to the $\langle 001\rangle$ axis and an angle $\psi=70$ μrad to the (110) plane. The emerging photons are converted into circularly polarized photons in the thick, central crystal aligned with an angle 2.3 mrad to the $\langle 110\rangle$ axis. The last crystal acts as an analyzer where the pair-production rate depends on the polarization state for photons incident with an angle 3 mrad to the $\langle 110\rangle$ axis.

found. It is thus possible that the highly polarized planar-channeling radiation emitted simultaneously with the strings-of-strings radiation was responsible for the comparatively large asymmetry.

2. Circular polarization

A later experiment at CERN, NA59 (Apyan *et al.*, 1998a, 2005), aimed to provide definite proof for the usefulness of the crystal equivalent of a quarter-wave plate (Unel *et al.*, 2001). In other words, it is a crystal that—as for normal optics—due to a difference in the refraction index along different planes can generate circularly polarized GeV photons from linearly polarized ones.

The setup of NA59 eventually came to be quite close to the later stages of NA43, but with a 10-cm-thick Si crystal acting as the quarter-wave plate. This thickness was carefully optimized as a tradeoff between attenuation of the photon beam and efficient conversion into circular polarization, taking into account a number of experimental effects such as divergence of the beam (Strakhovenko, 2001). An outline of the setup of the three crystals is shown in Fig. 38. Furthermore, substantial theoretical effort was put into an optimization of the radiating crystal orientation and thickness (Strakhovenko, 1998, 2002) expanding the applicability of earlier theoretical methods (Baier *et al.*, 1988b).

The polarization degree of coherent bremsstrahlung was used as a proof of principle of the technique used in NA59 (Apyan *et al.*, 2004a) [similar to that of Bussey *et al.* (1983)]. Furthermore, NA59 observed indications of the conversion from linear to circular polarization in a crystalline quarter-wave plate (Apyan *et al.*, 2004b) and demonstrated that the strings-of-strings mode—in agreement with recently developed theory—provided at most a polarization degree of 20% (Apyan *et al.*, 2004c).

Polarization properties in strong magnetic fields may be a route to investigating the structure of the magnetosphere of pulsars (Xu *et al.*, 2000).

E. Search for short-lived photoproduced particles

Strong crystalline fields were employed in the mid 1990s to search for the "Darmstadton"—the conjectured X particle responsible for the appearance of narrow lines of positron emission. These lines were superimposed on the expected contribution of positron creation from the strong-field QED in collisions of heavy ions, but were by the late 1980s considered doubtful as an indicator of new particles (Schäfer, 1989). The idea behind utilizing crystals was that a strong field was required for the production of the X particle (Bassompierre *et al.*, 1993, 1995). Indeed, by a comparison to a Monte Carlo–generated spectrum for the aligned $\langle 110\rangle$ Ge crystal, nine candidate events—of which only one could be accounted for by background—between 2.1 and 3.5 MeV/c^2 were found. However, as stated by the authors, "To be conclusive, an explicit measurement of the background with a misaligned crystal should have been done," i.e., the experiment could not provide a definite conclusion concerning the possible existence of a Darmstadton. Meanwhile, more accurate experiments investigating the positron emission lines have found no evidence for the effect (Ahmad *et al.*, 1997). However, the crystal-based technique utilized to examine the possible existence of strong-field generated short-lived particles was proven to be quite powerful.

X. CONCLUSION

It is perhaps surprising that the combination of ultrarelativistic particles (photons and/or leptons) and crystals allows us to investigate the behavior of fundamental processes in electromagnetic fields that are so strong that, for example, the emission of synchrotron radiation changes character. Nevertheless, since the mid 1980s, a number of experiments and theoretical developments have led to a thorough understanding of strong crystalline fields. Among the many interesting future possibilities are measurements of photon splitting and "Klein-like" trident production in strong fields.

A number of parallels and analogies exist, relevant to, for example, beamstrahlung, radiation from highly magnetized pulsars, and the processes in the "strong" geomagnetic field. Furthermore, strong crystalline fields find applications in subjects ranging from efficient $\gamma \rightarrow e^+e^-$ conversion through extraction of particles from accelerators to γ-ray sources.

Finally, it seems useful to continue this investigation in which the foundations are known to be on a fundamentally valid basis as for quantum electrodynamics, and then draw parallels to other, less-well-established fields such as QCD, e.g., in the strong-field or shortened formation length domains. Crystals present a uniquely simple tool for such a scenario.

ACKNOWLEDGMENTS

The author gratefully acknowledges the strong support from the members of the NA43, NA59, and LPM Collaborations at CERN, notably Poul Aggerholm, Per Christensen, Konrad Elsener, Kim Kirsebom, Søren Pape Møller, Pietro Sona, Erik Uggerhøj, and Mayda Velasco. Discussions with R. Avakian, V. Baier, V. Biryukov, P. Chen, S. Darbinian, S. Dumas, J. Ellison, K. Ispirian, M. Khokonov, S. Klein, Yu. Kononets, Jens Lindhard (deceased), H. Nitta, H. Rosu, J. P. F. Sellschop (deceased), N. Shul'ga, V. Strakhovenko, Allan Sørensen, and M. Ter-Mikaelian (deceased) over the years have been highly appreciated and most valuable. The author would also like to thank A. Richter for "igniting the flame" to write this review. Finally, financial support from the Danish Natural Science Research Council is acknowledged.

LIST OF SYMBOLS

a	acceleration
a_0	Bohr radius
a_s	(Thomas-Fermi) screening length
$\vec{a}_i$	lattice primitive vector
B	magnetic field
B_0	critical magnetic field
$\vec{b}_i$	reciprocal-lattice primitive vector
c	speed of light
C_L	Lindhard's constant
d	atomic spacing along axial direction
d_p	planar spacing
e	electron charge
$e_{\lambda\mu\nu\rho}$	antisymmetric unit tensor
E	energy
$E_\perp$	transverse energy
F	force
F_D	dechanneling fraction
$F_{1,2}$	CFA correction coefficients
$F_{\mu\nu}$	electromagnetic field strength tensor
$F(q)$	atomic form factor
g	gravitational acceleration
G	Newton's gravitational constant
g_μ	gyromagnetic ratio
$\vec{g}$	reciprocal-lattice vector
$G(\vec{q})$	potential Fourier coefficient
$\hbar$	Planck's constant $(/2\pi)$
I	intensity
I_Z	ionization potential
J_q	flux of equivalent photons
k	photon wave number
k_B	Boltzmann's constant
k^ν	photon wave number four-vector
K_ν	modified Bessel function of order ν
L	bent crystal length
L_ϕ	angular momentum
l_f	formation length
l_γ	multiple-scattering length
$l_{\gamma d}$	doughnut multiple-scattering length
L_D	dechanneling length
m	electron rest mass
m_p	proton rest mass
n	atomic density
$\vec{n}$	propagation direction
N	number of atoms
N_p	number of pairs
N_γ	number of photons
n_i	integer
n_r	index of refraction
p	momentum
p^ν	momentum four-vector
$q_\parallel$	longitudinal momentum transfer
$q_\perp$	transverse momentum transfer
$\vec{q}$	reciprocal-lattice vector
r_c	gyromagnetic curvature radius
r_e	classical electron radius
R	radius of curvature
R_c	critical radius of curvature
R_S	Schwarzschild radius
$S(\vec{g})$	lattice structure factor
t	time
T	temperature
T_0	Hawking temperature
U	transverse potential
U_0	transverse-potential height
u_1	one-dimensional thermal vibration amplitude
v	speed
V	atomic potential
W	radiation probability per unit time
W_p	pair-production probability per unit time
$W_{\gamma\rightarrow\gamma\gamma}$	photon splitting probability per unit time
X_0	radiation length
$\vec{x}$	position
Z_1	projectile atomic number
Z_2	target atomic number
α	fine-structure constant
β	speed in units of c
δ	minimum longitudinal momentum transfer
δ_c	classical field-reduced fractional photon energy
$\delta(\vec{q}-\vec{g})$	Dirac delta function

δ_p	field-reduced fractional pair energy
δ_q	quantum field-reduced fractional photon energy
Δ	unit-cell volume
Δ_θ	angular cooling variable
$\mathcal{E}$	electric field
$\mathcal{E}_0$	critical electric field
ε	deflection efficiency
$\varepsilon(\omega)$	dielectric function
ε_S	surface transmission
η	enhancement
η_F	dechanneling fraction scaling variable
$\eta_\pm$	fractional energy of lepton
γ	Lorentz factor
Γ	Lorentz invariant field strength parameter
γ_p	photon "Lorentz factor"
κ	curvature
κ_c	critical curvature
κ_f	field strength in units of critical field
χ	Lorentz invariant field strength parameter
$\lambda\!\!\!^{-}_c$	Compton wavelength ($/2\pi$)
λ	photon wavelength
$\lambda_\perp$	transverse (doughnut) equalization length
λ_γ	field deflection length
μ	magnetic moment
μ_B	Bohr magneton
μ_N	nuclear magneton
ν	number of quantum states
ω	photon angular frequency
ω_p	plasma frequency
ω_0	Larmor angular frequency
Ω	solid angle
ρ	density
ρ_t	thermal vibration amplitude
ψ	particle angle
ψ_c	critical (Lindhard) angle
ψ_p	planar critical (Lindhard) angle
ψ_1	axial critical (Lindhard) angle
σ	cross section
Δt_f	foil thickness
τ	polarization time
θ	photon angle
θ_{in}	entry angle
θ_{out}	exit angle
Θ_0	Baier angle
Υ	same as χ
Δx	transverse displacement
ξ	fractional photon energy
Ξ	Lorentz invariant field strength parameter

REFERENCES

Adams, D., *et al.*, 1997, "Spin structure of the proton from polarized inclusive deep-inelastic muon-proton scattering," Phys. Rev. D **56**, 5330–5358.

Ahmad, I., *et al.*, 1997, "Search for monoenergetic positron emission from heavy-ion collisions at Coulomb-barrier energies," Phys. Rev. Lett. **78**, 618–621.

Akhiezer, A. I., and N. F. Shul'ga, 1982, "Radiation of relativistic particles in single crystals," Usp. Fiz. Nauk **137**, 561–604 [Sov. Phys. Usp. **25**, 541–564 (1982)].

Akhiezer, A. I., V. I. Truten, and N. F. Shul'ga, 1991, "Dynamic chaos in the motion of charged particles through a crystal," Phys. Rep. **203**, 289–343.

Akhmadaliev, Sh. Zh., *et al.*, 1997, in *Photon '97*, International workshop on gamma-gamma coll., edited by A. Buijs and F. C. Erne (World Scientific, Singapore), pp. 246–250.

Akhmadaliev, Sh. Zh., *et al.*, 2002, "Experimental investigation of high-energy photon splitting in atomic fields," Phys. Rev. Lett. **89**, 061802.

Andersen, J. U., 1980, "Channeling radiation and coherent bremsstrahlung," Nucl. Instrum. Methods **170**, 1–5.

Andersen, J. U., S. K. Andersen, and W. M. Augustyniak, 1977, "Channeling of electrons and positrons," K. Dan. Vidensk. Selsk. Mat. Fys. Medd. **39** (10), 1–58.

Andersen, J. U., E. Bonderup, E. Laegsgaard, B. B. Marsh, and A. H. Sørensen, 1982, "Axial channeling radiation from MeV electrons," Nucl. Instrum. Methods Phys. Res. **194**, 209–224.

Andersen, J. U., E. Bonderup, and R. H. Pantell, 1983, "Channeling radiation," Annu. Rev. Nucl. Part. Sci. **33**, 453–504.

Andersen, J. U., K. R. Eriksen, and E. Lægsgaard, 1981, "Planar-channeling radiation and coherent Bremsstrahlung for MeV electrons," Phys. Scr. **24**, 588–600.

Andersen, S. K., *et al.*, 1980, "Influence of channeling on scattering of 2–15 GeV/c protons, π^+, and π^- on Si and Ge crystals," Nucl. Phys. B **167**, 1–40.

Apyan, A. B., R. O. Avakian, P. O. Bosted, S. M. Darbinian, and K. A. Ispirian, 1998b, "Circularly polarized photon beam produced by channeled longitudinally polarized electrons," Nucl. Instrum. Methods Phys. Res. B **145**, 142–145.

Apyan, A. B., R. O. Avakian, S. M. Darbinian, K. A. Ispirian, S. P. Taroian, U. Mikkelsen, and E. Uggerhøj, 2001, "Improved crystal method for photon beam linear polarization measurement at high energies," Nucl. Instrum. Methods Phys. Res. B **173**, 149–153.

Apyan, A., *et al.*, 1998a, "Proposal to study the use of a crystal as a 'quarter-wave plate' to produce high energy circularly polarized photons," CERN/SPSC 98-17, SPSC/P308.

Apyan, A., *et al.*, 2004a, "Coherent pair production by photons in the 20–170 GeV energy range incident on crystals and birefringence," e-print hep-ex/0306028.

Apyan, A., *et al.*, 2004b, "Linear to circular polarization conversion using birefringence properties of aligned crystals for multi-GeV photons," e-print hep-ex/0306041.

Apyan, A., *et al.*, 2004c, "Measurement of coherent emission and linear polarization of photons emitted by electrons in the strong fields of aligned crystals," e-print hep-ex/0406026.

Apyan, A., *et al.*, 2005, "Results on the coherent interaction of high energy electrons and photons in oriented single crystals," Nucl. Instrum. Methods Phys. Res. B **234**, 128–137.

Artru, X., 1988, "Self-amplification of channeling radiation of ultrarelativistic electrons due to loss of transverse energy," Phys. Lett. A **128**, 302–306.

Artru, X., 1990, "A simulation code for channeling radiation by ultrarelativistic electrons or positrons," Nucl. Instrum. Methods Phys. Res. B **48**, 278–282.

Artru, X., and G. Bignon, 2001, "A semiclassical approach to the radiation damping force," in *Electron-Photon Interaction in Dense Media*, NATO ARW Vol. 49, edited by H. Wiedemann (Kluwer, London), pp. 85–90.

Artru, X., *et al.*, 1993, "Observation of channeling and blocking effect in pair creation in a Ge crystal," Phys. Lett. B **313**, 483–490.

Ashcroft, N. W., and N. D. Mermin, 1976, *Solid State Physics* (Saunders College, Philadelphia).

Augustin, J., A. Schäfer, and W. Greiner, 1995, "Quantum-mechanical treatment of high-energy channeling radiation," Phys. Rev. A **51**, 1367–1373.

Avakian, R. O., L. A. Gevorgian, K. A. Ispirian, and R. K. Ispirian, 2001, "Spontaneous and stimulated radiation of particles in crystalline and nanotube undulators," Nucl. Instrum. Methods Phys. Res. B **173**, 112–120.

Bagrov, V. G., I. M. Ternov, and B. V. Kholomai, 1984, "Radiative self-polarization of electron-positron beams in axial channeling," Zh. Eksp. Teor. Fiz. **86**, 1066–1072]. [Sov. Phys. JETP **59**, 622–625 (1984)].

Baier, V. N., V. S. Fadin, V. M. Katkov, and E. A. Kuraev, 1974, "Photon splitting into two photons in a Coulomb field," Phys. Lett. **49B**, 385–387.

Baier, V. N., and V. M. Katkov, 1967, "Processes involved in the motion of high energy particles in a magnetic field," Zh. Eksp. Teor. Fiz. **53**, 1478–1491 [Sov. Phys. JETP **26**, 854–860 (1968)].

Baier, V. N., and V. M. Katkov, 1997, "On radiation damping in planar channeling in the presence of multiple scattering," Phys. Lett. A **232**, 456–462.

Baier, V. N., and V. M. Katkov, 2002, "Deviation from standard QED at large distances: Influence of transverse dimensions of colliding beams on bremsstrahlung," Phys. Rev. D **66**, 053009.

Baier, V. N., and V. M. Katkov, 2005a, "Concept of formation length in radiation theory," Phys. Rep. **409**, 261–359.

Baier, V. N., and V. M. Katkov, 2005b, "Coherent and incoherent pair creation by a photon in oriented single crystal," e-print hep-ph/0503005

Baier, V. N., V. M. Katkov, and V. M. Strakhovenko, 1970, "Kinetics of radiative polarization," Zh. Eksp. Teor. Fiz. **58**, 1695–1702 [Sov. Phys. JETP **31**, 908–911 (1970)].

Baier, V. N., V. M. Katkov, and V. M. Strakhovenko, 1981, "Radiation of relativistic particles moving quasiperiodically," Zh. Eksp. Teor. Fiz. **80**, 1348–1360 [Sov. Phys. JETP **53**, 688–693 (1981)].

Baier, V. N., V. M. Katkov, and V. M. Strakhovenko, 1983, "Radiation of ultrarelativistic particles moving near crystalline axes," Phys. Lett. **95A**, 403–406.

Baier, V. N., V. M. Katkov, and V. M. Strakhovenko, 1984, "Mechanism of electron-positron pair production by high-energy photons in a single crystal," Phys. Lett. **104A**, 231–234.

Baier, V. N., V. M. Katkov, and V. M. Strakhovenko, 1985, "Electron-positron pair creation by photons in an aligned single crystal: Comparison of theory with experiment," Phys. Lett. **109A**, 179–182.

Baier, V. N., V. M. Katkov, and V. M. Strakhovenko, 1986a, "Theory of pair creation in aligned single crystals," Nucl. Instrum. Methods Phys. Res. B **16**, 5–21.

Baier, V. N., V. M. Katkov, and V. M. Strakhovenko, 1986b, "On the radiation theory of high energy electrons in aligned single crystals," Phys. Lett. A **117**, 251–256.

Baier, V. N., V. M. Katkov, and V. M. Strakhovenko, 1986c, "Quantum effects in radiation emitted by ultrahigh energy electrons in aligned crystals," Phys. Lett. **114A**, 511–515.

Baier, V. N., V. M. Katkov, and V. M. Strakhovenko, 1987, "Cascade processes in the fields of the axes of aligned single crystals," Nucl. Instrum. Methods Phys. Res. B **27**, 360–367.

Baier, V. N., V. M. Katkov, and V. M. Strakhovenko, 1988a, "Theory and experiment for pair production in crystals," Nucl. Instrum. Methods Phys. Res. B **34**, 521–522.

Baier, V. N., V. M. Katkov, and V. M. Strakhovenko, 1988b, "Electron-positron pair creation by high-energy photons incident near crystalline planes," Nucl. Instrum. Methods Phys. Res. B **35**, 21–35.

Baier, V. N., V. M. Katkov, and V. M. Strakhovenko, 1989a, "Interaction of high-energy electrons and photons with crystals," Usp. Fiz. Nauk **159**, 455–491 [Sov. Phys. Usp. **32**, 972–992 (1989)].

Baier, V. N., V. M. Katkov, and V. M. Strakhovenko, 1989b, "Pair creation by a photon in oriented single crystals," Nucl. Sci. Appl. (Dhaka) **3**, 245–258.

Baier, V. N., V. M. Katkov, and V. M. Strakhovenko, 1991, "A simple model of kinetic phenomena for the description of radiation in single crystals," Nucl. Instrum. Methods Phys. Res. B **62**, 213–217.

Baier, V. N., V. M. Katkov, and V. M. Strakhovenko, 1992, "Hard photon emission from high energy electrons and positrons in single crystals," Nucl. Instrum. Methods Phys. Res. B **69**, 258–267.

Baier, V. N., V. M. Katkov, and V. M. Strakhovenko, 1995, "Electromagnetic showers in crystals at GeV energies," Nucl. Instrum. Methods Phys. Res. B **103**, 147–155.

Baier, V. N., V. M. Katkov, and V. M. Strakhovenko, 1998, *Electromagnetic Processes at High Energies in Oriented Single Crystals* (World Scientific, Singapore).

Baier, V. N., A. I. Milstein, and R. Zh. Shaisultanov, 1986, "Photon splitting in a strong electromagnetic field," Zh. Eksp. Teor. Fiz. **90**, 1141–1153 [Sov. Phys. JETP **63**, 665–671 (1986)].

Baier, V. N., A. I. Milstein, and R. Zh. Shaisultanov, 1987, "Photon splitting in a strong electromagnetic field and the possibility of its observation in single crystals," Phys. Lett. A **120**, 255–258.

Bak, J. F., *et al.*, 1985, "Channeling radiation from 2–55 GeV/c electrons and positrons, (I) planar case," Nucl. Phys. B **254**, 491–527.

Bak, J. F., *et al.*, 1988a, "e^+-e^- pair creation by 40–150 GeV photons incident near the $\langle 110\rangle$ axis in a germanium crystal," Phys. Lett. B **202**, 615–619.

Bak, J. F., *et al.*, 1988b, "Channeling radiation from 2 to 20 GeV/c electrons and positrons, (II) axial case," Nucl. Phys. B **302**, 525–558.

Bamber, C., *et al.*, 1999, "Studies of nonlinear QED in collisions of 46.6 GeV electrons with intense laser pulses" Phys. Rev. D **60**, 092004.

Baryshevskii, V. G., 1979, "Spin rotation of ultrarelativistic particles in a crystal," Pis'ma Zh. Tekh. Fiz. **5**, 182–184 [Sov. Tech. Phys. Lett. **5**, 73 (1979)].

Baryshevskii, V. G., and I. Ya. Dubovskaya, 1977, "Radiation cooling of charged beams," Phys. Lett. **62A**, 45–46.

Baryshevskii, V. G., and A. O. Grubich, 1983, "Self-polarization and spin precession of channeled particles," Yad. Fiz. **37**, 1093–1100 [Sov. J. Nucl. Phys. **37**, 648–652 (1983)].

Baryshevskii, V. G., and V. V. Tikhomirov, 1982, "Birefringence of the high-energy γ-quanta in monocrystals," Phys. Lett. **90A**, 153–155.

Baryshevskii, V. G., and V. V. Tikhomirov, 1986, "The role of incoherent scattering in radiation processes at small angles of

incidence of particles on crystallographic axes or planes," Zh. Eksp. Teor. Fiz. **90**, 1908–1921 [Sov. Phys. JETP **63**, 1116–1123 (1986)].
Baryshevskii, V. G., and V. V. Tikhomirov, 1988, "Possibilities of obtaining polarized $e^{\pm}$ beams in proton accelerators," Yad. Fiz. **48**, 670–678 [Sov. J. Nucl. Phys. **48**, 429–434 (1988)].
Baryshevskii, V. G., and V. V. Tikhomirov, 1989, "Synchrotron-type radiation processes in crystals and polarization phenomena accompanying them," Usp. Fiz. Nauk **159**, 529–565 [Sov. Phys. Usp. **32**, 1013–1032 (1989)].
Bassompierre, G., *et al.*, 1993, "A search on 1.8 MeV neutral-particle photoproduction in a QED strong field," Europhys. Lett. **22**, 239–244.
Bassompierre, G., *et al.*, 1995, "Search for light neutral objects photoproduced in a crystal strong field and decaying into e^+e^- pairs," Phys. Lett. B **355**, 584–594.
Baublis, V. V., *et al.*, 1994, "Measuring the magnetic moments of short-lived particles using channeling in bent crystals," Nucl. Instrum. Methods Phys. Res. B **90**, 112–118.
Baurichter, A., *et al.*, 1995, "Enhancement of electromagnetic showers initiated by ultrarelativistic electrons in aligned thick germanium crystals," Nucl. Phys. B (Proc. Suppl.) **44**, 79–81.
Baurichter, A., *et al.*, 1996, "New results from the CERN-SPS beam deflection experiments with bent crystals," Nucl. Instrum. Methods Phys. Res. B **119**, 172–180.
Baurichter, A., *et al.*, 1997, "Radiation emission and its influence on the motion of multi-GeV electrons and positrons in strong crystalline fields," Phys. Rev. Lett. **79**, 3415–3418.
Baurichter, A., *et al.*, 1999, "Enhanced electromagnetic showers initiated by 20–180 GeV gamma rays on aligned thick germanium crystals," Nucl. Instrum. Methods Phys. Res. B **152**, 472–478.
Baurichter, A., *et al.*, 2000, "Channeling of high-energy particles in bent crystals—Experiments at the CERN SPS," Nucl. Instrum. Methods Phys. Res. B **164–165**, 27–43.
Belkacem, A., *et al.*, 1984, "Observation of enhanced pair creation for 50–110 GeV photons in an aligned Ge crystal," Phys. Rev. Lett. **53**, 2371–2373.
Belkacem, A., *et al.*, 1985, "Erratum: Observation of enhanced pair creation for 50–110 GeV photons in an aligned Ge crystal," Phys. Rev. Lett. **54**, 852(E) (1985).
Belkacem, A., *et al.*, 1986a, "Measurement of axial effects on the pair creation by 3–150 GeV photons and on the radiation emitted by 150 GeV electrons and positrons in Ge crystals," Nucl. Instrum. Methods Phys. Res. B **13**, 9–14.
Belkacem, A., *et al.*, 1986b, "New channeling effects in the radiative emission of 150 GeV electrons in a thin germanium crystal," Phys. Lett. B **177**, 211–216.
Belkacem, A., *et al.*, 1987, "Study of e^+-e^- pair creation by 20–150-GeV photons incident on a germanium crystal in alignment conditions," Phys. Rev. Lett. **58**, 1196–1199.
Belkacem, A., *et al.*, 1988, "Strong field interactions of high energy electrons and photons in Ge crystals," Nucl. Instrum. Methods Phys. Res. B **33**, 1–10.
Bellucci, S., *et al.*, 2003, "Experimental study for the feasibility of a crystalline undulator," Phys. Rev. Lett. **90**, 034801.
Bellucci, S., *et al.*, 2004, "Crystal undulator as a new compact source of radiation," Phys. Rev. ST Accel. Beams **7**, 023501.
Beloshitski, V. V., M. A. Kumakhov, and A. Kh. Khokonov, 1991, "Radiation energy loss of high energy electrons channeling in thick single crystals," Nucl. Instrum. Methods Phys. Res. B **62**, 207–212.
Berestetskii, V. B., E. M. Lifshitz, and L. P. Pitaevskii, 1971, *Relativistic Quantum Theory* (Pergamon Press, New York).
Berestetskii, V. B., E. M. Lifshitz, and L. P. Pitaevskii, 1982, *Quantum Electrodynamics* (Pergamon Press, New York).
Bethe, H., and W. Heitler, 1934, "On the stopping of fast particles and on the creation of positive electrons," Proc. R. Soc. London, Ser. A **146**, 83–112.
Bilokon, H., G. Bologna, F. Celani, B. D'Ettore Piazzoli, R. Falcioni, G. Mannocchi, and P. Picchi, 1983, "Coherent bremsstrahlung in crystals as a tool for producing high energy photon beams to be used in photoproduction experiments at CERN SPS," Nucl. Instrum. Methods Phys. Res. **204**, 299–310.
Biryukov, V. M., Y. A. Chesnokov, and V. I. Kotov, 1997, *Crystal Channeling and Its Application at High-Energy Accelerators* (Springer, Heidelberg).
Biryukov, V. M., *et al.*, 1994, "On measuring 70 GeV proton dechanneling lengths in silicon crystals (110) and (111)," Nucl. Instrum. Methods Phys. Res. B **86**, 245–250.
Blankenbecler, R., and S. D. Drell, 1987, "Quantum treatment of beamstrahlung," Phys. Rev. D **36**, 277–288.
Blankenbecler, R., and S. D. Drell, 1988, "Quantum beamstrahlung: Prospects for a photon-photon collider" Phys. Rev. Lett. **61**, 2324–2327.
Bulanov, S. V., T. Esirkepov, and T. Tajima, 2003, "Light intensification towards the Schwinger limit," Phys. Rev. Lett. **91**, 085001.
Burke, D. L., *et al.*, 1997, "Positron production in multiphoton light-by-light scattering," Phys. Rev. Lett. **79**, 1626–1629.
Bussey, P. J., C. N. Paterson, C. Raine, R. E. Hughes-Jones, G. D. Lafferty, J. B. Lane, and D. Mercer, 1983, "A polarized high energy tagged photon beam," Nucl. Instrum. Methods Phys. Res. **211**, 301–308.
Cabibbo, N., G. Da Prato, G. De Franceschi, and U. Mosco, 1962, "Circular polarization of high-energy γ rays by birefringence in crystals," Phys. Rev. Lett. **9**, 435–437.
Chen, D., *et al.*, 1992, "First observation of magnetic moment precession of channeled particles in bent crystals," Phys. Rev. Lett. **69**, 3286–3289.
Chen, P., and V. I. Telnov, 1989, "Coherent pair creation in linear colliders," Phys. Rev. Lett. **63**, 1796–1799.
Chen, P., and K. Yokoya, 1988, "Field-gradient effect in quantum beamstrahlung," Phys. Rev. Lett. **61**, 1101–1104.
Cue, N., and J. C. Kimball, 1984, "Tilt-angle dependence of the crystal-assisted pair creation process," Nucl. Instrum. Methods Phys. Res. B **2**, 29–34.
Cue, N., and J. C. Kimball, 1987, "Coherent pair production in axial alignment," Phys. Lett. A **124**, 191–194.
Cue, N., *et al.*, 1984, "Observation of electric synchrotron radiation in a crystal," Phys. Rev. Lett. **53**, 972–974.
Darbinian, S. M., K. A. Ispirian, and A. T. Margarian, 1989, "New mechanism for Unruh radiation of channeled particles," Yerevan Physics Institute preprint, YERPHY-1188(65)-89.
Darbinyan, S. M., and N. L. Ter-Isaakyan, 1999, "The polarization of radiation in single crystals in the semiclassical approach," Pis'ma Zh. Eksp. Teor. Fiz. **69**, 171–175 [JETP Lett. **69**, 180–186 (1999)].
Darbinyan, S. M., and N. L. Ter-Isaakyan, 2002, "Hard polarized photon emission in single crystals by high energy electrons for planar crystal orientations," Nucl. Instrum. Methods Phys. Res. B **187**, 302–310.
Davies, P. C. W., 1975, "Scalar particle production in Schwarzschild and Rindler metrics," J. Phys. A **8**, 609–616.

Davies, P. C. W., 1978, "Thermodynamics of black holes," Rep. Prog. Phys. **41**, 1313–1355.

Doyle, P. A., and P. S. Turner, 1968, "Relativistic Hartree-Fock x-ray and electron scattering factor," Acta Crystallogr., Sect. A: Cryst. Phys., Diffr., Theor. Gen. Crystallogr. **A24**, 390–397.

Dumas, H. S., J. A. Ellison, and F. Golse, 2000, "A mathematical theory of planar particle channeling in crystals," Physica D **146**, 341–366.

Duncan, R. C., 2000, "Physics in ultra-strong magnetic fields," e-print astro-ph/0002442.

Dyson, F. J., and H. Überall, 1955, "Anisotropy of bremsstrahlung and pair production in single crystals," Phys. Rev. **99**, 604–605.

Emma, P., R. Iverson, P. Krejcik, P. Raimondi, and J. Safranek, 2001, "Femtosecond electron bunch lengths in the SLAC FFTB beamline," SLAC-PUB-8850.

Erber, T., 1966, "High-energy electromagnetic conversion processes in intense magnetic fields," Rev. Mod. Phys. **38**, 626–659.

Feinberg, E. L., 1966, "High energy successive interactions," Zh. Eksp. Teor. Fiz. **50**, 202–214 [Sov. Phys. JETP **23**, 132–140 (1966)].

Feinberg, E. L., 1994, "Effect confirmed 40 years later," Priroda (Sofia) **11**, 30. English translation available at http://www.phys.au.dk/~ulrik/lpm/Nature.doc

Feynman, R. P., 1948, "A relativistic cut-off for classical electrodynamics," Phys. Rev. **74**, 939–946.

Fomin, S. P., A. Jejcic, J. Maillard, N. F. Shul'ga, and J. Silva, 1996, "Suppression effect of high energy electron radiation in a thin crystal," Nucl. Instrum. Methods Phys. Res. B **119**, 59–62.

Gemmell, D. S., 1974, "Channeling and related effects in the motion of charged particles through crystals," Rev. Mod. Phys. **46**, 129–227.

Ginzburg, I. F., G. L. Kotkin, V. G. Serbo, and V. I. Telnov, 1983, "Colliding ge and gg beams based on the single-pass $e^{\pm}e^{-}$ colliders (VLEPP type)," Nucl. Instrum. Methods Phys. Res. **205**, 47–68.

Greiner, W., B. Müller, and J. Rafelski, 1985, *Quantum Electrodynamics of Strong Fields* (Springer-Verlag, Berlin).

Gyulassy, M., and X.-N. Wang, 1994, "Multiple collisions and induced gluon bremsstrahlung in QCD," Nucl. Phys. B **420**, 583–614.

Hansen, H. D., U. I. Uggerhøj, C. Biino, S. Ballestrero, A. Mangiarotti, P. Sona, T. J. Ketel, and Z. Z. Vilakazi, 2003, "Is the electron radiation length constant at high energies?," Phys. Rev. Lett. **91**, 014801.

Hansen, H. D., U. I. Uggerhøj, C. Biino, S. Ballestrero, A. Mangiarotti, P. Sona, T. J. Ketel, and Z. Z. Vilakazi, 2004, "The LPM effect for multi-hundred GeV electrons," Phys. Rev. D **69**, 032001.

Heitler, W., 1954, *The Quantum Theory of Radiation* (Dover, New York).

Huang, Z., P. Chen, and R. D. Ruth, 1995, "Radiation reaction in a continuous focusing channel," Phys. Rev. Lett. **74**, 1759–1762.

Huang, Z., P. Chen, and R. D. Ruth, 1996, "A semi-classical treatment of chenneling radiation reaction," Nucl. Instrum. Methods Phys. Res. B **119**, 192–198.

Ibrahim, A. I., J. H. Swank, and W. Parke, 2003, "New evidence of proton-cyclotron resonance in a magnetar strength field from SGR 1806-20," Astrophys. J. Lett. **584**, L17–L21.

Jackson, J. D., 1975, *Classical Electrodynamics* (Wiley, New York).

Jarlskog, G., L. Jönsson, S. Prünster, H. D. Schulz, H. J. Willutzki, and G. G. Winter, 1973, "Measurement of Delbrück scattering and observation of photon splitting at high energies," Phys. Rev. D **8**, 3813–3823.

Kasper, P., 1996, private communication.

Khokonov, M. Kh., 1992, "Self-focusing and angular distribution of electrons moving in the field of atomic rows," Pis'ma Zh. Eksp. Teor. Fiz. **56**, 349–351 [JETP Lett. **56**, 333–336 (1992)].

Khokonov, A. Kh., M. Kh. Khokonov, and R. M. Keshev, 1998, "Features of the emission spectrum of relativistic electrons moving in an ultraintense laser field," Pis'ma Zh. Tekh. Fiz. **24**, 20–27 [Tech. Phys. Lett. **24**, 797–799 (1998)].

Khokonov, A. Kh., M. Kh. Khokonov, and A. A. Kizdermishov, 2002, "Possibility of generating high-energy photons by ultrarelativistic electrons in the field of a terawatt laser and in crystals," Zh. Tekh. Fiz. **72**, 69–75 [Tech. Phys. Lett. **47**, 1413–1419 (2002)].

Khokonov, M. Kh., and H. Nitta, 2002, "Standard radiation spectrum of relativistic electrons: beyond the synchrotron approximation," Phys. Rev. Lett. **89**, 094801.

Kimball, J. C., and N. Cue, 1984a, "Synchrotron radiation and channeling of ultrarelativistic particles," Phys. Rev. Lett. **52**, 1747–1750.

Kimball, J. C., and N. Cue, 1984b, "Constant field approximation for the crystal-assisted pair-creation process," Nucl. Instrum. Methods Phys. Res. B **2**, 25–28.

Kimball, J. C., and N. Cue, 1985, "Quantum electrodynamics and channeling in crystals," Phys. Rep. **125**, 69–101.

Kimball, J. C., N. Cue, and A. Belkacem, 1986, "Crystal-assisted quantum electrodynamics: Pair production and radiation," Nucl. Instrum. Methods Phys. Res. B **13**, 1–8.

Kimball, J. C., N. Cue, L. M. Roth, and B. B. Marsh, 1983, "New crystal-assisted pair-creation process," Phys. Rev. Lett. **50**, 950–953.

Kirsebom, K., U. Mikkelsen, E. Uggerhøj, K. Elsener, S. Ballestrero, P. Sona, and Z. Z. Vilakazi, 2001a, "First measurements of the unique influence of spin on the energy loss of ultrarelativistic electrons in strong electromagnetic fields," Phys. Rev. Lett. **87**, 054801.

Kirsebom, K., U. Mikkelsen, E. Uggerhøj, K. Elsener, S. Ballestrero, P. Sona, S. H. Connell, J. P. F. Sellschop, and Z. Z. Vilakazi, 2001b, "Radiation emission and its influence on the motion of multi-GeV electrons and positrons incident on a single diamond crystal," Nucl. Instrum. Methods Phys. Res. B **174**, 274–296.

Kirsebom, K., *et al.*, 1996, "Experimental investigation of photon multiplicity and radiation cooling for 150 GeV electrons/positrons traversing diamond and Si crystals," Nucl. Instrum. Methods Phys. Res. B **119**, 79–95.

Kirsebom, K., *et al.*, 1998, "Pair production by 5–150 GeV photons in the strong crystalline fields of germanium, tungsten and iridium," Nucl. Instrum. Methods Phys. Res. B **135**, 143–148.

Kirsebom, K., *et al.*, 1999, "Generation and detection of the polarization of multi-GeV photons by use of two diamond crystals," Phys. Lett. B **459**, 347–353.

Klein, O., 1929, "Die reflexion von elektronen an einem potentialsprung nach der relativistischen dynamik von dirac," Z. Phys. **53**, 157–165.

Klein, S., 1999, "Suppression of bremsstrahlung and pair pro-

duction due to environmental factors," Rev. Mod. Phys. **71**, 1501–1538.
Klenner, J., J. Augustin, A. Schäfer, and W. Greiner, 1994, "Photon-photon interaction in axial channeling," Phys. Rev. A **50**, 1019–1026.
Kononets, Yu. V., 1988, "The quantum recoil effects in radiative losses of superrelativistic electrons in crystals," Nucl. Instrum. Methods Phys. Res. B **33**, 22–25.
Kononets, Yu. V., 1992, "Theoretical investigations of hard gamma radiation and radiative kinetics of superrelativistic electrons in oriented crystals in connection with recent precision experiments of the Aarhus/CERN group," J. Mosc. Phys. Soc. **2**, 71–100.
Kononets, Yu. V., 1996, private communication.
Kononets, Yu. V., 1999, in *Quantum Aspects of Beam Physics, Monterey 1998*, edited by Pisin Chen (World Scientific, Singapore).
Kononets, Yu. V., and V. A. Ryabov, 1988, "Photon showers and the Belkacem peak in the radiation from channeled ultrarelativistic electrons," Pis'ma Zh. Eksp. Teor. Fiz. **48**, 303–306 [JETP Lett. **48**, 333–337 (1988)].
Kononets, Yu. V., and V. A. Ryabov, 1990a, "Radiative-cooling and multiple-scattering effects in the deceleration kinetics of superrelativistic channeled electrons," Nucl. Instrum. Methods Phys. Res. B **48**, 274–277.
Kononets, Yu. V., and V. A. Ryabov, 1990b, "Cascade processes in radiation by high-energy electrons in crystals: The radiation peak," Nucl. Instrum. Methods Phys. Res. B **48**, 269–273.
Kononets, Yu. V., and I. S. Tupitsyn, 1993, "Coherent resonances in the spectra of e^+-e^- pairs created by hard γ rays in aligned single crystals," Pis'ma Zh. Eksp. Teor. Fiz. **57**, 148–153 [JETP Lett. **57**, 151–156 (1993)].
Kononets, Yu. V., and I. S. Tupitsyn, 1994, "Above-barrier γ-ray emission by ultrahigh-energy electrons in oriented single crystals," Pis'ma Zh. Eksp. Teor. Fiz. **59**, 491–497 [JETP Lett. **59**, 516–523 (1994)].
Korol, A. V., A. V. Solov'yov, and W. Greiner, 1998, "Coherent radiation of an ultra-relativistic charged particle channeled in a periodically bent crystal," J. Phys. G **24**, L45–L53.
Korol, A. V., A. V. Solov'yov, and W. Greiner, 1999, "Photon emission by an ultra-relativistic charged particle channeling in a periodically bent crystal," Int. J. Mod. Phys. E **8**, 49–100.
Korol, A. V., A. V. Solov'yov, and W. Greiner, 2001, "The influence of the dechanneling process on the photon emission by an ultra-relativistic positron channeling in a periodically bent crystal," J. Phys. G **27**, 95–125.
Korol, A. V., A. Solov'yov, and W. Greiner, 2002, "The influence of spin-flip transitions on the photon spectrum from ultra-relativistic electrons in the field of a crystal," J. Phys. G **28**, 627–641.
Krause, W., A. V. Korol, A. V. Solov'yov, and W. Greiner, 2000, "Total spectrum of photon emission by an ultra-relativistic charged particle channeling in a periodically bent crystal," J. Phys. G **26**, L87–L95.
Krause, W., A. V. Korol, A. V. Solov'yov, and W. Greiner, 2001, "Spontaneous and stimulated undulator radiation by an ultra-relativistic positron channeling in a periodically bent crystal," Nucl. Instrum. Methods Phys. Res. A **475**, 441–444.
Krejcik, P., 2001, private communication.
Krekora, P., Q. Su, and R. Grobe, 2004, "Klein paradox in spatial and temporal resolution," Phys. Rev. Lett. **92**, 040406.
Kurilin, A. V., 1999, "Particle physics in intense electromagnetic fields," Nuovo Cimento Soc. Ital. Fis., A **112**, 977–1000.
Landau, L. D., 1965, *The Collected Papers of L. D. Landau* (Pergamon, New York).
Landau, L. D., and I. J. Pomeranchuk, 1953a, "The limits of applicability of the theory of bremsstrahlung by electrons and of the creation of pairs at large energies," Dokl. Akad. Nauk SSSR **92**, 535 (English translation available in Landau, 1965, pp. 586–588).
Landau, L. D., and I. J. Pomeranchuk, 1953b, "Electron-cascade processes at ultra-high energies," Dokl. Akad. Nauk SSSR **92**, 735 (English translation available in Landau, 1965, pp. 589–593).
Lindhard, J., 1965, "Influence of crystal lattice on motion of energetic charged particles," K. Dan. Vidensk. Selsk. Mat. Fys. Medd. **34** (14), 1–64.
Lindhard, J., 1991, "Quantum-radiation spectra of relativistic particles derived by the correspondence principle," Phys. Rev. A **43**, 6032–6037.
MacDonald, K., 1998, in *Quantum Aspects of Beam Physics*, edited by P. Chen (World Scientific, Singapore), p. 643.
McBreen, B., and C. J. Lambert, 1981, "Interactions of high-energy ($E>5\times10^{19}$ eV) photons in the Earth's magnetic field," Phys. Rev. D **24**, 2536–2538.
Medenwaldt, R., *et al.*, 1989a, "Hard-photon emission from 150-GeV electrons incident on Si and Ge single crystals near axial directions," Phys. Rev. Lett. **63**, 2827–2829.
Medenwaldt, R., *et al.*, 1989b, "Detailed investigations of shower formation in Ge- and W-crystals traversed by 40–287 GeV/c electrons," Phys. Lett. B **227**, 483–488.
Medenwaldt, R., *et al.*, 1990, "Hard photon yields from (70–240) GeV electrons incident near axial directions on Si, Ge and W single crystals with a large thickness variation," Phys. Lett. B **242**, 517–522.
Medenwaldt, R., *et al.*, 1991, "Coherent bremsstrahlung and channeling radiation from 40 and 150 GeV electrons and positrons traversing Si and diamond single crystals near planar directions," Phys. Lett. B **260**, 235–239.
Medenwaldt, R., *et al.*, 1992, "Experimental investigations of hard photon emission from strong crystalline fields," Phys. Lett. B **281**, 153–158.
Mikkelsen, U., and E. Uggerhøj, 2000, "A crystalline undulator based on graded composition strained layers in a superlattice," Nucl. Instrum. Methods Phys. Res. B **160**, 435–439.
Molière, G., 1947, "Theorie der Streuung schneller geladener Teilchen I," Z. Naturforsch. A **2**, 133–145.
Møller, S. P., 1995, "High-energy channeling—applications in beam bending and extraction," Nucl. Instrum. Methods Phys. Res. A **361**, 403–420.
Moore, R., *et al.*, 1996, "Measurement of pair-production by high energy photons in an aligned tungsten crystal," Nucl. Instrum. Methods Phys. Res. B **119**, 149–155.
Müller, B., W. Greiner, and J. Rafelski, 1977, "Interpretation of external fields as temperature," Phys. Lett. **63A**, 181–183.
Müller, C., A. B. Voitkiv, and N. Grün, 2003, "Nonlinear Bound-Free Pair Creation in the Strong Electromagnetic Fields of a Heavy Nucleus and an Intense X-Ray Laser," Phys. Rev. Lett. **91**, 223601.
Nikishov, A. I., and V. I. Ritus, 1964, "Quantum processes in the field of a plane electromagnetic wave and in a constant field," Zh. Eksp. Teor. Fiz. **46**, 776–796 [Sov. Phys. JETP **19**, 529–541 (1964)].
Nitta, H., M. Kh. Khokonov, Y. Nagata, and S. Onuki, 2004, "Electron-positron pair production by photons in nonuniform

strong fields," Phys. Rev. Lett. **93**, 180407.
Nitta, H., T. Kudo, and H. Minowa, 1999, "Motion of a wave packet in the Klein paradox," Am. J. Phys. **67**, 966–971.
Olinto, A. V., 2000, "Ultra high energy cosmic rays: The theoretical challenge," Phys. Rep. **333-334**, 329–348.
Palazzi, G. D., 1968, "High-energy bremsstrahlung and electron pair production in thin crystals," Rev. Mod. Phys. **40**, 611–631.
Pedersen, O., J. U. Andersen, and E. Bonderup, 1986, "Coherence lengths for emission of classical channeling radiation," Nucl. Instrum. Methods Phys. Res. B **13**, 27–31.
Pedersen, O., J. U. Andersen, and E. Bonderup, 1987, in *Relativistic channeling*, NATO Advanced Study Institute Vol. 165, edited by R. A. Carrigan, Jr. and J. A. Ellison (Plenum, New York), pp. 207–226.
Plyasheshnikov, A. V., and F. A. Aharonian, 2002, "Characteristics of air showers produced by extremely high energy gamma-rays," J. Phys. G **28**, 267–288.
Pomeranchuk, I., 1940, "On the maximum energy which the primary electrons of cosmic rays can have on the Earth's surface due to radiation in the Earth's magnetic field," J. Phys. (Moscow) **2**, 65–69.
Rosu, H., 2004, in *Quantum Aspects of Beam Physics, Hiroshima 2002*, edited by Pisin Chen (World Scientific, in press).
Samsonov, V. M., 1996, "On the possibility of measuring charm baryon magnetic moments with channeling," Nucl. Instrum. Methods Phys. Res. B **119**, 271–279.
Sauter, F., 1931a, "Über das Verhalten eines Elektrons im homogenen elektrischen Feld nach der relativistischen Theorie Diracs," Z. Phys. **69**, 742–764.
Sauter, F., 1931b, "Zum Kleinschen Paradoxon," Z. Phys. **73**, 547–552.
Schäfer, A., 1989, "New particles in strong fields?," J. Phys. G **15**, 373–416.
Schäfer, A., S. Graf, J. Augustin, W. Greiner, and E. Uggerhøj, 1990, "High energy two-gamma physics using channeling," J. Phys. G **16**, L131–L133.
Schumacher, M., 1999, "Delbrück scattering," Radiat. Phys. Chem. **56**, 101–111.
Schwinger, J., 1954, "The quantum correction in the radiation by energetic accelerated electrons," Proc. Natl. Acad. Sci. U.S.A. **40**, 132–136.
Schwinger, J., and W. Tsai, 1974, "Radiative polarization of electrons," Phys. Rev. D **9**, 1843–1845.
Schwinger, J., and W. Tsai, 1978, "New approach to quantum corrections in synchrotron radiation," Ann. Phys. (N.Y.) **110**, 63–84.
Shinozaki, K., *et al.*, 2002, "Upper limit on gamma-ray flux above 10^{19} eV estimated by the Akeno giant air shower array experiment," Astrophys. J. Lett. **571**, L117–L120.
Shul'ga, N. F., and S. P. Fomin, 1998, "Bremsstrahlung of ultrarelativistic electrons in a thin layer of substance," Nucl. Instrum. Methods Phys. Res. B **145**, 73–39.
Shul'ga, N. F., and V. V. Syshchenko, 2002, "On the coherent radiation of relativistic electrons and positrons in crystal in the range of high energies of gamma-quanta," Nucl. Instrum. Methods Phys. Res. B **193**, 192–197.
Sokolov, A. A., and I. M. Ternov, 1964, "On polarization and spin effects in the theory of synchrotron radiation," Dokl. Akad. Nauk SSSR **153**, 1052–1054 [Sov. Phys. Dokl. **8**, 1203–1205 (1964)].
Sokolov, A. A., and I. M. Ternov, 1986, *Radiation from Relativistic Electrons* (AIP, New York).
Stanev, T., 1998, "The nature and the origin of the highest energy cosmic rays," Nucl. Phys. B (Proc. Suppl.) **60**, 181–190.
Stanev, T., and H. P. Vankov, 1998, "Nature of the highest energy cosmic rays," Phys. Rev. D **55**, 1365–1371.
Stark, J., 1912, "Bemerkung über zerstreuung und absorption von β-strahlen und röntgenstrahlen in kristallen," Phys. Z. **13**, 973–977.
Sørensen, A. H., 1983, Ph.D. thesis (Aarhus University).
Sørensen, A. H., 1987, in *Relativistic Channeling*, NATO Advanced Study Institute Vol. 165, edited by R. A. Carrigan, Jr. and J. A. Ellison (Plenum, New York), pp. 331–337.
Sørensen, A. H., 1991, in *Vacuum Structure in Intense Fields*, NATO Advanced Study Institute Vol. 255, edited by H. M. Fried and B. Müller (Plenum, New York), pp. 91–118 [reprinted in "Channeling, bremsstrahlung and pair creation in single crystals," Nucl. Instrum. Methods Phys. Res. B **119**, 2–29 (1996)].
Sørensen, A. H., 1992, "On the suppression of the gluon radiation for quark jets penetrating a dense quark gas," Z. Phys. C **53**, 595–600.
Sørensen, A. H., 2001, "Impact-parameter dependence of the relativistic photoeffect and other high-energy photoprocesses," Phys. Rev. A **64**, 012703.
Sørensen, A. H., and E. Uggerhøj, 1989, "Channeling, radiation and applications," Nucl. Sci. Appl. (Dhaka) **3**, 147.
Strakhovenko, V. M., 1998, "A practical method for calculation of photon emission and pair production probabilities in crystals," Nucl. Instrum. Methods Phys. Res. B **145**, 120–127.
Strakhovenko, V. M., 2001, "Propagation of polarized high-energy photons in crystals," Nucl. Instrum. Methods Phys. Res. B **173**, 37–47.
Strakhovenko, V. M., 2002, "Emission of polarized photons from unpolarized electrons moving in crystals," e-print hep-ph/0301149.
Tajima, T., and M. Cavenago, 1987, "Crystal x-ray accelerator," Phys. Rev. Lett. **59**, 1440–1443.
Ter-Mikaelian, M. L., 1972, *High-Energy Electromagnetic Processes in Condensed Media* (Wiley Interscience, New York).
Ter-Mikaelian, M. L., 2001, "Electromagnetic radiative processes in periodic media at high energies," Usp. Fiz. Nauk **171**, 597–624 [Phys. Usp. **44**, 571–596 (2001)].
Ternovskii, F. F., 1960, "On the theory of radiative processes in piecewise homogeneous media," Zh. Eksp. Teor. Fiz. **39**, 171–180 [Sov. Phys. JETP **12**, 123–129 (1960)].
Tikhomirov, V. V., 1987a, "The position of the peak in the spectrum of 150 GeV electron energy losses in a thin germanium crystal is proposed to be determined by radiation cooling," Phys. Lett. A **125**, 411–415.
Tikhomirov, V. V., 1987b, "On the theory of electron-positron pair production in crystals," J. Phys. (Paris) **48**, 1009–1016.
Tikhomirov, V. V., 1989, "Simulation of multi-GeV electron energy losses in crystals," Nucl. Instrum. Methods Phys. Res. B **36**, 282–285.
Timm, U., 1969, "Coherent bremsstrahlung of electrons in crystals," Fortschr. Phys. **17**, 765–808.
Tsai, W., 1973, "Magnetic bremsstrahlung and modified propagation function: Spin-0 charged particles in a homogeneous magnetic field," Phys. Rev. D **8**, 3460–3469.
Tsai, Y., 1974, "Pair production and bremsstrahlung of charged leptons," Rev. Mod. Phys. **46**, 815–851; **49**, 421–423(E) (1977).
Tsai, W., and A. Yildiz, 1973, "Motion of an electron in a ho-

mogeneous magnetic field—modified propagation function and synchrotron radiation," Phys. Rev. D **8**, 3446–3460.
Uggerhøj, U. I., 2003, "An experimental foundation for electromagnetic shower formation in the geomagnetic field," Nucl. Phys. B (Proc. Suppl.) **122**, 357–363.
Uggerhøj, U. I., 2004a, "The Landau-Pomeranchuk-Migdal effect for amorphous and crystalline matter," Mod. Phys. Lett. B **18**, 309–325.
Uggerhøj, U. I., 2004b, in *Quantum Aspects of Beam Physics, Hiroshima 2003*, edited by Pisin Chen and Kevin Reil (World Scientific, Singapore).
Uggerhøj, U. I., and E. Uggerhøj, 2005, "Strong crystalline fields—a possibility for extraction from the LHC," Nucl. Instrum. Methods Phys. Res. B, **234**, 31–39.
Unel, G., *et al.*, 2001, "Na59 Experiment at CERN," Int. J. Mod. Phys. A **16**, Suppl. 1C, 1071–1073.
Unruh, W. G., 1976, "Notes on black-hole evaporation," Phys. Rev. D **14**, 870–892.
Waasmaier, D., and A. Kirfel, 1995, "New analytical scattering-factor functions for free atoms and ions," Acta Crystallogr., Sect. A: Found. Crystallogr. **51**, 416–431.
Watson, A. A., 1998, "The highest energy cosmic rays and the Auger project," Nucl. Phys. B (Proc. Suppl.) **60**, 171–180.
Weinmann, P. M., 1998, Ph.D. thesis (Technischen Universität München), e-print MPI-PhE/98-07.
Williams, E. J., 1935, "Correlation of certain collision problems with radiation theory," K. Dan. Vidensk. Selsk. Mat. Fys. Medd. **13** (4), 1–50.
Xu, R. X., J. F. Liu, J. L. Han, and G. J. Qiao, 2000, "An inverse Compton scattering model of pulsar emission. III. Polarization," Astrophys. J. **535**, 354–364 (2000).
Yamazaki, R., K. Ioka, F. Takahara, and N. Shibazaki, 2005, "Giant flare of SGR 1806-20 from a relativistic jet," e-print astro-ph/0502320.